Title
A Novel Overtopping Wave Energy Device Concept Applied to California

Author
Imamura, John

Publication Date
2009

Peer reviewed|Thesis/dissertation

A Novel Overtopping Wave Energy Device Concept Applied to California

by

John Imamura

B.S. (University of California, Berkeley) 2000
M.S. (University of California, Berkeley) 2006

A dissertation submitted in partial satisfaction of the

requirements for the degree of

Doctor of Philosophy

in

Engineering - Mechanical Engineering

in the

Graduate Division

of the

University of California, Berkeley

Committee in charge:

Professor Alaa Mansour, Chair
Professor Ömer Savaş
Professor Mark Stacey

Fall 2009

Abstract

A Novel Overtopping Wave Energy Device Concept Applied to California

by

John Imamura

Doctor of Philosophy in Engineering - Mechanical Engineering

University of California, Berkeley

Professor Alaa Mansour, Chair

This thesis explores a novel concept in the area of overtopping ocean wave energy devices. Current models of overtopping devices are limited to locations which experience large wave activity. The high energy associated with large waves enables the ocean water waves to overtop the device ramp into the collection reservoir which discharges through a power generating turbine. The ramp height is necessarily large to establish a sufficient collection reservoir head. The proposed design concept can utilize small waves by implementing a gearing system which can transfer water to the collection reservoir. This allows for greater access to the wave energy resource at more locations than currently possible.

After providing background to ocean wave energy devices the wave resources of the California coast is investigated. The formulation for wave energy is established and a statistical analysis of eight locations from northern to southern California is provided. Next important aspects for overtopping as well as overtopping formulas are presented.

The modeling of an overtopping device with a gearing system is presented and examined for a range of variables important to overtopping. An analysis of the proposed design concept shows promise for higher power output in the smaller wave

environments of southern California. Additionally for all locations considered the gearing system concept improves power output over a conventional overtopping device for some portion of the time. In addition, survivability issues important for devices in the ocean environment are treated using extreme value analysis and further areas of research are suggested for future work.

.....

Professor Alaa Mansour

Committee Chairman

Contents

List of Figures

List of Tables

Acknowledgments

I am extremely grateful to my advisor, Professor Alaa Mansour, for helping me complete this thesis. He is a renowned scholar with many professional obligations yet under unusual circumstances he generously accepted me as his student and discussions with him contributed greatly to this work. He is always helpful and relaxed and you always leave his office better off than when you entered. His outlook towards research and style of mentoring his students has vastly enhanced my perspective and has been of tremendous benefit to me.

I would also like to thank my thesis committee members, Professor Ömer Savaş and Professor Mark Stacey for their insightful comments. In addition I've benefitted from the instruction of Professors Ömer Savaş, Stanley Berger, Andrew Szeri, and the other instructors I have had courses with, from which I have greatly broadened my knowledge of fluid mechanics and engineering.

My friends and labmates have helped me in countless ways over the years. I value the helpful talks and fun times I've had with Hui Wan, Robert Seah, Alexia Aubault, Jean Toilliez, Grégoire Poupard, Juan Perri, Jon Elkin, Hobin Kang, Tomasz Matlak, Fred Toh, Martin Petricic, Vincent Escobedo, and Antoine Peiffer. In addition, I cherish Whiskers and Han Solo for never failing to make me smile when times were tough.

Finally, I am thankful for the support and encouragement from my family without which this work would not be possible.

Chapter 1

Introduction

1.1 Wave Energy Background

The useful extraction of energy from the oceans has intrigued scientists and inventors around the world for more than two centuries. Indeed, the first patent for an ocean energy device, filed by the Girards in Paris, dates back to 1799. The first British patent was in 1855. In 1892, one of the earliest papers on wave power was presented at the American Society of Mechanical Engineers by A.W. Stahl. Research programs in this field has been active for the past 60 to 70 years. In the late 1940's wave-power pioneer Yoshio Masuda began testing and developing wave energy devices for the oceanographic unit of the Japanese Defense Department. During the early 1970's wave power research was initiated at universities in Scotland and Norway. Many theoretical advances were accomplished by applied mathematicians during this decade. Larger government funded research and development programs were started in the UK, Sweden, Norway and other countries in the late 70's ([13], [38]). Much of the current level of success in wave energy is due to these efforts.

A few developments stand out as significant advances. In 1965, the Masuda Buoy was developed. This was an air turbine buoy with an output of 60 watts. Hundreds

of these wave powered navigation buoys have been deployed off the coasts of Japan, Canada, the UK, and other locations demonstrating the potential of wave energy. In 1974, the "Salter's Duck" created a lot of interest due to its publication in *Nature*. This cam-shaped floating device by professor Stephen Salter of the University of Edinburgh, was extremely efficient at absorbing energy. As the oil crisis of the 1970's was occurring this development had a great impact on promoting wave energy. The Well's Turbine was also developed during this time period. This turbine used in conjunction with oscillating water columns (to be described below) greatly improved the power take-off aspect of such devices.

Historically the interest and development of wave energy by the government and investors has been intermittent and strongly dependent on the conditions of the larger economic climate. Specifically, during the 1970's tremendous progress was made theoretically and analytically in the design and modeling of wave energy devices. Naturally this was a consequence of increased funding and interest in alternative energy in response to the oil crisis at the time. In the 1980's much of the funding stopped, coinciding with a precipitous drop in the price of oil. A halt in the advancement of wave energy development resulted. However, starting in the mid 1990's there has been an renewed push for renewable energy. The impetus this time was the Kyoto Protocol on reduction of carbon dioxide emissions to the atmosphere as well as energy independence and the rising costs of oil. Within California, state mandates on electrical utilities for minimum renewable energy goals is a driving force. Therefore, once again there has been a growing interest in wave energy around the world.

Significant advancements have led to the point where some full-scale prototypes have been tested and connected to national electrical grids. Development centers helped accomplish this by subsidizing costly infrastructure costs because though the resource is free, wave energy projects are very capital intensive. In Europe, the European Marine Energy Centre (EMEC) as well as the England's Wave Hub are

supporting various device concepts by providing a test center for many pre-commercial groups. The UK and Portugal, in particular, are greatly supporting development of this young industry. In the United States, smaller scale prototype testing has occurred off the Oregon coast and near Hawaii. Many feasibility studies and site location studies have been performed for the West Coast. Applications have been filed with government agencies to test off the coast from California to Washington. Similar to wind energy fifteen years ago, there are many competing approaches. Many young companies exist with their own design concepts spanning the globe from Australia to Ireland to Norway to the United States. Much progress has been made however continued support from energy associated industries and government agencies remains crucial. ([8], [35], [46]).

The history and scope of research programs and designs in wave energy has been only briefly described here. Interested readers should consult the above references.

1.2 Literature Review

As the wave energy field grows the sources of information has similarly increased. Many conference proceedings dating back to the 1970's exist showing the continued interest and development of theoretical and design concepts by the scientific community. A well-referenced collection of papers edited by Count [7] describes the state of the field as of 1979. Evans established the theoretical principles of wave energy conversion in his journal papers in 1976 and 1981 ([10], [11]). These principles involve the motions of wave energy structures in response to water waves. Therefore it is not surprising that much of the mathematical treatment is related to ship hydrodynamic theory for which there is a long established wealth of knowledge. The basic difference in treatment to that of ship theory is wave energy structures have zero forward speed. This simplifies the problem from that of ship motions. However wave energy

designs may involve articulated motions unaccounted for in ship theory. Nevertheless, references to start from with regard to response to water waves are the well-known classic works on the theory of floating bodies by Wehausen [45] and Newman [32]. Mei's book [29] is another well known reference and provides a sub-chapter on wave energy analysis. Another thorough description of the mathematical analysis of the absorption of waves by oscillating bodies can be found in Falnes [12].

References more suitable for a wider engineering audience are also available. McCormick [27] presented many initial design concepts with a clear presentation of the fundamentals of wave energy conversion back in 1981. Practical issues such as mooring and anchoring as well as electrical transmission is discussed in addition to the fluid dynamic aspects. Shaw [38] published a similar book on the design challenges of wave energy in 1982. More recently Brooke [3] edited a compilation of work ranging from economics and resource assessment to power take-off mechanisms and contributions from various geographical areas. In 2008, Cruz [8] edited the most current reference on the status of ocean wave energy. Full scale prototype experiences and future perspectives are analyzed for four prominent devices in his book.

Industrial and professional organizations have also contributed to the growing pool of information. International Ship and Offshore Structures Congress (ISSC) specialist committees for ocean, wind and wave utilization now provide report with concern for the structural design of ocean energy utilization devices [31]. The Electric Power Research Institute (EPRI) has conducted several feasibility and siting studies particularly in California to help the state move forward with wave energy conversion. Their work explores topics such as grid infrastructure, installation and maintenance, performance prediction, environmental issues and permitting through the regulation process [35].

1.3 Device Classifications

One way of several ways that wave energy devices are classified is based on their location from the shoreline. Onshore (or shoreline) devices are embedded or fixed to the shore. This is advantageous for transmitting power to electrical substations, installation and maintenance, and does not require mooring systems. However the wave energy resource that reaches the shore is not as great as offshore. Offshore devices on the other hand have the greatest potential to produce energy because they are exposed to much larger waves. The drawback is the device must withstand a harsher environment, costly electrical cables back to shore must be installed, installation and maintenance costs are far more expensive, and mooring systems are required. Nearshore (or shallow water) devices can be varients of the other two types. Closer to shore the wave energy tends to diminish however the cabling, maintenance, and mooring costs decrease as well. The suitability for which style of device to install therefore depends greatly on the features of the particular site.

Another way of classifying devices is by how they interact mechanically with waves. All of these devices require some kind of relative motion to produce power. There are several hundreds of proposed device designs [19], however the means by which the relative motion in response to the waves places them in one of the following categories; point absorbers, oscillating water columns, articulated motion devices, or overtopping devices.

Point absorbers are buoy-like devices that oscillate vertically in response to incoming waves. Generally they are designed or can be tuned to have large motions in response to a desired frequency. The large oscillations serve to drive a working fluid to power a turbine or move magnets through electric coils in 'direct drive' power take-off systems to produce electricity. The key characteristic of a point absorber is that it can potentially absorb more energy than available within the device's width of

wave front. Ideally many of these devices are to be deployed in arrays as offshore wave energy 'farms'. Point absorbers are conducive to mathematical analysis because the formulation is similar as that in other fields involving wave theory such as in acoustics and electromagnetics. Budal and Falnes have pioneered much theoretical work on these devices [4]. Prominent examples of this type of device are the PowerBuoy by Ocean Power Technology and Finavera Renewable's AquaBuoy.

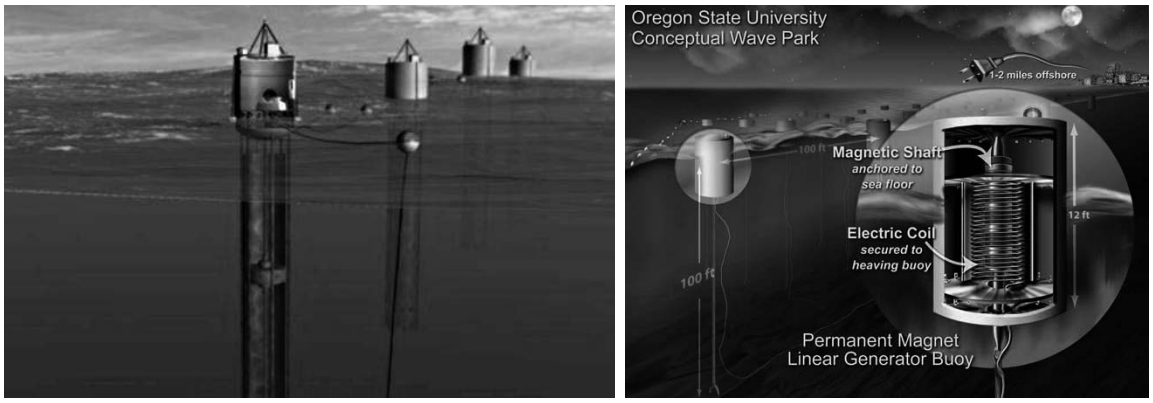

Figure 1.1: Example of point absorbers in wave farms.

Oscillating water columns operate by employing the rise and falls of the ocean surface to cyclically compress and expand an enclosed air space. When the air is compressed the resulting increased pressure drives a turbine to produce electricity. A cleverly designed turbine known as the Well's Turbine allows for electricity generation as the air space is compressed and expanded. This type of device was the world's first wave power plant. A Scottish company, Wavegen, installed the LIMPET device on Islay Island and produced peak power of 500 kW for the UK grid. Another leading design is by Energetech of Australia, which uses an offshoot of the Well's Turbine and a parabolic wall to focus waves to its device.

The articulated motion category is a wide ranging category to account for devices which bend or rotate at joints and hinges. The Pelamis by Ocean Power Delivery

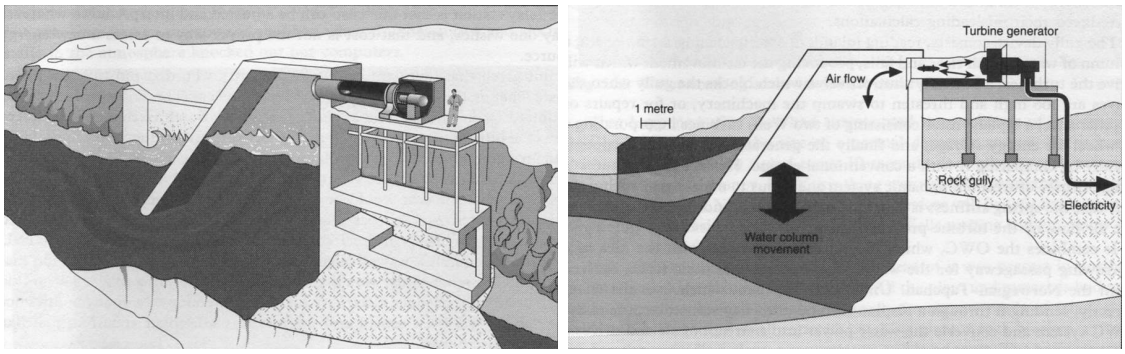

Figure 1.2: Example of a basic Oscillating Water Column.

is one such device. It is a semi-submerged system of four cylinders joined by three articulating joints. It is moored such that it can align itself lengthwise in the direction of wave propagation and as waves propagate along its length the articulating joints actuate hydraulic rams to pump fluid to run a motor. Like point absorbers the Pelamis is expected to operate offshore in large wave farms.

Figure 1.3: Photo of a prototype Pelamis and conceptualized Pelamis wave farm.

Overtopping devices are those which operate by collecting water from waves of sufficient size and energy to 'overtop' a ramp into a reservoir at an elevated position. The height difference between the reservoir and mean sea level, or head, is utilized to

produce energy by releasing the stored water through low-head turbines back to the sea. These types of devices can be located onshore but are not required to be so. The initial concept of an overtopping device, the TapChan by Mehlum in 1985 [28] and another design called the Sea-Slot Cone Generator (SSG) are onshore devices. The most prominent overtopping device called the Wave Dragon can be located nearshore or offshore.

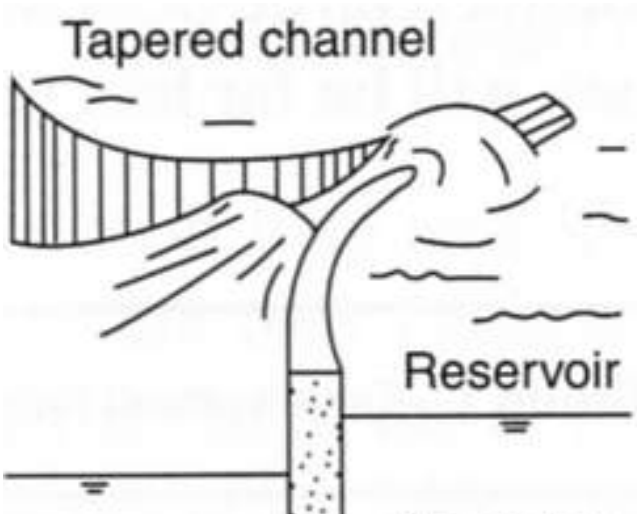

Figure 1.4: Schematic of a basic overtopping device.

1.4 Main Purpose and Contents of This Thesis

The main purpose of this thesis is to propose and analyze a novel overtopping device concept and apply it to the waters off the California coast. An explanation of the source of wave energy and how it is quantified will be presented in chapter 2. The wave climate off the California coast will also be described and the wave energy will be estimated. Chapter 3 discusses various aspects of overtopping devices. For overtopping devices, the critical factor in determining the energy produced is the overtopping volume of water which enters the reservoir. Methods to determine

how to obtain this parameter are described. Particularly, the formulas for seawall and offshore volumetric overtopping rates are given. Also descriptions of overtopping devices such as the Wave Dragon and the Sea-Slot Cone Generator are given and their applicability along California's coast are analyzed.

The key points of this thesis is presented in the remaining chapters. It will be demonstrated in chapter 4 that gearing systems can be used to allow overtopping devices access to low sea-states previously largely unusable to conventional overtopping devices. Conventional systems have a minimum crest freeboard which serve as a cutoff on the sea-states for which overtopping will occur. Gearing systems will allow this crest freeboard to be lowered and transfer the previously unaccessible low-head water to a higher head. This increases the usable wave resource in many locations because oftentimes wave activity is low. This proposed novel overtopping device concept which is more appropriate for many locations in California will be analyzed in chapter 5 and conclusions and future work are given in chapter 6.

This page intentionally left blank.

Chapter 2

California's Wave Resource

2.1 Origin of Ocean Waves

The energy in ocean waves can be thought of as a secondary form of solar energy. Sun-rays heat up the Earth's surface in an uneven fashion which creates wind which in turn can generate waves. On the global scale the Equator heats up more than the North and South poles do. The temperature gradient between the Equator and the poles establishes global circulation patterns. Generally speaking the air at the Equator would rise up into the atmosphere due to natural convection and cooler air from the poles would flow towards the Equator along the surface. In this way, simplified three-dimensional circulation patterns would form in both hemispheres. However, Earth's rotation, its axial tilt of 23.5° and its distribution of land masses complicate the circulation patterns. These features additionally serve to produce the high and low pressure systems which are responsible for the wind generated waves as well as the seasonal variations in global wave production ([2], [5]).

When the conditions are right, depressions or storms form and generate the waves desirable for wave energy extraction. A depression is simply a cell of air at lower pressure than its surroundings. The pressure gradient between the low pressure cell

and the surrounding space causes air to move quickly towards the cell. In combination with the Coriolis force due to Earth's rotation, fast moving air creates a spiral pattern. In the Northern Hemisphere these spirals are counter-clockwise. The drag of the fast moving air over the ocean causes the generation of waves. The deeper the depression, the faster the air moves. Depending on its severity and which hemisphere it is in, the depression may possibly be categorized as a cyclone or a hurricane.

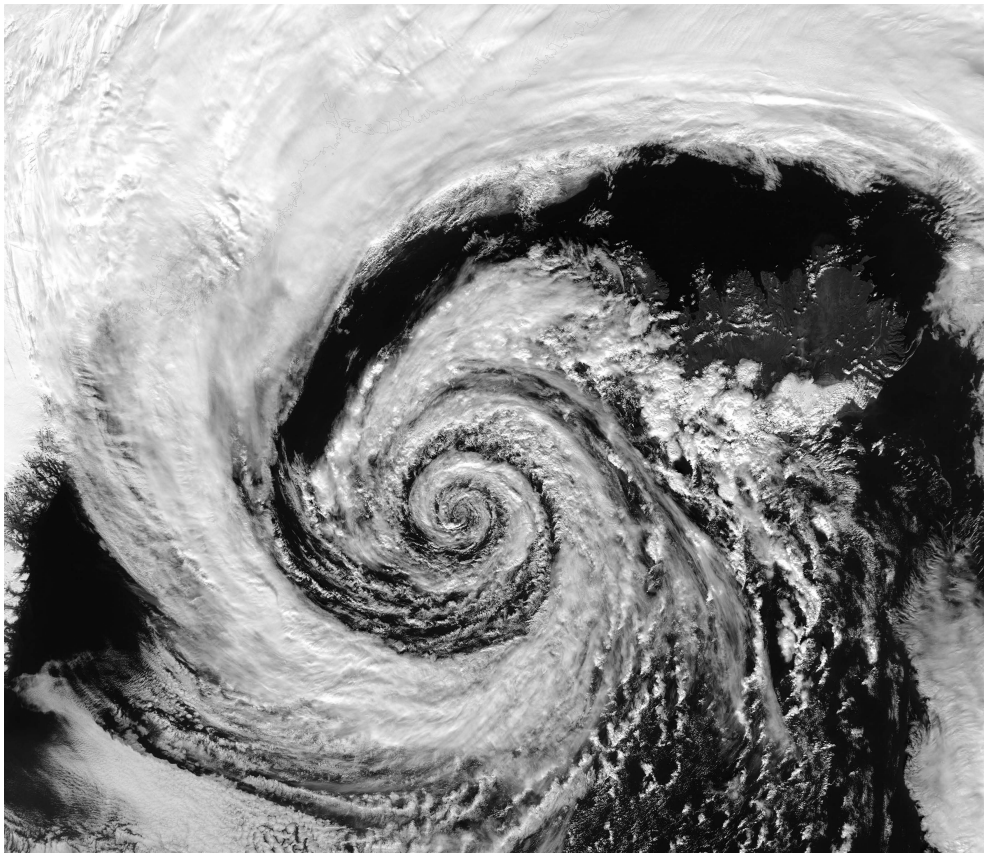

Figure 2.1: Low pressure in the Northern Hemisphere.

The basic mechanisms of wind waves generation are generally agreed upon. These mechanisms are Phillips' resonance theory and Miles' shear flow theory by oceanographers O.M. Phillips and J.W. Miles [39]. The first mechanism begins creating small waves by blowing wind over a flat sea. This creates capillary waves as little random disturbances of the wind push down on the sea. The wind continues to interact with

the small up-and-down motions of the water surface by adding more motion and energy and once these initial excitations have grown linearly the second mechanism takes over. At this stage the water surface is ruffled and the wind forms turbulent eddies in the troughs of the small waves. The eddies grow the waves by increasing pressure in the trough and decreasing pressure at the crest. As the eddies grow they are feed more energy by the wind. Through this coupling and feedback the waves grow exponentially into gravity waves. This process continues until a limiting factor is reached as depicted in Figure (2.2).

When the waves grow to a certain height a balance is reached between the generating force of the wind and the restoring force of gravity. Whitecapping also occurs to dissipate energy when wave become to big or steep and the wind blows the top off them. Two other limits on wave growth are due to generation time and distance. Duration-limited seas are those for which the wind stops blowing before the waves can grow to their maximum size. Fetch-limited seas are those for which the area (or fetch) over which the wind is blowing is restricted. In this case the waves move out of that area before growing to maximum size.

Within the wave generating area corresponding to the location of the depression, the sea contains a wide range of waves of different size, shape, length, and direction. Once the waves leave the generation area they propagate away as free-traveling swell. As the waves move away they decrease in size while spreading out over a progressively wider area. This is called circumferential dispersion if we view the generation area as a point source. The swell also disperses in the radial direction because the speed of a wave depends on its wavelength. (See Appendix A). Therefore as waves propagate away those with longer wavelengths go faster. As time progresses the swell will 'stretch out'. Additionally, waves lose very little energy as they propagate. Unless they encounter obstacles or head winds they can travel thousands of miles over several days. Thus far away from the storms from which they originated the swell can arrive

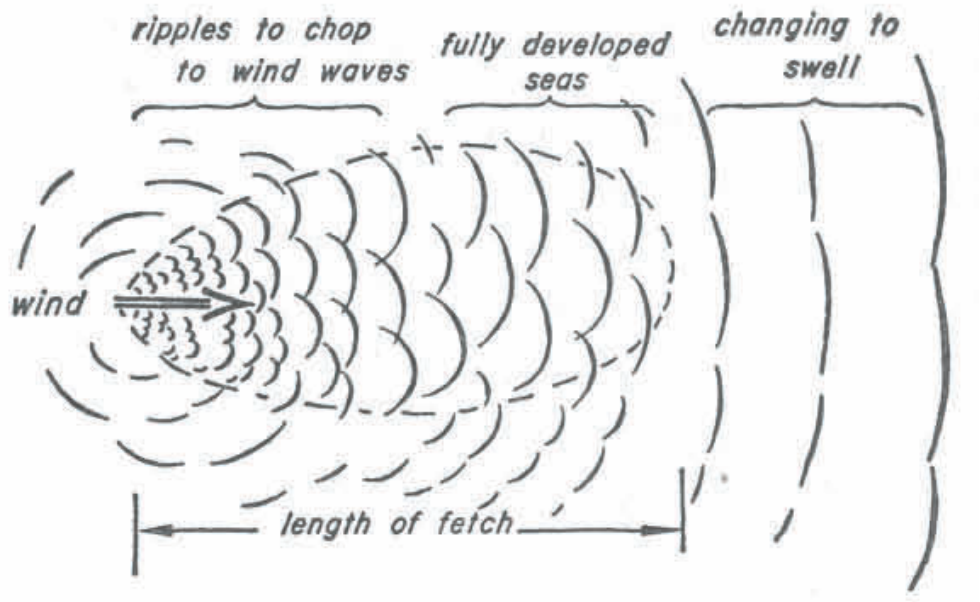

Figure 2.2: Wind wave generation/growth (from [2]).

as wave after wave of consistent, high power density energy.

Wave activity varies throughout the year because of Earth's axial tilt and land distribution. Earth's tilt causes the temperature to vary considerably between the summer and winter at the poles whereas throughout the year the temperature at the Equator is relatively constant. During the winter months the North Pole is tilted away from the sun resulting in less heating while the opposite occurs during the summer months. Therefore there is a much greater temperature gradient providing energy for storms during the winter months. Another factor in the seasonal variation is the difference in heat capacity between water and land. Water has a greater heat capacity than land so while the temperature of the continents varies in the tens of degrees from summer to winter the ocean stays at a relatively constant temperature throughout the year. Hence during the summer months low pressure tends to exist over land as the warm air over land rises and high pressure exists over the ocean. During the winter the sea can be warmer than the land and the low pressure moves offshore. For

these reasons winter is the season when most swell producing depressions occur and thus the season when wave activity is the greatest for California.

2.2 Stochastic View of Ocean Waves

Ocean waves of course do not have regular and precise properties of wave height and period. For mathematical analysis it is extremely convenient to make such assumptions, however typical sea surfaces look like that shown in Figure (2.3a). Clearly the sea is a mix of many waves of different heights, lengths, and directions. Even when high energy swells appear as large, periodic, consistent waveforms the 'old seas' generated from different winds can ride on top of these swells. Therefore this situation requires a statistical approach to describe the properties of waves.

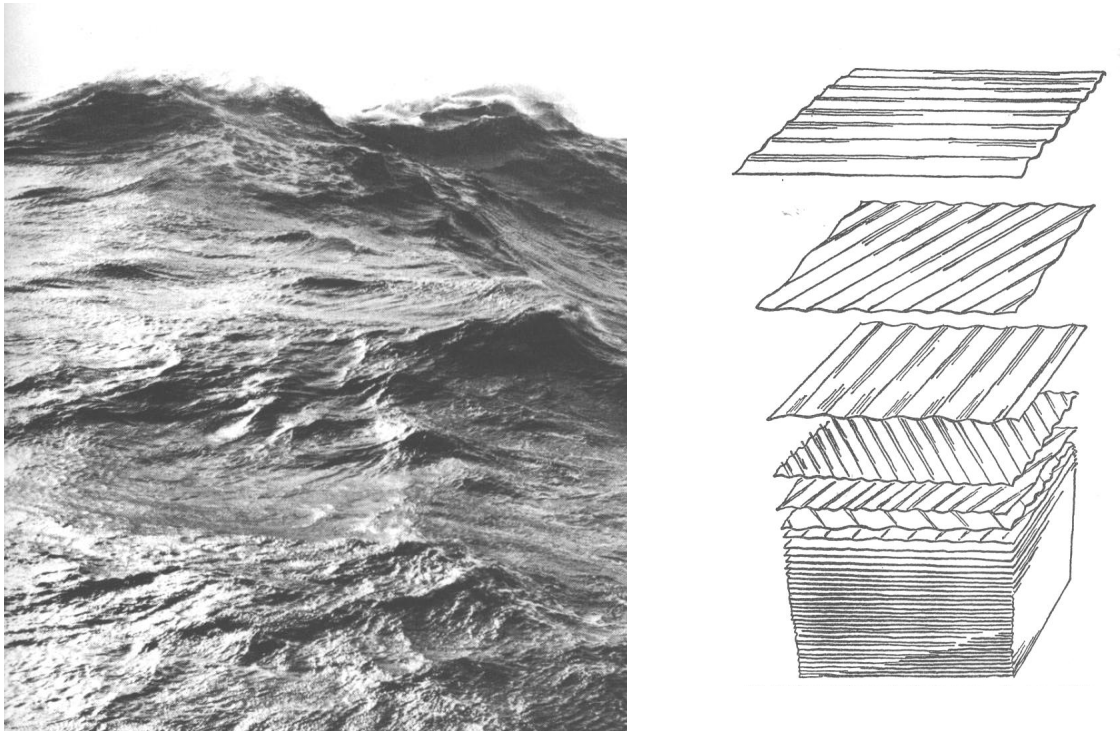

Figure 2.3: a). Typical sea surface (from [2]). b). Superposition (from [2]).

Typical wave records such as Figure (2.4) give the vertical position time history at a point on the sea surface. These records need to be represented statistically in a useful way to adequately characterize the energy in the waves. We will assume that these recordings are stationary, ergodic processes thereby allowing for meaningful values to be obtained from single wave records.

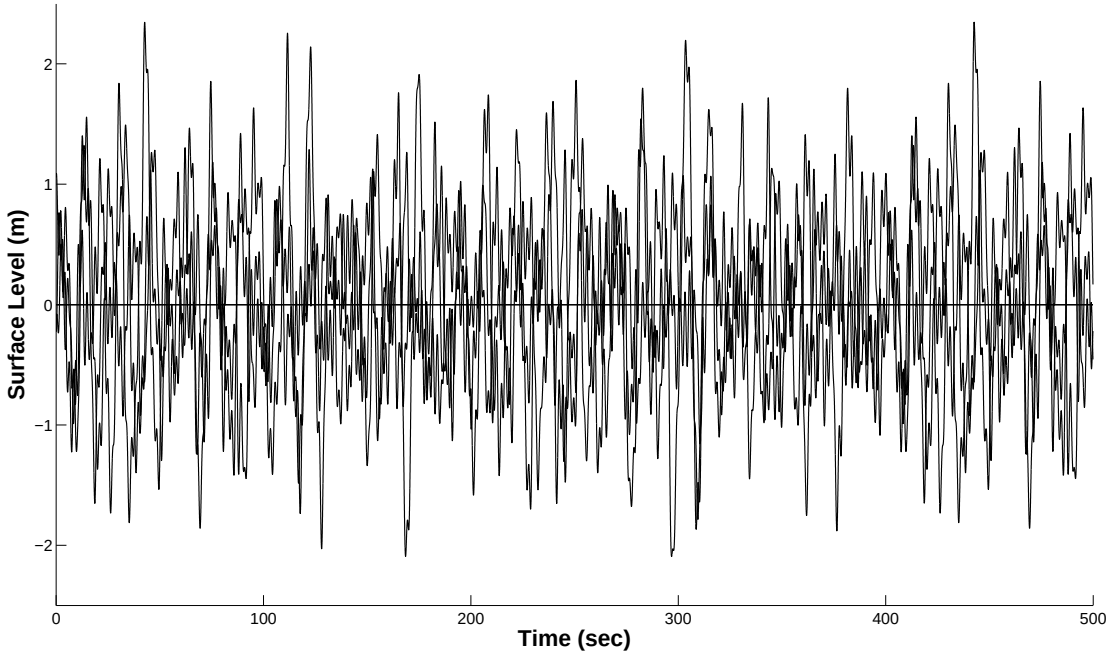

Figure 2.4: Typical time history at a point on the sea surface.

As shown in Figure (2.3b) the sea surface elevation ζ can be thought of as a superposition of many different sine waves of varying height and period (or frequency).

$$\zeta(t) = \sum_n A_n sin(\omega_n t + \phi_n) \tag{2.1}$$

The varience E, which is the mean square of ζ can be computed as

$$E = \overline{\zeta^2(t)} = \sum_n \tfrac{1}{2} A_n^2 \tag{2.2}$$

where after taking the long-term average, all the oscillatory terms go to zero leaving only the steady component. Thus the varience of the sea surface elevation equals the sum of the variences of its component wave trains and is therefore proportional to the energy of the wave system.

An important way of representing a wave system is by means of the spectral density function, $S(f)$. Also known as the 'omnidirectional spectral density function' or 'point spectrum' it has units of m^2/Hz. The spectral density function is a representation of the varience as a continuous function of frequency. By filtering the sea elevation signal (equation 2.1) around a small frequency range around f to get a corresponding ΔE, the spectral density function $S(f)$ can be defined as $S(f) = \Delta E/\Delta f$ where $S(f)$ remains finite as $\Delta f \to 0$. Thus it can be seen that

$$\int_0^\infty S(f)df = E = \sum_n \tfrac{1}{2} A_n^2 \tag{2.3}$$

Many useful definitions and statistics are expressed in terms of the moments of the spectral density [42]. The n^{th} spectral moment is defined as

$$m_n = \int_0^\infty f^n S(f)df \tag{2.4}$$

The varience of the wave system is $m_0 = \int_0^\infty S(f)df$. The significant wave height is commonly defined as:

$$H_{m0} = 4\sqrt{m_0} \tag{2.5}$$

The "energy period", sometimes called the spectral period is defined as:

$$T_e = m_{-1}/m_0 \tag{2.6}$$

In practice, the spectral density function can be measured from a wave record

through a process of filtering around a central frequency f_0 with bandwidth Δf, squaring the filtered signal, and time averaging the new signal. This must be done for large numbers of frequencies to get the spectrum. An alternative method involves using the Wiener-Khintchine relations to obtain the spectral density function from the autocorrelation of the wave record. Figure (2.5) shows the spectral density function for the wave record in figure (2.4).

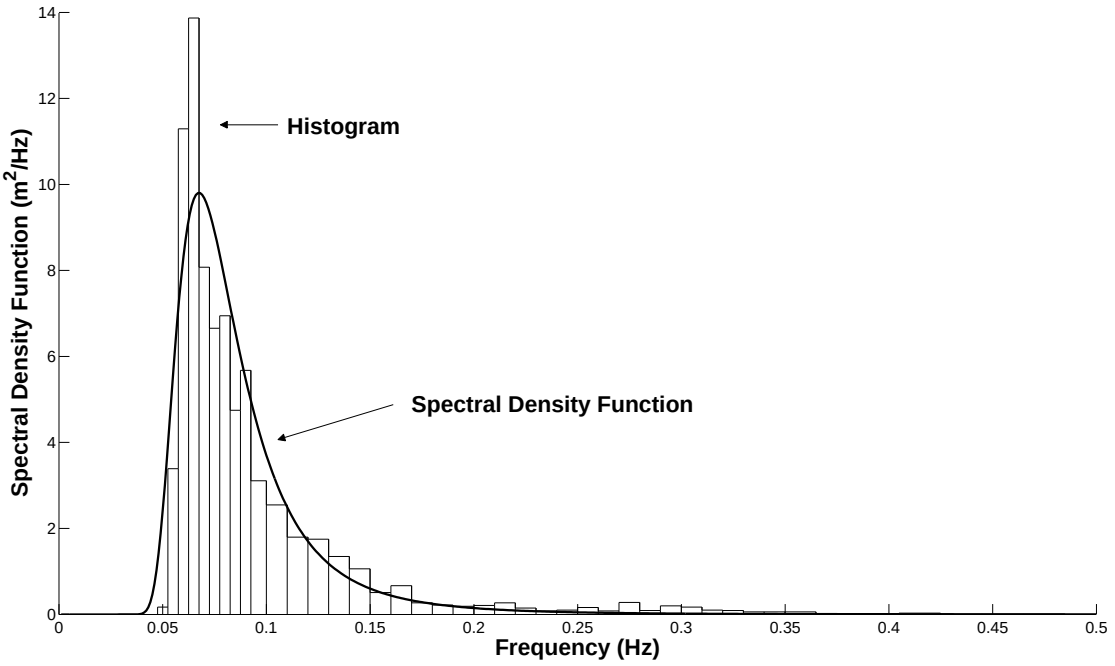

Figure 2.5: Histogram and spectral density function of the wave record in Figure 2.4.

2.2.1 Traditional Wave Energy Formulation

For simple, regular, gravity waves in deep water the power per unit length of wave crest (or energy flux) is:

$$P = (\tfrac{1}{2}\rho g A^2) * \left(\frac{d\omega}{dk}\right) \tag{2.7}$$

The first term is the energy density and the second term is the group velocity of the wave. A is the wave amplitude, g is gravitational acceleration, ρ is water density, k is wavenumber, ω is angular frequency, and T is wave period. Using the dispersion relationship:

$$\omega^2 = gk \tag{2.8}$$

and knowing that wave height, $H = 2A$, the equation for the power per unit length can be given as a function of wave period and wave height:

$$P = \frac{\rho g^2 T H^2}{32\pi} \tag{2.9}$$

For a wave system, using the concept of superposition the power is given as:

$$P = \rho g \int c_g(f) S(f) df \tag{2.10}$$

where $c_g(f)$ is the group velocity as a function of frequency.

We can obtain a more convenient expression for power by using the expression for group velocity in deepwater $c_g = g/4\pi f$.

$$P = \frac{\rho g^2}{4\pi} \int f^{-1} S(f) df = (\rho g^2/4\pi) m_{-1} \tag{2.11}$$

Utilizing the expressions for energy period and significant wave height we can write power as:

$$P = \left(\frac{\rho g^2}{64\pi}\right) \cdot T_e \cdot H_{m0}^2 \tag{2.12}$$

In general significant wave height and average period are available for one hour length wave records from wave buoys. T_e is taken to be the average period which is the average of the zero up-crossing wave periods of a wave record. In practice average and energy period are very close. Estimates to determine the wave energy resource

available typically average these parameters over a long time series. Stochastically this is written as

$$E(P) = \left(\frac{\rho g^2}{64\pi}\right) \cdot E(T_e) \cdot E(H_{m0}^2) \tag{2.13}$$

where $E(\cdot)$ is the expectation operation. In the above analysis an implied assumption was T_e is independent from H_{m0}. Appendix B provides the analysis accounting for the cross stochastic properties between energy period and significant wave height which provides higher estimates of wave energy.

2.3 Wave Energy Estimates

The stochastic view of ocean waves provides a method to estimate the wave energy potential at a given location. To utilize this method we need to obtain wave record data from the field. This section describes how the data is obtained for the estimates and shows how California's wave energy potential compares to other locations around the world.

2.3.1 Data Sources

Wave measurement techniques have advanced greatly over the past thirty years as a result of significant advances in technology. *In situ* instruments now have greater resolution and are more reliable. These advancements produce accurate data valuable for ship and port operations and engineering projects as well as for calibration and validation of global wave and ocean process models. Recently, remote sensing instruments such as land, aircraft, and orbiting satellites are showing promise for wave measurements at far greater number of locations [47].

Currently, surface following wave buoys provide the bulk of data used for wave energy estimates. An example of a typical wave buoy is shown in Figure (2.6). These

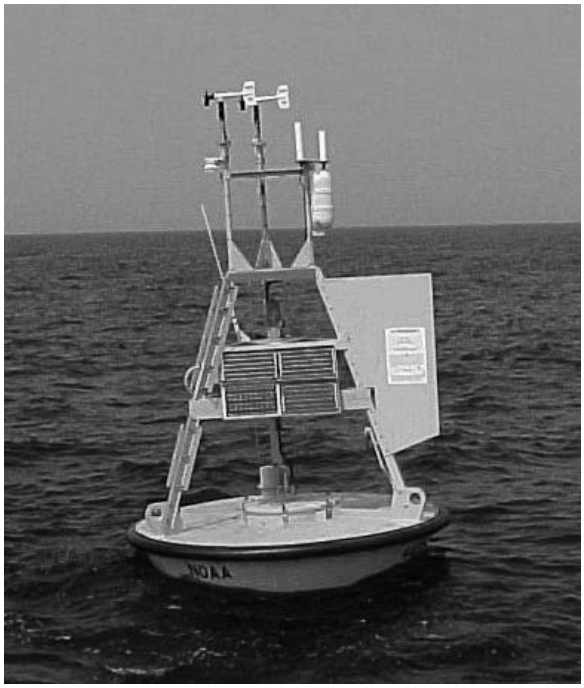

Figure 2.6: Typical wavebuoy.

are the type of instruments used by the two main providers of free, readily available wave data in the United States. Through their wave buoy network covering the West coast, Gulf of Mexico, East coast, and Hawaii both the National Oceanic and Atmospheric Administration (NOAA) National Data Buoy Center (NDBC) and the Coastal Data Information Program (CDIP) provide current and archived ocean related data accessible via the internet. These sites provide hourly records of spectral density as well as significant wave height and average wave period amongst many other types of information such as salinity, temperature, wind speed, etc. Their buoys measure heave acceleration or vertical displacement and after factoring in the buoy's own disturbance, the time history of surface elevation is known. A fast Fourier Transform of the time history is performed and transmitted to shore. This spectral information is saved and analyzed to determine the significant wave height and average period.

2.3.2 Global Overview

It has been estimated that the total wave resource available in all the oceans is approximately 2 Terawatts. This is the same order of magnitude to the worldwide consumption of electricity [8]. The exploitable limit is approximated at 10-25%. Therefore wave energy has the potential to contribute significantly to the energy mix. Additionally, ocean wave energy is one of the most concentrated (relative to solar or wind energy) and widely available forms of renewable energy in coastal areas. These characteristics combined with the fact that 37% of the worlds population lives within 60 miles of a coastline establishes a good match between resource and demand [35].

Several studies to map the worldwide wave energy potential have been performed. These studies used the *in-situ* and satellite instrument and wind-wave model data sources described above as well as visual observations in remote areas for their assessments. Figure (2.7) shows the global variation of yearly-averaged wave energy potential resulting from such a study [1]. The two shaded bands represent latitudes where wave activity is greatest. They correspond to latitudes between $40-70°$, those

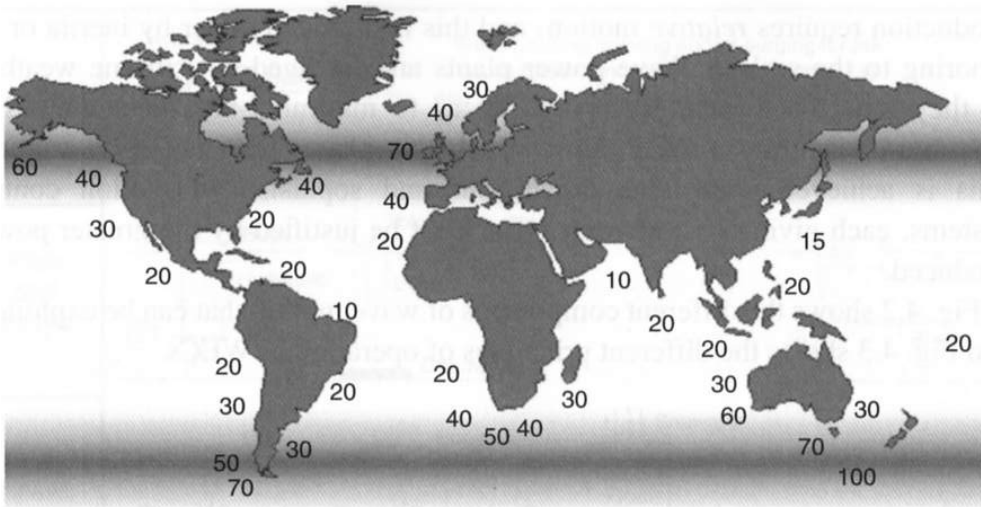

Figure 2.7: Shading shows latitudes of very high wave energy (kW/m of crest length).

favorable to formation of low pressure systems. In the Southern hemisphere this band is known as the "Roaring 40's". Its interesting to note that the highest average levels of wave energy are on the lee side of these ocean zones due to the origins of oceanic winds.

In general the Southern hemisphere has more wave energy potential. Additionally it experiences a smaller season variation. This has to do with the lack of land masses to complicate the circulation patterns. In latitudes such as the Roaring 40's there are very few obstructions to formation of depressions and wind wave generation. Therefore locations in South Africa, south and southwest Australia, and southern Chile have tremendous (50-100 kW/m), relatively consistent wave activity. On the contrary, in the Northern hemisphere the seasonal variation is sharper. Nevertheless the west coast of the UK, Iceland, and Greenland as well as the northwestern United States have high levels of wave energy as well.

2.3.3 California Estimate

California has a very long coast and the wave energy potential varies considerably by location. Northern California has an excellent wave climate, with wave power densities in suitable locations between 15 kW/m and 40 kW/m. In southern California, south of Point Conception, the wave energy drops of considerably. This is due to the obstruction of the Channel Islands and the change of direction in the coastline. Very far off the coast (hundreds of miles) the wave energy is pretty uniform throughout the coast. Nevertheless it is approximated that 37,000 MW of energy dissipates on California's 1,200 km of coastline. If a conversion rate of 20% is possible, this is enough to meet 23% of California's electricity needs. In general, California features a high energy wave climate and a fast dropping ocean floor, resulting in deep water close to shore and an excellent wave power resource that is located close to shore and

major coastal population centers [35].

2.4 Statistical Analysis of locations in California

In this section we will explore the wave energy potential at various locations off the California coast. Our analysis applies the stochastic wave energy formulation of Appendix B. As depicted in Figure (2.8) eight NOAA buoy locations were chosen.

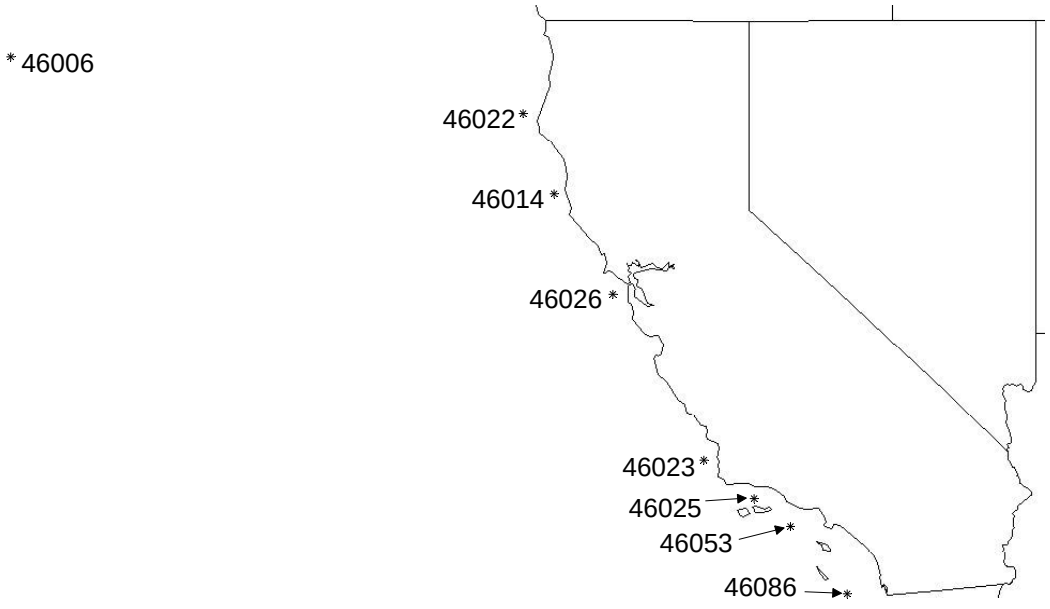

Figure 2.8: Location of the eight NOAA buoys.

Buoy 46006 is 600 nautical miles west of Eureka, CA. Buoy 46014 is 19 nautical miles northwest of Point Arena, CA. Buoy 46022 is 17 nautical miles west-southwest of Eureka, CA. Buoy 46026 is 18 nautical miles west of San Francisco, CA. Buoy 46023 is 17 nautical miles northwest of Pt. Arguello, CA. Buoy 46053 is 12 nautical miles southwest of Santa Barbara, CA. Buoy 46025 is 33 nautical miles west-southwest of Santa Monica, CA. Buoy 46086 is in the San Clemente Basin, CA.

Figure (2.9) is representative of the data used. In some years only incomplete

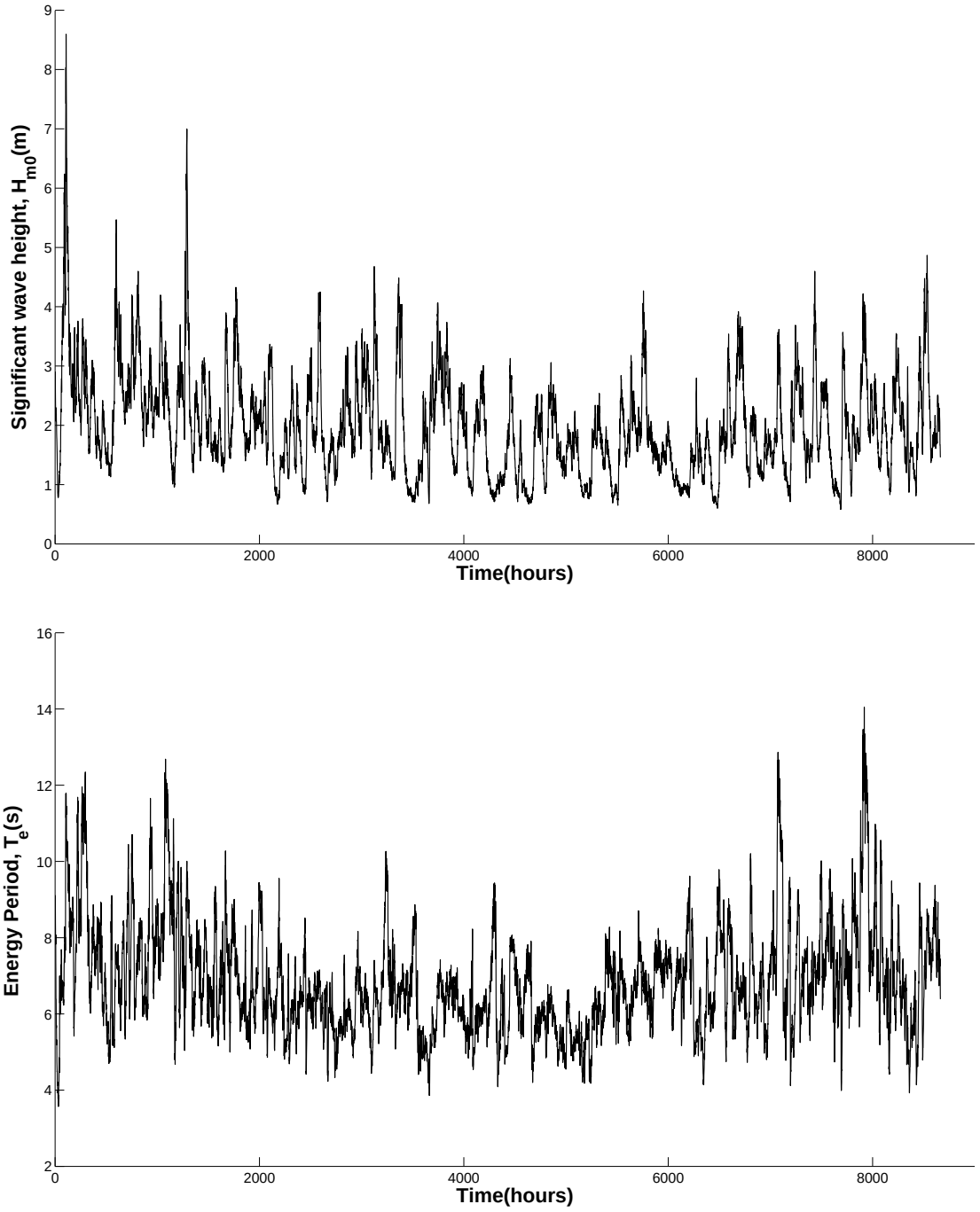

Figure 2.9: San Francisco (46026) station significant wave height and energy period variation for year 2008.

data was available, however generally a complete data set was used. All the buoys may be considered to be in deep water. The shallowest depth a buoy is operating in is 52 m. These buoys are the surface following type as described above. The wave data we consider here was obtained from the NDBC (National Data Buoy Center) website [33]. Data from the past ten years were analyzed.

Table 2.1 shows the statistical properties of this data averaged over the past ten years. Figure (2.10) shows yearly annual average wave power. Those years that are missing markers indicate years of incomplete data. The trend indicated by these results is that wave energy increases as you travel north along the California coast which is expected from standard weather patterns.

Figure (2.11) shows that the winter months clearly have greater wave activity. This is expected as California experiences typical seasonal wave patterns expected in the Northern hemisphere. Table (2.2) show how great the range in significant wave heights can be within a month. The maximum significant wave heights are 3-4 times greater than that of the average in most months including the summer months.

Table 2.1: Station statistics averaged over the past 10 years.

Buoy	Station name	Northing (°)	Westing (°)	10 year Averages		
				$T_e(s)$	$H_{m0}(m)$	$P(kW/m)$
46006	SE PAPA	40.89	137.45	7.12	2.90	43.29
46022	Eel River	40.75	124.58	7.42	2.42	30.09
46014	Pt. Arena	39.20	123.97	7.35	2.43	27.56
46026	San Francisco	37.76	122.83	7.03	1.95	16.68
46023	Pt. Arguello	34.71	120.97	7.74	2.18	22.83
46053	Santa Barbara	34.25	119.84	6.21	1.29	6.52
46025	Santa Monica	33.74	119.06	6.18	1.16	4.87
46086	San Clemente	32.50	118.00	7.06	1.55	9.81

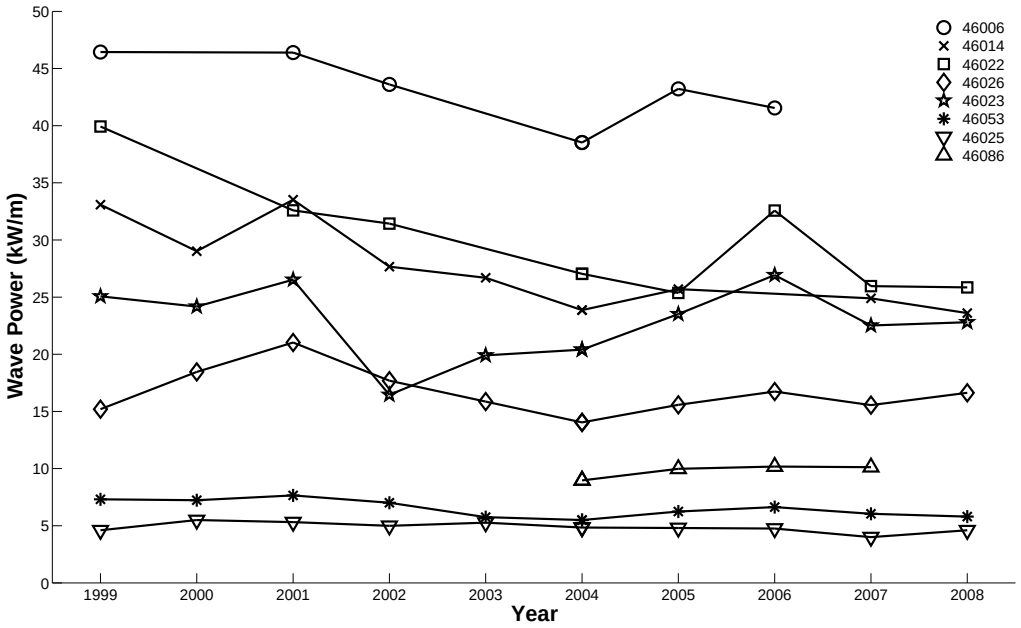

Figure 2.10: Yearly power.

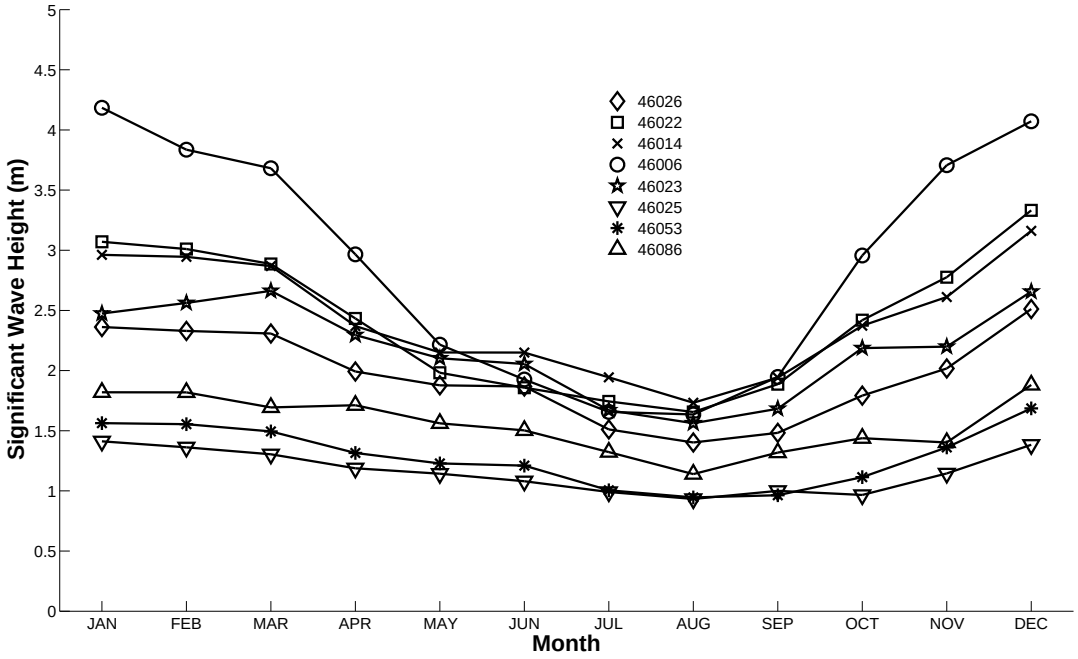

Figure 2.11: Variation by month.

Table 2.2: Maximum, minimum, and average significant wave height in meters per month over the past 10 years at each buoy.

	46086			46025			46053			46023		
	Max	Min	Avg	Max	Min	Avg	Max	Min	Avg	Max	Min	Avg
Jan	5.26	0.47	1.82	3.88	0.38	1.41	4.55	0.26	1.56	7.66	0.49	2.47
Feb	4.99	0.52	1.82	5.38	0.18	1.36	5.37	0.24	1.55	7.42	0.83	2.56
Mar	4.27	0.61	1.69	3.38	0.49	1.30	3.72	0.36	1.49	6.14	0.50	2.66
Apr	4.56	0.68	1.71	3.69	0.38	1.19	3.28	0.28	1.31	6.58	0.65	2.30
May	3.52	0.71	1.56	3.27	0.45	1.14	2.92	0.34	1.23	6.02	0.71	2.10
Jun	2.79	0.70	1.50	2.48	0.47	1.08	2.75	0.30	1.21	4.68	0.64	2.06
Jul	2.21	0.74	1.32	1.83	0.48	0.99	2.20	0.34	1.01	3.30	0.66	1.67
Aug	1.87	0.56	1.14	1.70	0.41	0.93	1.97	0.32	0.95	3.64	0.68	1.56
Sep	2.88	0.71	1.32	2.45	0.50	1.00	2.52	0.30	0.96	4.43	0.73	1.68
Oct	3.19	0.58	1.44	2.75	0.43	0.97	3.15	0.34	1.11	7.45	0.76	2.19
Nov	4.06	0.73	1.40	3.80	0.38	1.15	3.85	0.35	1.36	6.33	0.80	2.20
Dec	5.76	0.67	1.88	4.30	0.42	1.38	5.49	0.42	1.69	7.10	0.79	2.26

	46026			46022			46014			46006		
	Max	Min	Avg	Max	Min	Avg	Max	Min	Avg	Max	Min	Avg
Jan	8.60	0.72	2.36	10.79	0.70	3.07	9.32	0.63	2.96	15.47	1.16	4.18
Feb	7.00	0.67	2.33	8.73	1.07	3.01	7.59	0.75	2.95	12.83	1.09	3.84
Mar	5.93	0.57	2.31	8.77	0.60	2.89	7.53	0.63	2.87	10.23	1.32	3.68
Apr	5.85	0.67	1.99	7.72	0.59	2.43	7.69	0.66	2.37	8.18	0.90	2.97
May	5.36	0.64	1.88	6.34	0.54	1.98	6.15	0.59	2.15	6.87	0.78	2.22
Jun	4.99	0.58	1.87	6.05	0.58	1.86	5.07	0.42	2.15	7.23	0.64	1.93
Jul	4.15	0.58	1.51	4.70	0.51	1.74	4.54	0.57	1.94	3.63	0.77	1.66
Aug	4.27	0.39	1.40	4.39	0.44	1.66	4.40	0.52	1.73	5.65	0.62	1.64
Sep	3.88	0.42	1.48	4.95	0.57	1.89	4.59	0.55	1.94	5.15	0.75	1.95
Oct	6.80	0.54	1.79	10.67	0.67	2.42	9.06	0.72	2.37	16.3	0.81	2.96
Nov	7.26	0.58	2.02	9.72	0.57	2.78	8.72	0.74	2.61	14.23	1.21	3.71
Dec	7.95	0.56	2.51	9.41	0.76	3.33	9.74	0.80	3.16	12.49	1.22	4.07

2.5 Propagation to Nearshore and Determining Site Location

The above buoy data provides accurate wave information for specific locations far offshore in deep water. However, wave conditions will evolve as the waves propagate closer to shore. For nearshore and shoreline devices more accurate wave information is required. Wave models can provide this information by simulating the evolution of offshore wave fields as they propagate towards the shore.

Currently, third generation wave models are the state of the art for wave climate modeling. Third generation refers to the level of development of the radiative transfer equation also known as the action balance equation. This is the fundamental equation used in modern wave prediction models. Massive weather prediction models such as the Wave Analysis Model (WAM) and NOAA's WAVEWATCH III model solve this equation on a global scale using tremendous computational resources. Wave climate forecasts are based on these models.

The Simulating Waves Nearshore (SWAN) model is also a third-generation wave model for obtaining realistic estimates of wave parameters in coastal areas, and inland waters from given wind, sea bottom, and current conditions. It differs from the WAM and WAVEWATCH III model in this regard because nearshore wave propagation undergo different processes than offshore deepwater propagation. SWAN has been developed by Delft University of Technology and is distributed freely under the terms of the GNU General Public License [40].

The applications of SWAN are numerous. It can be used for nearshore wave modeling for harbor and offshore installation design, coastal development and management, and wave hindcasting. Recently, researchers have used it for estimating wave energy potential nearshore and exploring optimal locations for wave farms ([15],[20]). Figure

(2.12) shows an example of the necessary bathymetry information required as input for SWAN. Once the bathymetry information along with additional input data such as

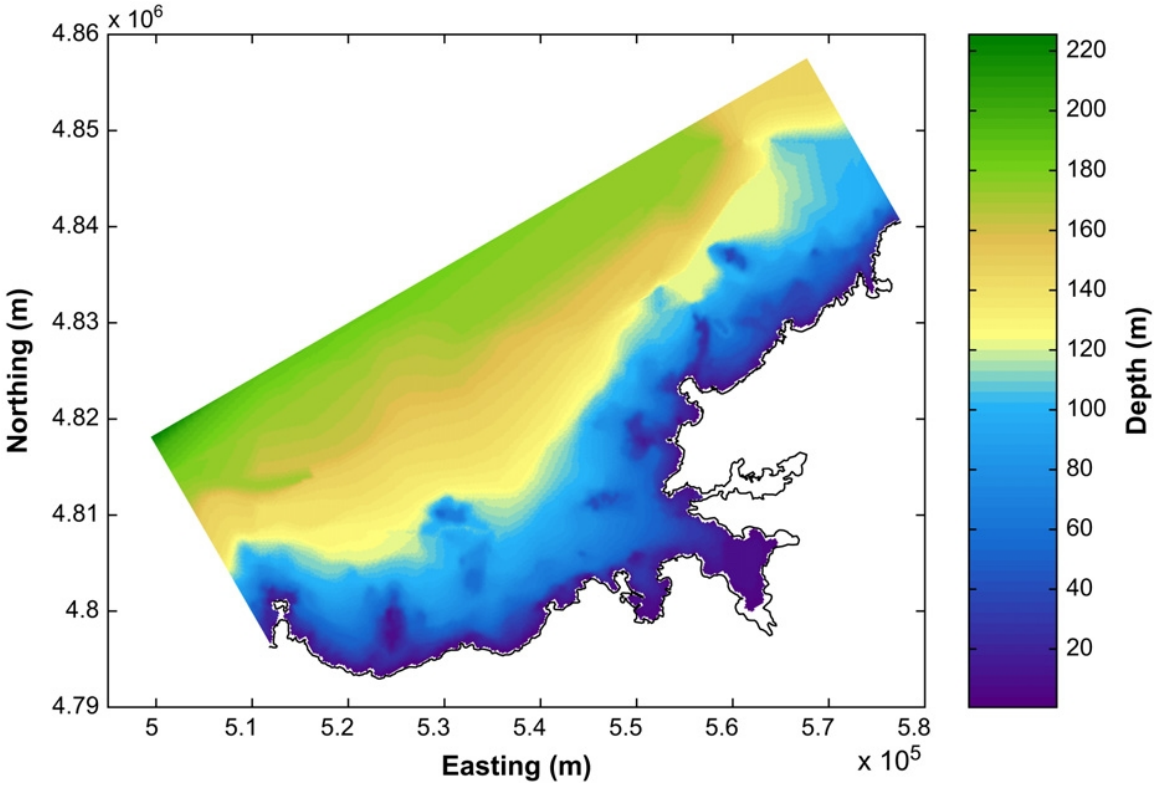

Figure 2.12: Bathymetry input to the SWAN example.

current and wind conditions, and wave climate boundary conditions are entered into the model, SWAN will numerically compute the evolution of waves as the propagate to the coast. SWAN can account for the coastal processes of shoaling, refraction, diffraction, whitecapping, and bottom friction. Figure (2.13) shows one important output of feature of SWAN which is the computation of significant wave height. This is a necessary parameter for the overtopping formulas to be described in chapter 3.

Figures (2.12) and (2.13) are results of work done by Iglesias et.al. to explore the wave energy potential in the region of Galicia in northwest Spain. An interesting result of this work was that for a limited set of offshore wave conditions the wave power can vary remarkably as it propagates to nearshore locations. It was found that

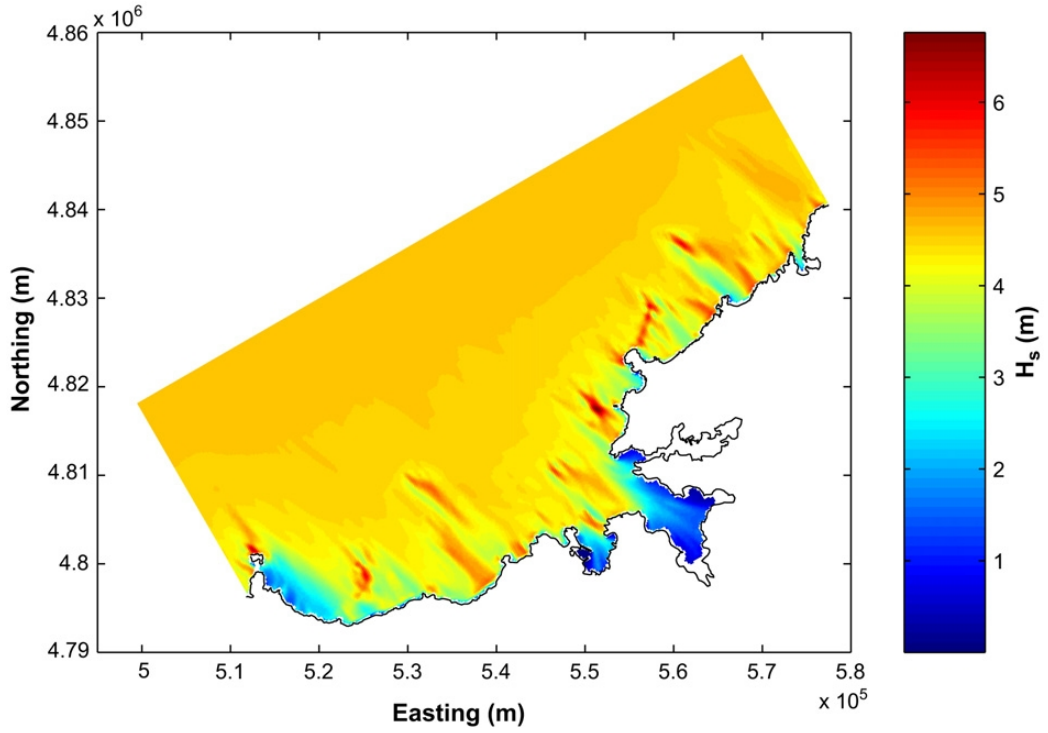

Figure 2.13: Output significant wave height from SWAN.

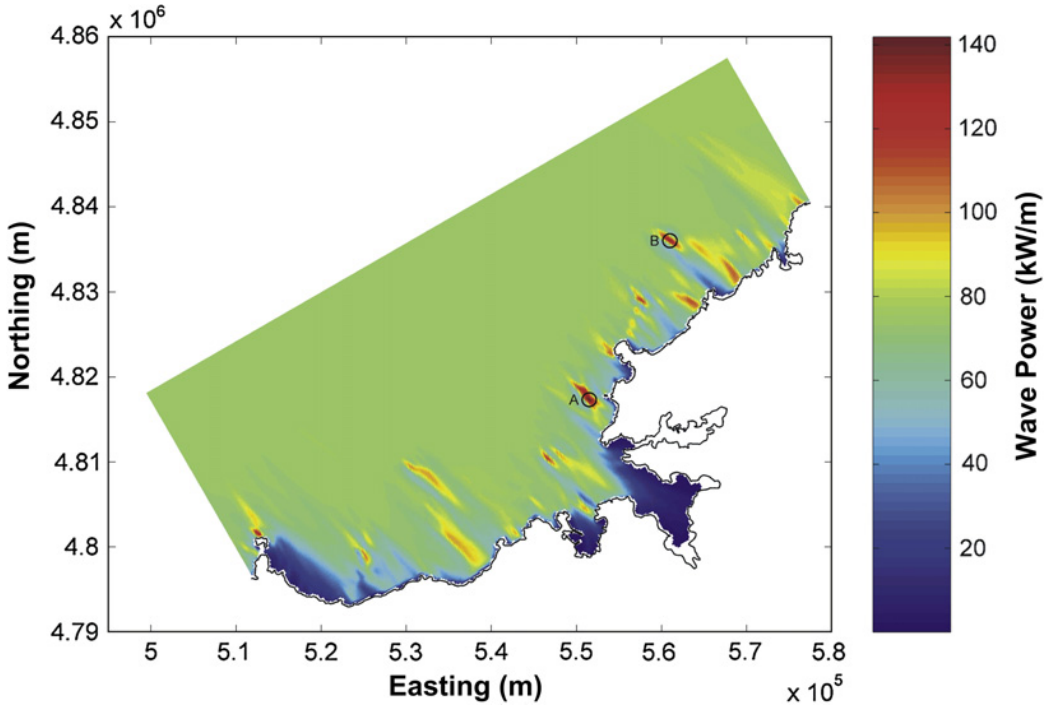

Figure 2.14: Output wave power from SWAN.

in most of the area the average wave power was 70 kW/m however in two specific spots the average wave power rose to 135 kW/m and fell to below 40 kW/m in other spots. Figure (2.14) illustrates this range where A and B refer to the high power spots. It may be concluded that the nearshore processes of shoaling, refraction, bottom friction, and in some cases sheltering by the shoreline can modify the wave power considerably in Galicia . The same is presumably true for the California coast. Hence careful analysis of the nearshore processes should be performed before deciding on a wave energy location. Similar work will need to be done for the California coast to identify promising high power locations. The effort will be quite extensive due to the length of the coastline and variability in bathymetry as shown in Figure (2.15). Localized bathymetry images are given for individual buoys in Figure (2.16) for all buoys except 46006 which is too far offshore.

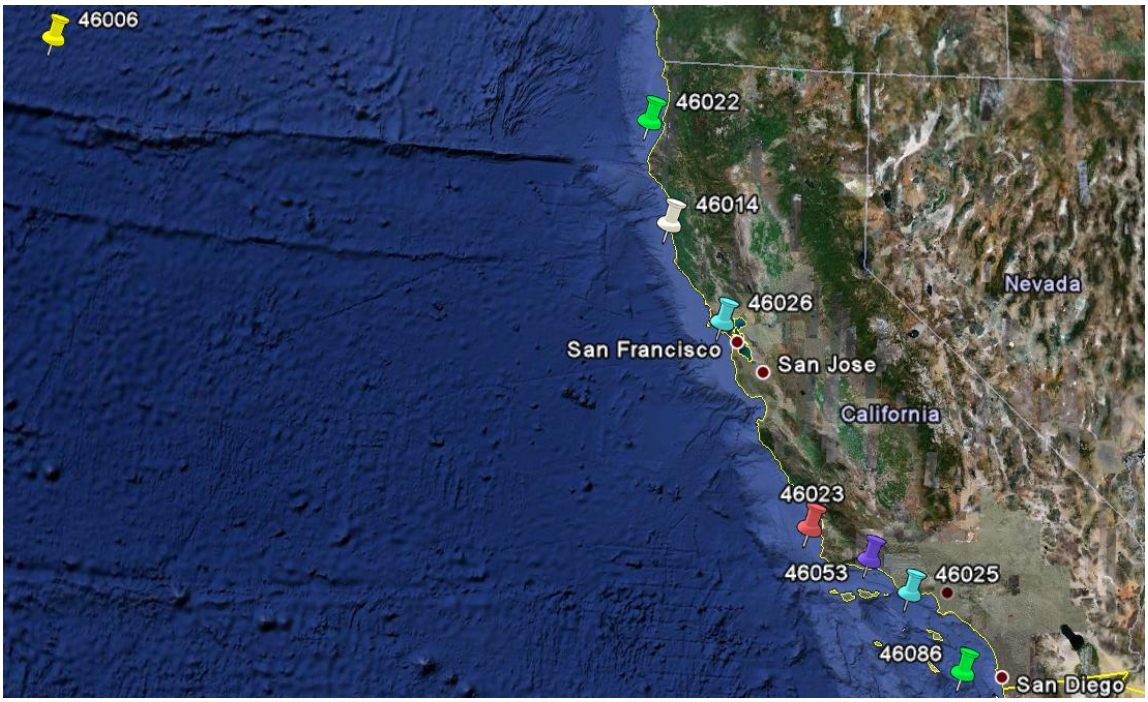

Figure 2.15: Bathymetry off the coast of California.

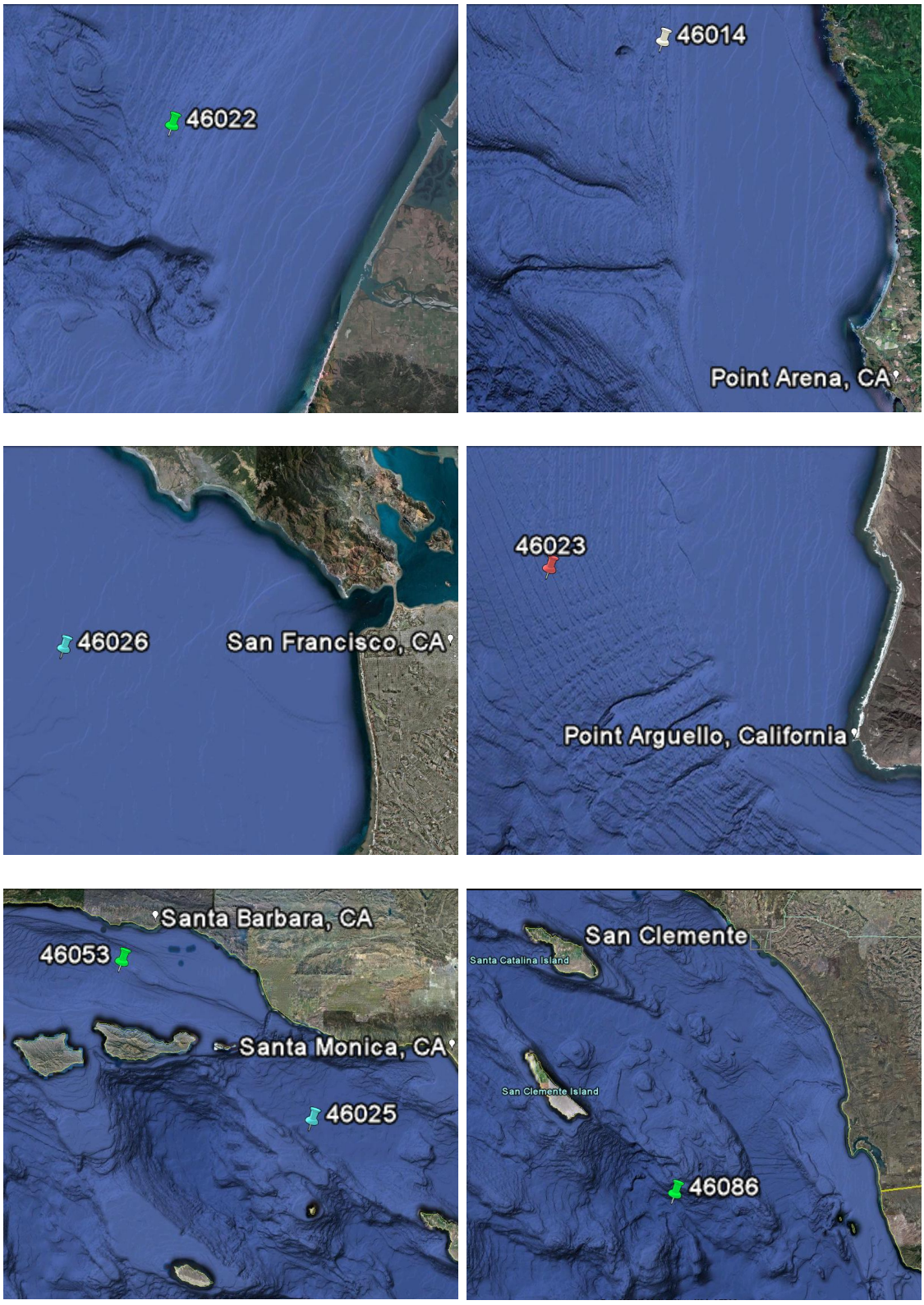

Figure 2.16: Local bathymetry for the various buoys.

2.6 Extreme Wave Analysis

As illustrated in the above sections the significant wave heights off the California coast can become very high. This brings up the issue of survivability for devices operating is such environments. This section will describe the analysis used in chapter 5 to determine the most probable extreme value significant wave heights for given numbers of years. Knowledge of these most probable extreme values provides criteria and insight for design in these environments.

The estimates of most probable extreme value significant wave heights will be determined through extreme value analysis of the prior ten years of data at each location. This analysis [25] will done using order statistics. We begin with our dataset of n points $(X_1, X_2, ..., X_n)$. We order these data points as follows:

$$\begin{aligned} Y_1 &= \min(X_1, X_2, ..., X_n) \\ Y_2 &= \text{second smallest}(X_1, X_2, ..., X_n) \\ &\vdots \\ Y_n &= \max(X_1, X_2, ..., X_n) \end{aligned}$$

We are interested in the largest significant wave height Y_n. Now consider the event $Y_n \leq y$.

$$[Y_n \leq y] \equiv [X_1 \leq y \cap X_2 \leq y \cap \ldots \cap X_n \leq y] \tag{2.14}$$

Then the cumulative distribution function of Y_n, $\Phi_{Y_n}(y)$ is given as:

$$\Phi_{Y_n}(y) = P[Y_n \leq y] = P[X_1 \leq y \cap X_2 \leq y \cap \ldots \cap X_n \leq y] \tag{2.15}$$

where $P[\cdot]$ is the probability. We will assume $(X_1, X_2, ..., X_n)$ are independent such

that

$$\begin{aligned}\Phi_{Y_n}(y) = P[Y_n \leq y] &= P[X_1 \leq y] \cdot P[X_2 \leq y] \cdot \ldots \cdot P[X_n \leq y] \\ &= \prod_{i=1}^{n} P[x_i \leq y]\end{aligned} \tag{2.16}$$

Now assuming $(X_1, X_2, ..., X_n)$ are identically distributed we have the cumulative distribution function of the extreme value Y_n.

$$\Phi_{Y_n}(y) = [F_X(y)]^n \tag{2.17}$$

where $F_X(\cdot)$ is the cumulative distribution function of any X_i. The corresponding probability distribution function for Y_n is

$$\phi_{Y_n}(y) = \frac{d\Phi_{Y_n}(y)}{dy} = n[F_X(y)]^{n-1} \cdot f_X(y) \tag{2.18}$$

where $f_X(\cdot)$ is the probability density function of any X_i. This equation shows that as n increases the probability distribution function of Y_n shifts to the right as shown in Figure (2.17). The most probable extreme value, $\bar{y}_n$ is determined by $\frac{d\phi_{Y_n}(y)}{dy} = 0$. Using the expressions for $\phi_{Y_n}(y)$ given above we get

$$f_X^{'}(y)F_X(y) + (n-1)f_X^2(y) = 0 \tag{2.19}$$

Here $f_X^{'}(y)$ is derivative of the probability distribution function. For any given value of n this equation can be solved iteratively to determine the most probable extreme value.

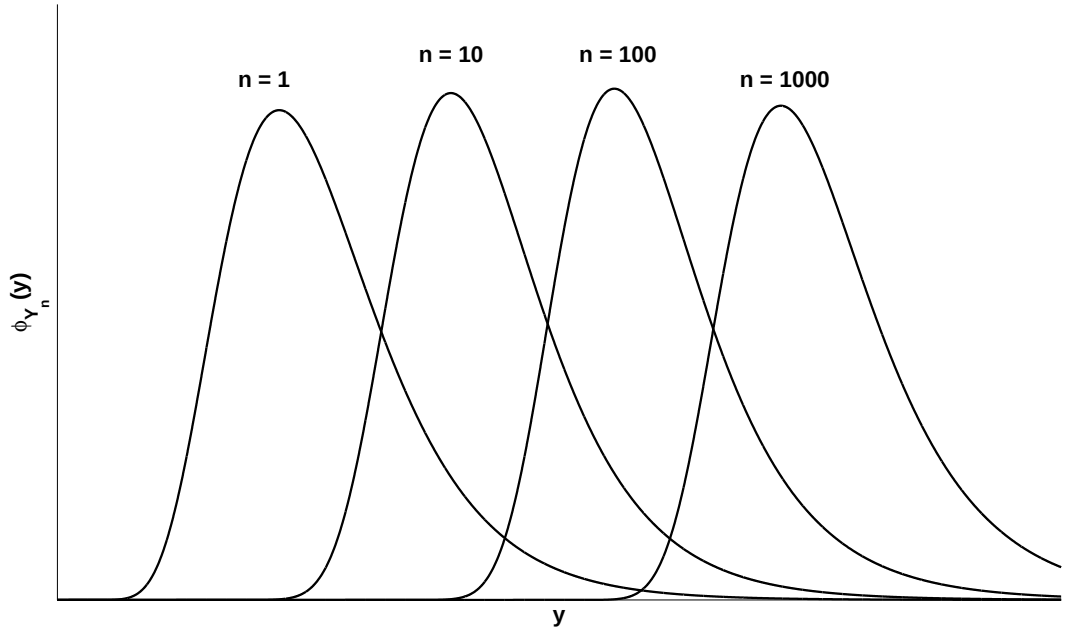

Figure 2.17: Example probability density functions of Y_n for increasing values of n.

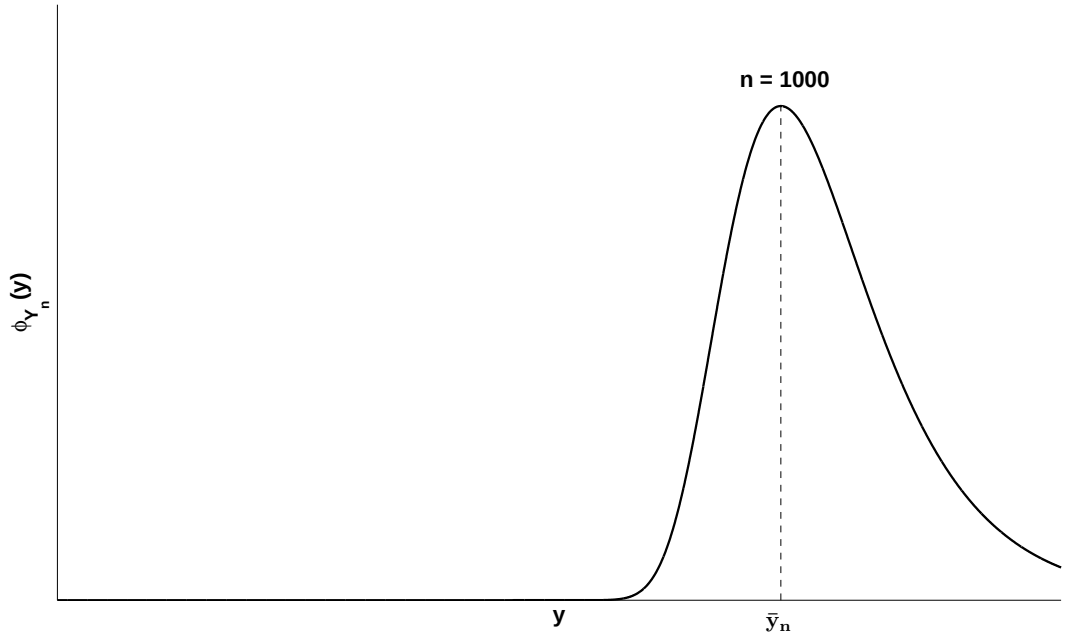

Figure 2.18: The most probable extreme value, $\bar{y}_n$.

An alternative approach exists for obtaining the most probable extreme value in a given number of years. For large values of observations the following approximate relationship relates the most probable extreme value with time:

$$n = \frac{1}{1 - F_x(\bar{y}_n)} \tag{2.20}$$

where n is the observation number, $F_x(\cdot)$ is the cumulative distribution function, and $\bar{y}_n$ is the most probable extreme value. The observation number is a function of time. Our datasets provide one significant wave height data point per hour for the last ten

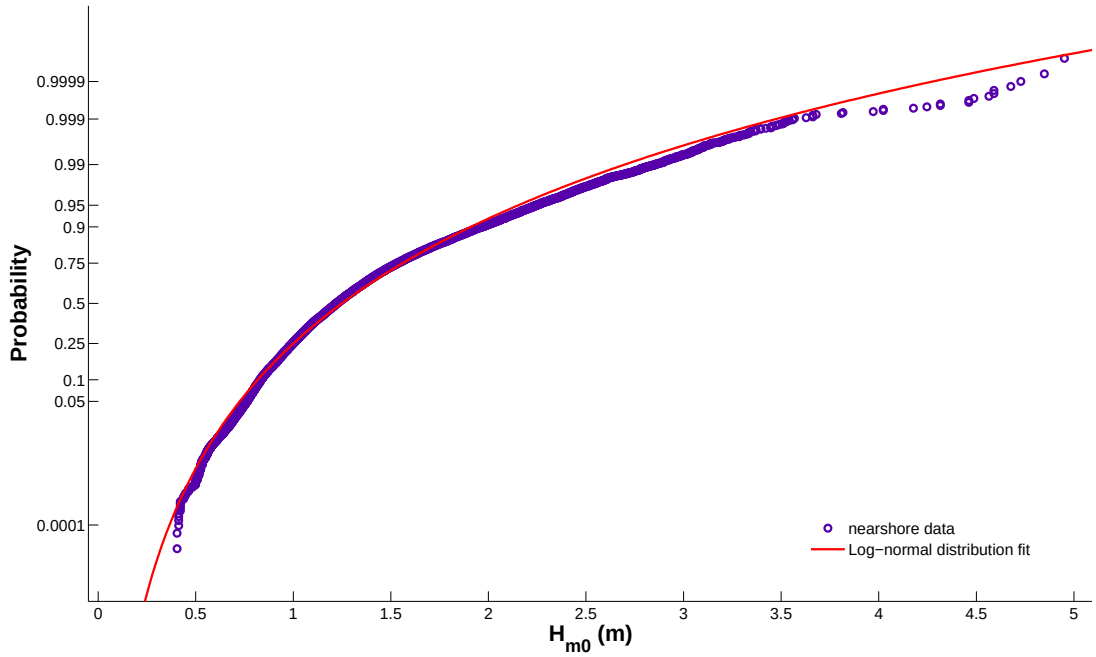

Figure 2.19: Sample probability plot.

years and exclude erroneous and missing data points. The numbers of years for which we seek the most probable extreme value relate to observation number through this relationship. We can approximate $F_x(\cdot)$ by ordering the dataset of significant wave heights in ascending order. The order number of each observation divided by the total

number of observations plus 1 is the corresponding cumulative distribution value for that observation. The cumulative distribution function can be plotted on probability paper and fitted with various distributions to determine which distribution is best. For our data a log-normal distribution fit matches very well as illustrated in Figure (2.19).

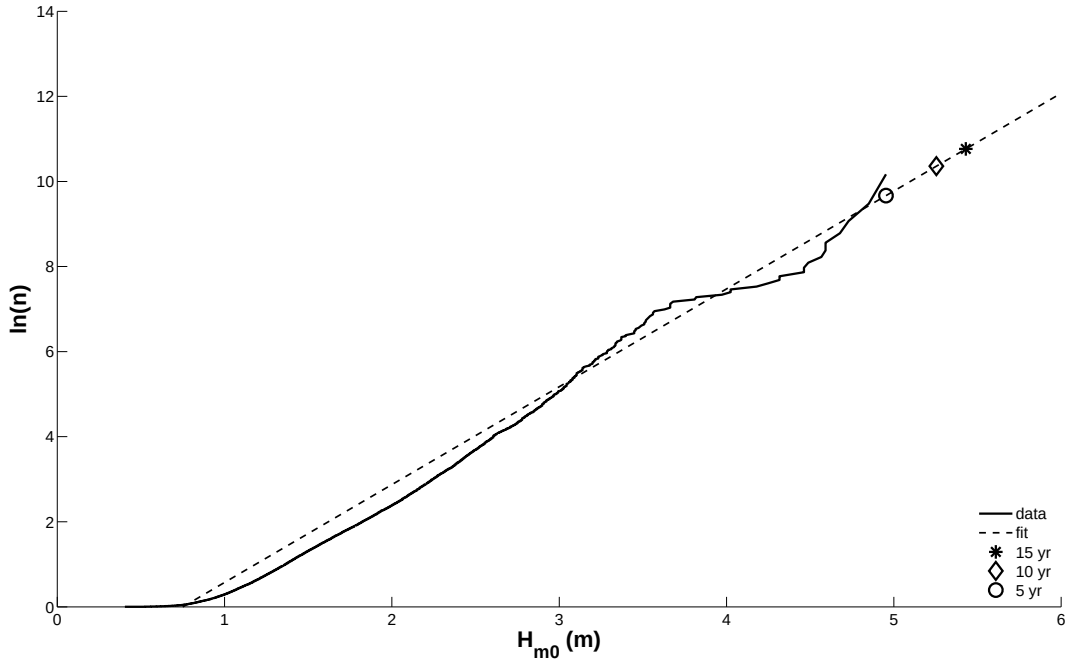

Figure 2.20: Sample plot useful for interpolation or extrapolation.

The approximate cumulative distribution function can then be used to compute n in equation (2.20). Taking the natural logarithm of n and plotting against the corresponding significant wave height results in a nearly linear slope as shown in Figure (2.20). This can be fitted using a linear fit or a piecewise-linear fit based on regression analysis or engineering judgement. The resulting fit can then be used for interpolation or extrapolation. Then for a given number of years converted to observation number, its natural log can be computed and the corresponding most

probable extreme value significant wave height for that return period can be attained by interpolation or extrapolation. This is shown on the figure for number of years of 5, 10, and 15 years.

This page intentionally left blank.

Chapter 3

Overtopping Devices

As introduced in chapter 1, overtopping devices utilize the energy of waves to establish a head of water above mean sea level in the reservoir of the device. The 'power take-off' component of the device, usually low-head turbines, then tries to maximize the potential energy of the stored water and convert it to electricity. In this chapter we will investigate the parameters integral to overtopping devices. The wave overtopping process is complex to describe and quantify, however current formulas for overtopping rate will be presented. Then we will describe the most prominent overtopping devices, the Wave Dragon and the Seawave Slot-Cone Generator, and analyze their suitability for use in California.

3.1 Important Aspects of Overtopping Devices

The appeal of overtopping devices for wave energy extraction is in their simplicity. Simplicity is essential for any device operating offshore or in marine environments where maintenance is difficult to perform and where extreme forces, fouling, and corrosion can seriously affect moving parts. Most overtopping designs have very few moving parts and these are usually the turbines comprising the power take-off

component of the device. The turbine technology for overtopping devices is similar to that which has successfully been used by the hydropower industry for a long time and is therefore reliable and well understood. Taking advantage of existing technology allows overtopping devices to remain relatively simple from both the design point of view as well as in terms of maintenance and operation.

The power available from an overtopping device operating at steady state is governed by the equation:

$$P = \rho Q g H \tag{3.1}$$

where

$$\begin{aligned} P &= \text{Power} \\ \rho &= \text{density} \\ Q &= \text{Volumetric flow rate} \\ g &= \text{gravity} \\ H &= \text{Head} \end{aligned}$$

The volumetric rate of water which successfully enters the reservoir is a crucial factor for overtopping devices because that is directly proportional to how much energy can be extracted. Significant wave height is a key parameter involved in determining this rate. Crest freeboard which is the maximum height the water must reach to spill into the reservoir is also an important parameter. Another element of the device shape is the surface slope which also influences the volumetric rate. Likewise, aspects important to the wave height such as water depth, seabed slope may need consideration.

Power extracted is directly proportional to the reservoir height, or head, above the turbine. The greater the head, the more energy extracted. However the reservoir

height must always be less than the crest freeboard. Increasing the head necessarily requires increasing the crest freeboard, thus reducing the volume of water which enters the reservoir. Therefore based on the expected wave conditions for a location optimum settings of crest freeboard or effectively reservoir height must be found.

Capacity factor is one metric for determining the suitability of a device for a particular location. This is the energy produced during a one year period divided by the energy that would have been produced had the device been running continually at its maximum rated output during that year. Lowering the crest freeboard is one way of improving capacity factor.

3.2 Overtopping Formulas

As discussed above, the volumetric rate of water which overtops the device and spills into the reservoir is fundamental for overtopping devices. Quantifying this rate is an important step for analysis and design. Yet, the mechanics of wave overtopping are very complex and dependent on device geometry and the specifics of the wave conditions. Therefore laboratory experiments are routinely conducted to determine expected overtopping rates. As a consequence, many types of overtopping rate formulas have been proposed. Most formulas are based on the formulations for wave overtopping of coastal structures intended for shore protection. Much research, including the well referenced work by van der Meer [43], has gone towards this area because of the importance of protecting land against storm waves, tides, and surges.

In this section, we will describe the basic formulas to determine wave overtopping for various applications. These formulas are based on experiments collected primarily from European research programs such as the EurOtop program [9] and the Crest Level Assessment of coastal Structure (CLASH) program [6]. An overview of overtopping of general coastal structures will give context to the formulas and establish

overtopping principles before relating this to wave energy applications. Goda [16] utilizing the CLASH dataset, calibrated the data and generalized wave overtopping formulas for cases of seawalls with smooth, impermeable surfaces. Overtopping wave energy designs are similar to seawalls and so we will use these formulas for shoreline and breakwater device analysis. Finally we will also consider the formula reported for use by the Wave Dragon. This has been fitted to experimental data for the Wave Dragon but can be useful to get a sense for wave overtopping rate for floating structures in deep water.

3.2.1 General Coastal Structure Overtopping

Coastal structures come in many shapes and sizes. Their effectiveness is dependent on their geometry, surface characteristics, and the wave conditions and shape. Therefore, the following parameters and influence factors must be determined in order to use the general formulas for overtopping. The significant wave height, H_{m0} (equation 2.5) and energy period, T_e (equation 2.6) must be known at the 'toe' of the structure where the slope of the structure changes into the foreshore. Oftentimes coastal structures do not have entirely straight slopes but contain sections of various slope or even berms (horizontal sections). An average coastal structure slope angle α must be determined and the affect of berms are contained in the berm influence factor γ_b. Figure (3.1) shows a generic coastal structure with one berm. Other influence factors handle the angle of wave attack γ_β and short vertical walls at the top of the crest γ_v. The roughness influence factor γ_f is dependent on the type of material used for the surface of the structure. Crest height, R_c is the height of the outer crest line. If water does not run-up to this height there will be no overtopping. Finally overtopping volume rate q varies linearly with the surf similarity parameter or breaker parameter ξ_0, which combines the wave steepness and slope information.

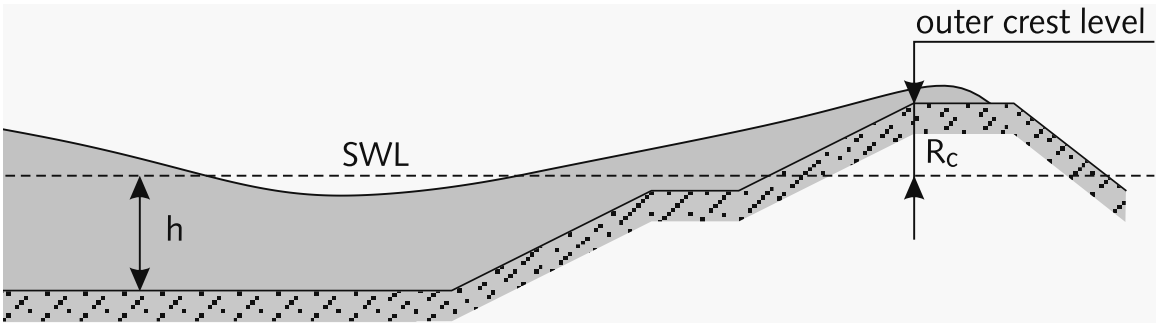

Figure 3.1: Generic coastal structure

The wave overtopping formulae are exponential functions with the general form:

$$q = a \cdot \exp(b \cdot R_c) \tag{3.2}$$

Wave overtopping is usually given as average discharge per meter of wavecrest (m^3/s per m). The coefficients a and b are functions of the wave height, slope angle, breaker parameter and influence functions. The complete formula as given in van der Meer [43] for non-dimensional overtopping is:

$$\frac{q}{\sqrt{gH_{m0}^3}} = \frac{0.067}{\sqrt{\tan(\alpha)}}\ \gamma_b \cdot \xi_0 \cdot \exp\left(-4.3\,\frac{R_c}{H_{m0}}\,\frac{1}{\xi_0 \cdot \gamma_b \cdot \gamma_f \cdot \gamma_\beta \cdot \gamma_v}\right) \tag{3.3}$$

Here g is gravity and the surf similarity parameter ξ_0 is given by

$$\xi_0 = \frac{\tan(\alpha)}{\sqrt{s_0}} \tag{3.4}$$

where $s_0 = 2\pi H_{m0}/\left(gT_e^2\right)$ is the wave steepness.

3.2.2 Seawall Overtopping

We will now consider simplified structures limiting our scope to seawalls with smooth and impermeable surfaces. By assuming smooth, impermeable surfaces for simple inclined structures perpendicularly aligned to the incoming waves we can neglect the effect of the influence factors. Goda proposed mean wave overtopping formu-

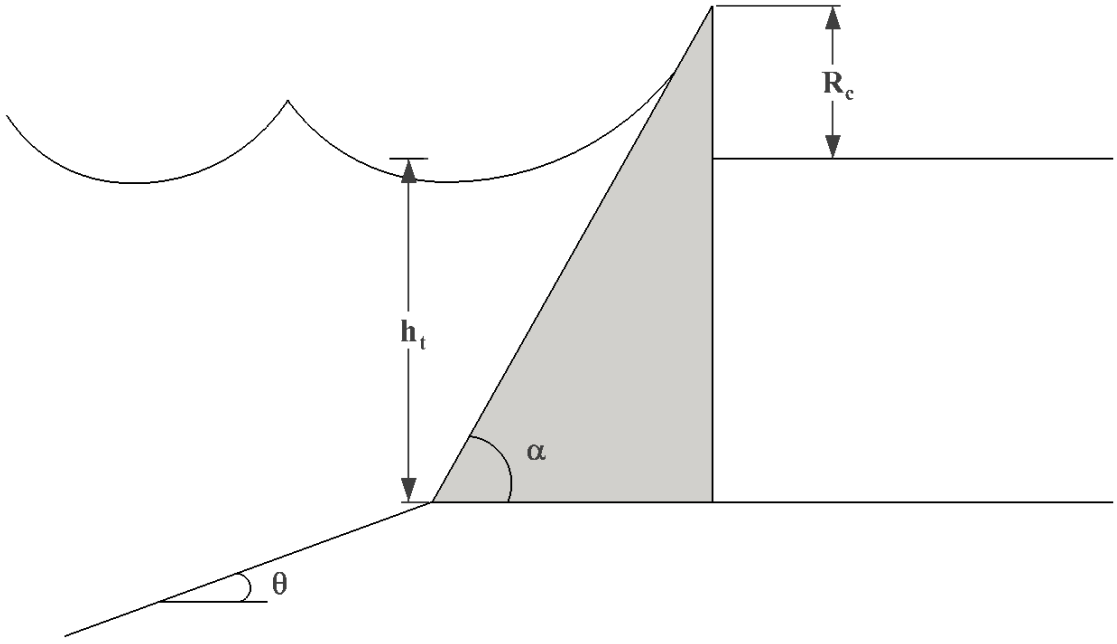

Figure 3.2: Schematic of a generic Seawall

las for this type of coastal structure by calibrating them to an appropriate set of data from the CLASH database. The CLASH database is a renowned accomplishment by the EU-financed CLASH project, consisting of 10,532 experimental runs from 163 experiments for overtopping from around the world. Goda extracted close to 2,000 runs from 36 datasets for smooth, impermeable seawalls for his calibration. His proposed formulas match the experimental results better than the formulas for overtopping of

general coastal structures shown above.

The ratio of crest freeboard relative to the significant wave height at the toe of the structure (R_c/H_{m0}) is the main parameter governing wave overtopping rate. Relative toe depth and seabed slope are previously unaccounted for parameters which can also affect the overtopping rate as will been seen in the following brief presentation of the new overtopping rate formula. The proposed overtopping formula employs a simple exponential relation given as:

$$\frac{q}{\sqrt{gH_{m0}^3}} = q^* = \exp\left[-\left(A + B\frac{R_c}{H_{m0}}\right)\right] \tag{3.5}$$

Goda's study tried to find the optimal formulations for A and B by incorporating the parameters of the surface slope angle, α, the relative toe depth h_t/H_{m0}, and the seabed slope $\tan(\theta)$. The relative toe depth is the ratio of water depth at the toe to significant wave height at the toe. The seabed slope is simply the average seabed slope leading up to the structure. Formulation of the coefficients A and B were made by fitting the following linear equation to the data:

$$y = -\ln(q^*) = A + Bx \tag{3.6}$$

where $x = R_c/H_{m0}$. Hyperbolic tangent functions were chosen to represent the relationship between the coefficients and the relative toe depth and seabed slope.

$$A = A_0 \tanh\left[(0.956 + 4.44\tan(\theta) \times (h_t/H_{m0} + 1.242 - 2.032\tan^{0.25}(\theta))\right] \tag{3.7}$$

$$B = B_0 \tanh\left[(0.822 - 2.22\tan(\theta) \times (h_t/H_{m0} + 0.578 + 2.22\tan(\theta))\right] \tag{3.8}$$

For inclined structures, the following equations which are functions of surface slope angle are used for the coefficients A_0 and B_0. They were obtained by regression

analysis to fit experimental data.

$$A_0 = 3.4 - 0.734\cot(\alpha) + 0.239\cot^2(\alpha) - 0.0162\cot^3(\alpha) \tag{3.9}$$

$$B_0 = 2.3 - 0.5\cot(\alpha) + 0.15\cot^2(\alpha) - 0.011\cot^3(\alpha) \tag{3.10}$$

for $0 \leq \cot(\alpha) \leq 7$. It is interesting to note that wave period is no longer a variable in these formulas for mean overtopping rate .

Goda's proposed formula is dependent on four variables which are significant wave height and water depth at the toe, inclined surface angle, and seabed angle. The influence of these variables on the wave overtopping rate is investigated in the following figures. Variable values for typical sea states and seawalls for overtopping energy devices were used. Figure (3.3) shows the trend for non-dimensional overtopping as a function of non-dimensional crest freeboard. Values of 1 to 10 m significant wave heights were chosen and the resulting plot lines are nearly stacked on top of each other. This indicates that this overtopping formulation is consistent over a wide range of sea states.

Figure (3.4) shows how the incline angle of the seawall affects overtopping. The range of angles corresponds to $0 < \cot(\alpha) < 7$ which is the range of applicability specified by Goda. For very small angles corresponding to a very long seawall ramp the overtopping rate falls drastically because the water from the waves do not have enough energy to flow up the whole length of the ramp. Under the conditions of the plot the overtopping peaks for an incline angle of approximately 30 degrees and gradually decreases as the seawall angle increases toward vertical.

Figure (3.5) shows the effect of the relative toe depth on the overtopping rate coefficients A and B. As their functional dependence is a hyperbolic tangent one for relative toe depth values greater than one the dependence is roughly constant. Hence

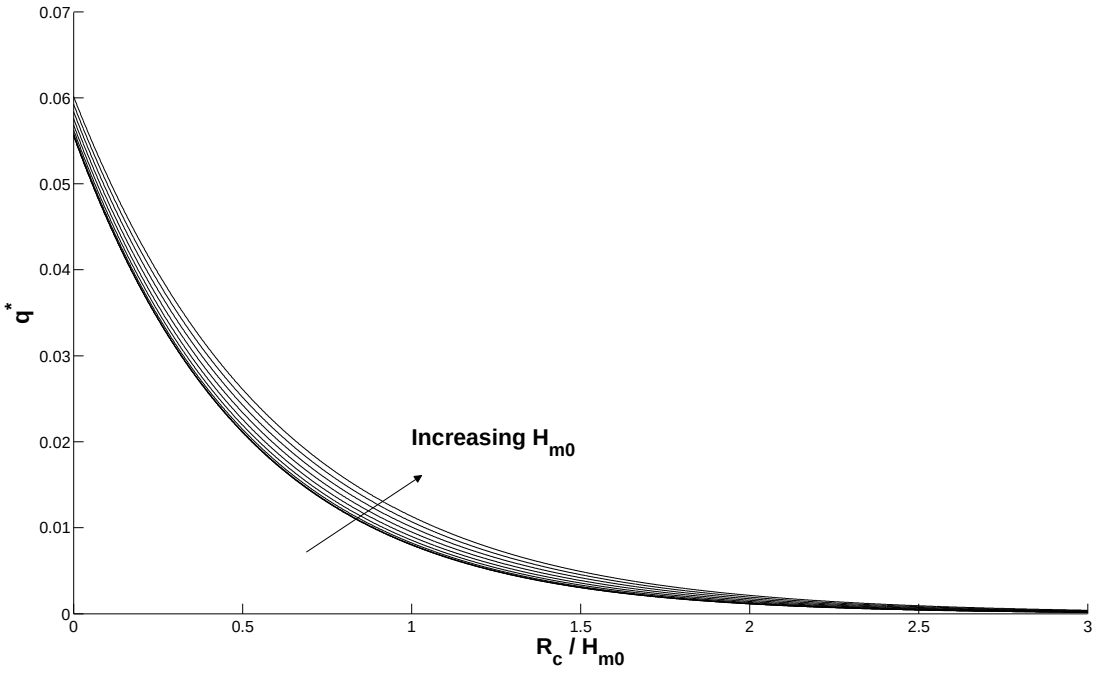

Figure 3.3: Non-dimensional overtopping for increasing H_{m0} from 1 m to 10 m.

given that we do not expect to operate in wave conditions where the significant wave height is greater than the toe depth we shall neglect the relative toe depth variable. We expect to operate only within the constant regime.

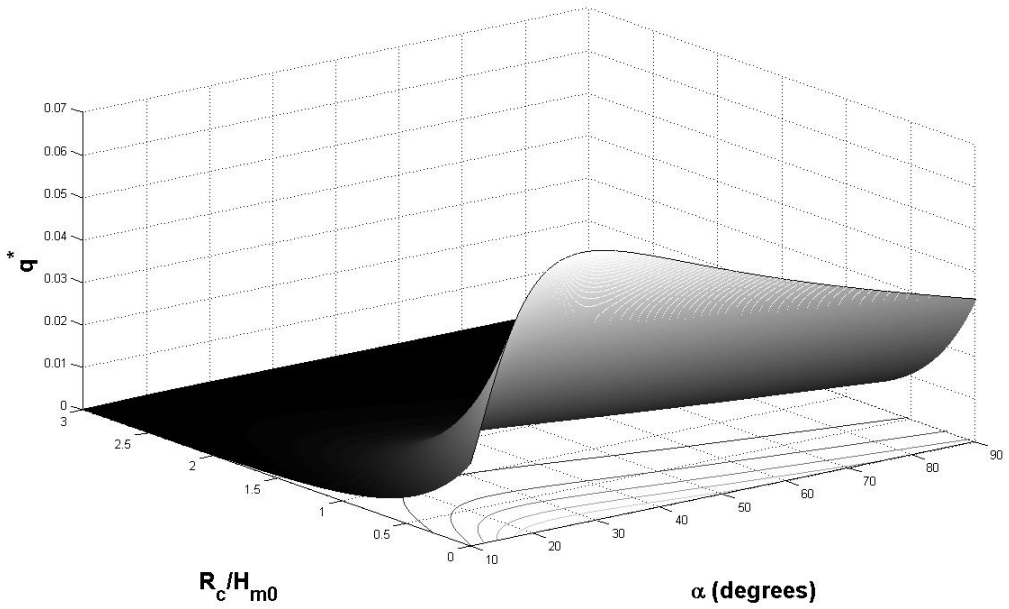

Figure 3.4: Effect of changing the inclined slope angle.

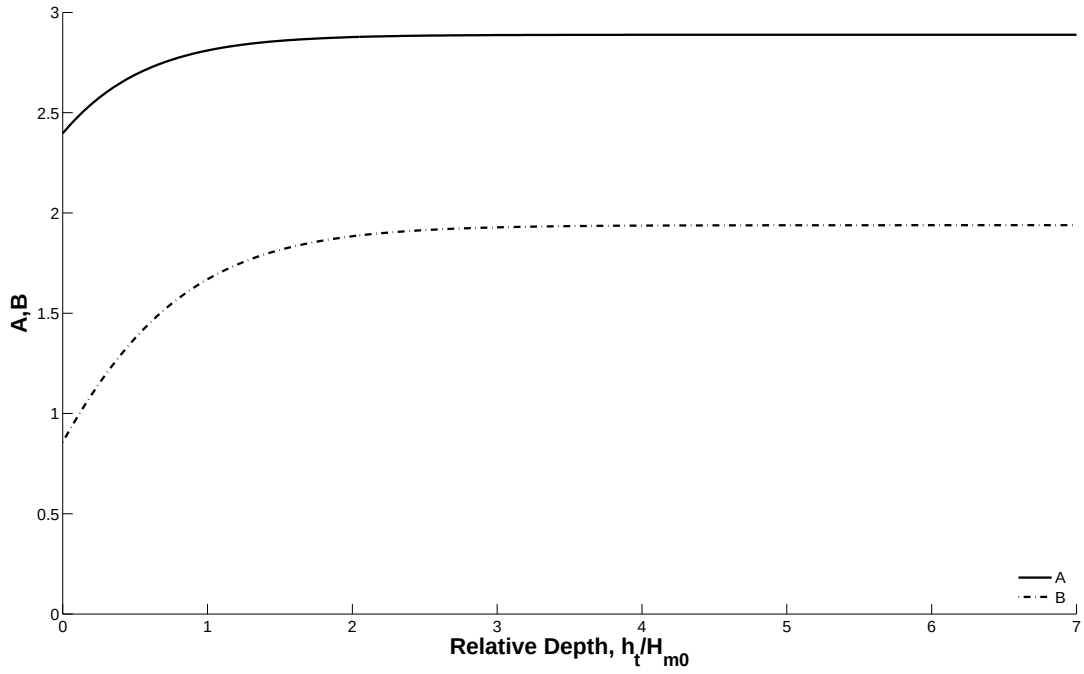

Figure 3.5: Influence on coefficients A and B by the relative depth at the toe.

Figure (3.6) shows how seabed slope angle influences overtopping rate. Here the available experimental data is limited. Goda seems to make a distinction between $\tan(\theta)$ angles of (1/10) and (1/100) in how he handles the experimental data. However as seen in the figure for such small angles corresponding to approximately 5.7 and 0.57 degrees, the impact on overtopping rate is close to zero.

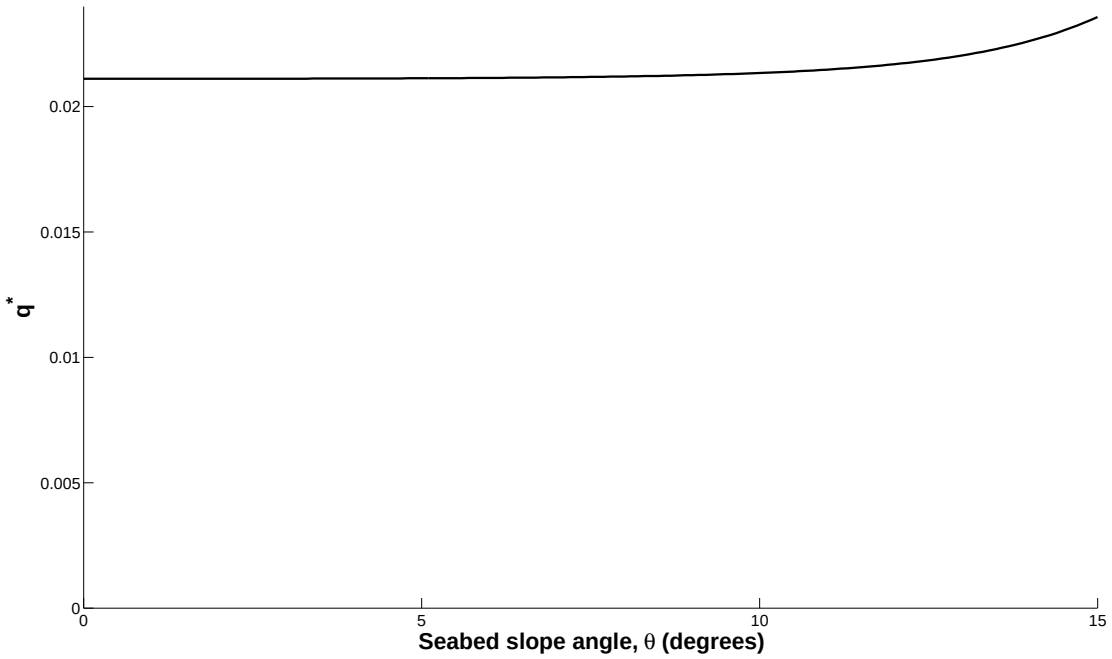

Figure 3.6: Influence on wave overtopping rate by the seabed slope angle.

Goda also provides an uncertainty range for his overtopping rate formula. It is based on his analysis of the experimental results. The spread of the ratio between the measured overtopping rate to the experimental overtopping rate is wide for low overtopping and decrease with greater overtopping.

$$\frac{q^*_{meas}}{q^*_{est}} = 1.0 \times q^{2/5}_{est} \leftrightarrow 1.0 \times q^{-1/3}_{est} \qquad : \qquad q^* < 1.0 \tag{3.11}$$

This uncertainty originates from the random nature of waves. The total volume of

overtopping by a random wave train is determined by the number and height of waves above the threshold for overtopping. When the random waves are generated by the wave generator for a specified wave spectrum different combinations of heights and periods are produced thus resulting in different volumes to total wave overtopping. Differences become pronounced as the overtopping volume decreases. For this reason these prediction formulas are intended only for preliminary design purposes. Scale model testing or numerical computation should be undertaken to obtain more reliable information on the wave overtopping rate.

We will use the above equations for analysis of nearshore overtopping devices. As these formulas are dependent on the significant wave height at the toe of the structure, this information will be needed accurately. The use of SWAN is highly valuable for this purpose.

3.2.3 Offshore Overtopping

Overtopping of offshore devices is not well established in the literature. Research on similar processes such as greenwater and wave run-up is available as these are concerns for the offshore oil industry. However preventing the occurrence of these processes rather than quantifying their rate is their primary interest. One approach to get a sense of offshore overtopping is to extend the use of the formula above to offshore. Indeed the seawall overtopping expression may also be used for offshore applications since the subset of data used by Goda included scale testing from the shoreline to deep water. For such deep water use, the hyperbolic tangent functions asymptote to 1 and the A and B coefficients reduce to A_0 and B_0. Unfortunately, construction of seawalls is likely cost prohibitive in deep water and this formula will probably have limited use.

Seemingly the only application for offshore overtopping is for wave energy devices. Thus, overtopping device makers must perform their own experiments to determine overtopping rates for their designs. The Wave Dragon group has published a handful of papers describing their experience with their 1 : 4.5 scale prototype deployed in Nissum Bredning, Denmark. They have conducted model testing and compared those results with *in situ* prototype results to obtain the following expression [14].

$$q = 0.025 \cdot c_d \cdot \exp\left(-40\frac{R_c}{H_{m0}}\sqrt{\frac{S_{op}}{2\pi}}\right)\frac{L\sqrt{gH_{m0}^3}}{\sqrt{\frac{S_{op}}{2\pi}}} \tag{3.12}$$

where,

$$\begin{aligned} q &= \text{overtopping volume} \\ c_d &= \text{coeff. for direction spreading effects} \\ L &= \text{length of the structure ramp} \\ S_{op} &= H_{m0}/L_{op} \\ L_{op} &= \frac{g}{2\pi}T_p^2 \\ T_p &= (\text{peak period}, \simeq 1.1T_e) \\ H_{m0} &= \text{significant wave height} \\ R_c &= \text{crest freeboard} \end{aligned}$$

This overtopping rate is based on the Wave Dragon design and thus it is quite limited in application to other device shapes. However, it can provide a rough estimate for initial design purposes of wave overtopping rate for floating structures. Indeed it is interesting to note that the exponential nature of the overtopping rate taken from the design of coastal structures continues to compare well with experimental data for an offshore floating structure.

3.2.4 Comparison of Seawall and Offshore Overtopping

Here we will look at the differences in the overtopping rates given by formulas (3.5) and (3.12), for seawall and offshore overtopping respectively. These overtopping rates are plotted in non-dimensional form in figure (3.7). Recall from equation (3.5) that non-dimensional overtopping is given by $q^* = \frac{q}{\sqrt{gH_{m0}^3}}$. The figure shows that

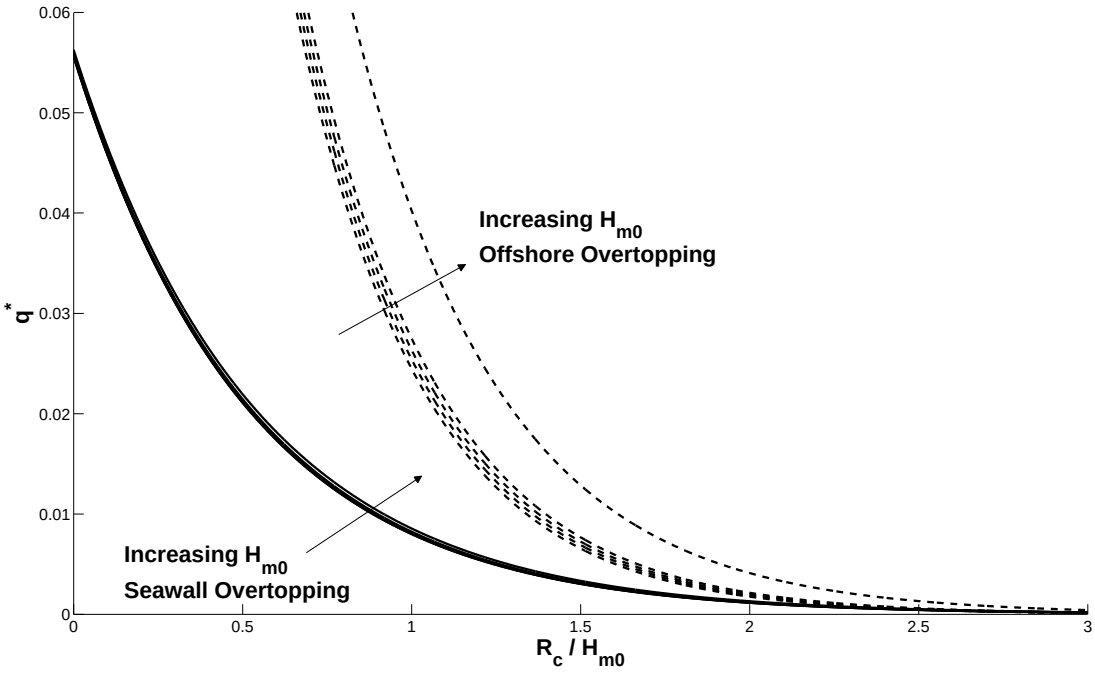

Figure 3.7: Comparison of non-dimensional overtopping for the seawall and offshore formulas for significant wave height varying every 1 m from 1-4 m.

the offshore overtopping is many times greater than the seawall overtopping at small values of non-dimensional crest freeboard. As the non-dimensional crest freeboard increases the difference in overtopping narrows. This can likely be attributed to the fact that seawalls in general are built to stop waves while the offshore overtopping formulation is for the Wave Dragon which has been designed to promote wave overtopping. Also the experiments for the Wave Dragon included reflecting arms and a specially designed ramp to improve overtopping considerably. These features of the

Wave Dragon are described in the next section. It is expected that such features can be similarly applied to the proposed device design in chapter 4 to improve overtopping as well. The difference in overtopping rate is significant as it may limit the power take-off options also described in the next chapter.

3.3 Description of Current Devices

3.3.1 Wave Dragon

The Wave Dragon (by Wave Dragon Ltd, Denmark) is a well known device and on-going research project originated in the late 1980s by the inventor MSc Erik Friis-Madsen. It is the first ocean wave energy convertor to produce power to the electrical grid. The device incorporates two large reflectors that stretch outwards from the device and direct wave energy towards the center. As shown in Figures (3.8, 3.9, 3.10) the main device body platform consists of a specially designed ramp, and a raised reservoir, which is filled by the action of the waves, and then drained via a set of low-head Kaplan turbines. The turbines have to operate in very low head

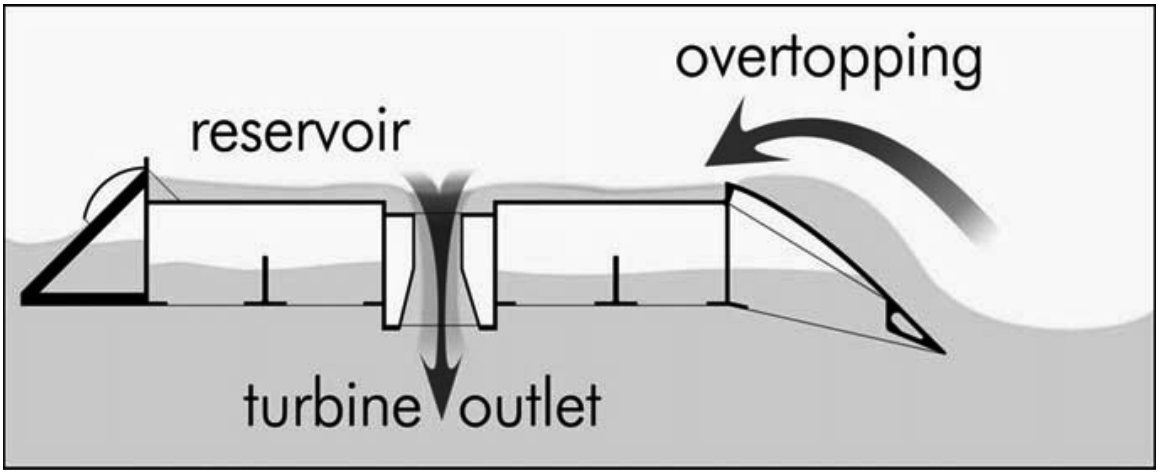

Figure 3.8: Schematic of the Wave Dragon.

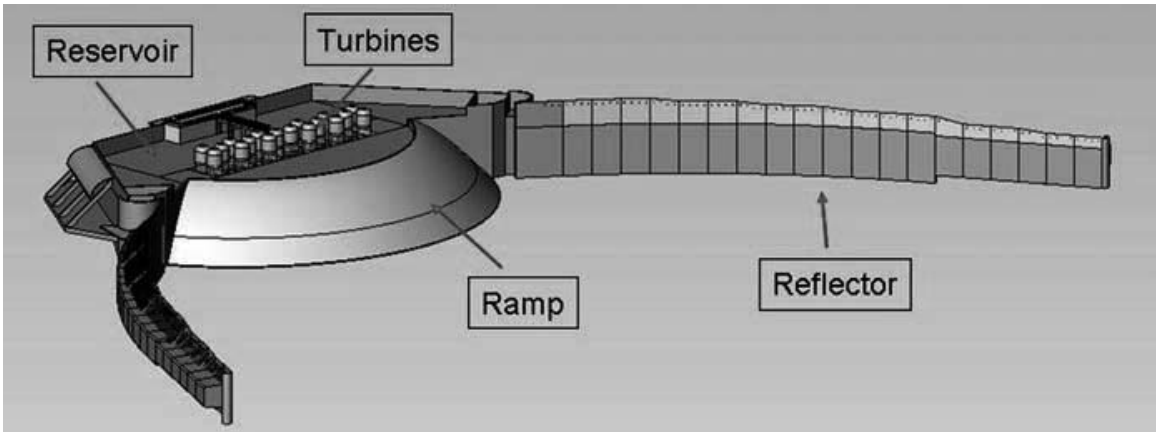

Figure 3.9: Solid model of the Wave Dragon.

values ranging from 0.4 to 4.0 m [22]. The Wave Dragon is constructed with open air chambers. A pressurized air system makes the floating height adjustable. This allows for an adjustable crest freeboard to adapt to different wave conditions. The ramp has a variable crest freeboard of 1-4 m [41]. Furthermore, the open air chambers reduce the movements of the main body, by acting as cushions to the wave induced pressure. It will be moored in relatively deep water (more than 25 m and preferably +40 m) to take advantage of the ocean waves before they lose energy as they reach the coastal area. Since 2003, a 1:4.5 scale prototype has been grid connected and undergoing sea trials in Nissum Bredning, Denmark. The company has plans for a 7 MW plant that would operate in wave climates of 36 kW/m [19].

Much work has gone into the design of the Wave Dragon to amplify the wave overtopping into the reservoir. Large wave reflectors have been studied, designed, and patented. These reflectors have the verified effect of increasing the significant wave height substantially and thereby increasing energy capture by 70% in typical conditions [22]. An earlier study showed that by the use of wave reflectors the wave energy is effectively focused and increased by approximately 130-140% [23]. Additionally, Kofoed tested various slope layouts in order to find a structure producing

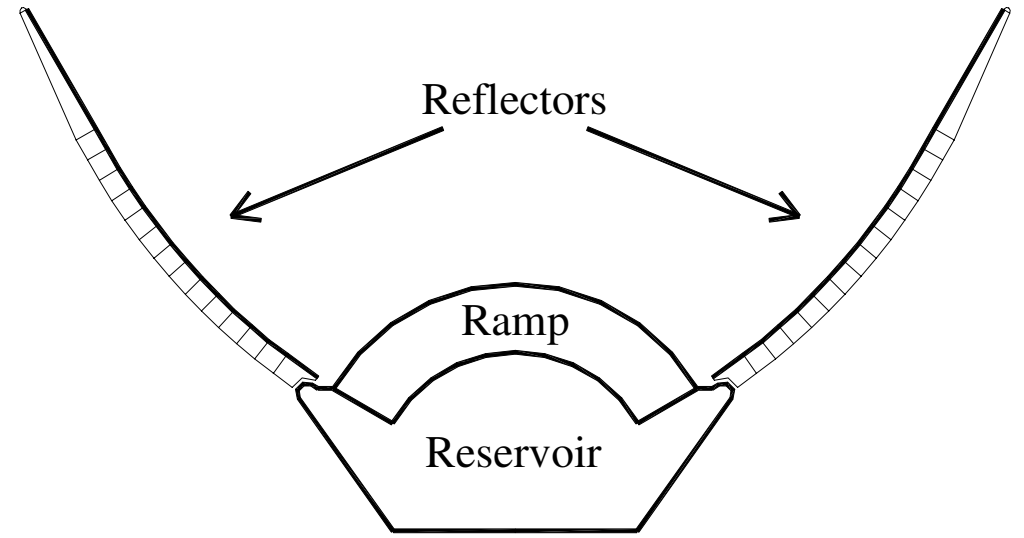

Figure 3.10: Top-down view of the Wave Dragon.

the maximum overtopping effect. These tests verified their patented doubly curved ramp to have a significantly positive effect [14].

An unresolved area of research interest for the Wave Dragon is in buoyancy control. As reported in their 2007 paper [21], performing active control automatically in real time is far from trivial. Yet it is desirable to achieve because the better the buoyancy control is, the better the energy capture is. There are two basic control loops. The first is a slow acting loop on the same time scale as for the change in sea states which is on the order of hours. Therefore the platform can change its buoyancy, and thus its floating level on that time scale for greater overtopping. The method for controlling the floating level as well as the heel and trim of the platform is by blowing air into, or venting air from open compartments beneath the reservoir. The faster acting loop maintains the correct level of water in the reservoir. Too high a water level means large waves will not be accommodated resulting in spilling from the reservoir. Too low of a level means the head across the turbine is not optimal and power production decreases. Control of the timing to open and close the turbines in relation to the water

level in the reservoir is determined by this loop. The buoyancy model and control algorithms of the Wave Dragon are still being developed. The prototype results have shown for large periods of operating time, a reduction of power production by a factor of more than two from optimal performance. This demonstrates the importance of maintaining optimal settings. Determining the right control algorithm will not be trivial, however to due to the complex geometry, the free surface of water in the reservoir, wave interaction with the reflectors, plus the mooring system and wind and wave forces.

3.3.2 Seawave Slot-Cone Generator

The Seawave Slot-Cone Generator (SSG) by WAVEenergy AS, in Norway is a shoreline based wave energy converter patented in 2003. The SSG concept consists of a number of reservoirs one on the top of the other above the mean water level in which the water from incoming waves is stored temporary and features a unique turbine design. The essential part of the device is a sloped wall, with water entry slots spaced at various heights from the bottom to the top. As a wave impacts the wall, water overtops some of the slots and collects into the series of separate, vertically spaced reservoirs. By directing the higher-energy water into higher reservoirs instead of using one large reservoir, the SSG performance should be better. The Multi-Stage Turbine (MST) as shown in Figure (3.11) operates by taking advantage of different heights of water head corresponding to the different reservoir levels. The MST technology can drain water from each reservoir sequentially or simultaneously and can also operate even if only one reservoir is supplying water. This results in a higher degree of efficiency by minimizing the start/stop sequences. ([19], [26]).

A key to success for the SSG will be the low cost of the structure and its robustness. The construction of the pilot plant is under consideration. The pilot plant is planned

Figure 3.11: Seawave Slot-cone Generator and Multi-Stage Turbine renderings.

to be an on-shore full-scale module of 3 levels with an expected power production of 320 MWh/y (40 kW device) in the North Sea. Additional concepts exist for coastal structure or breakwater designs and an offshore design. The breakwater design can possibly be built into existing breakwaters or designed into future constructions as seen in Figure (3.12). The coastal structure possibility will allow cost sharing and possibly better performance for reducing reflection by efficiently absorbing energy. The offshore concept is also being investigated to reach more energetic seas. As shown in Figure (3.13) the offshore design is a cone-shaped, seabed-anchored device.

The SSG is still in the development stage. The various components of the device need optimization. Further investigations are needed to test the behavior of the MST under varying conditions and in general to optimize the concept before manufacturing a full-scale machine [26]. For this reason Kaplan turbines currently are planned to be used instead. Ideally the power stored in the reservoirs is the power related to the potential energy in the incoming waves, but in reality this storage incurs a limitation due to the dimensions of the structure and turbine strategy. Thus, much like the Wave Dragon an optimizing strategy must be developed to maximize head and minimize spillage losses. An added variable for shoreline devices is the bathymetry of a location. Bathymetry plays an important role on the design of the frontal plates as well as the

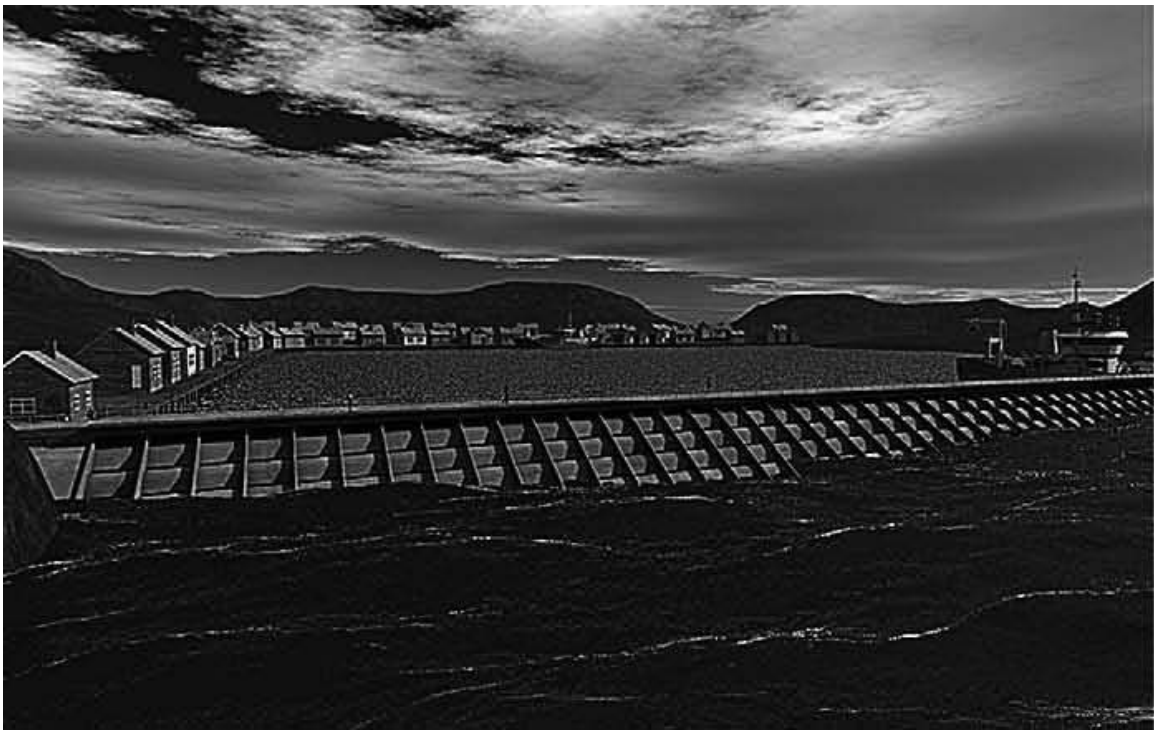

Figure 3.12: Seawave Slot-Cone Generator in breakwater configuration.

frontal 'apron' at the toe of the structure and must be taken into account when determining the water overtopping volume. Given that these individual component efficiencies vary with the sea state, it has been estimated that overall efficiency in the range of 10-26% can be obtained for different wave conditions.

3.4 Suitability of the Wave Dragon and SSG for California

The Wave Dragon is unlikely to be effective at many locations along the California coast. California's wave climate varies considerably along the length of its coast as seen in Section 2.4. For low wave energy sites, particularly in Southern California the capacity factor of the Wave Dragon will suffer. Indeed, the Wave Dragon was

Figure 3.13: Offshore design for the Seawave Slot-Cone Generator.

initially designed for deployment in the North Sea where the wave climate range is 40-70 kW/m . The Wave Dragon design plans have been scaled for wave climates of 24, 36, 48, and 60 kW/m. This is much greater than what can be expected in Southern California. Only the most northern part of the state is suitable for the Wave Dragon.

The operating range of the Wave Dragon suggest that it may operate in small sea states. The stated low end values of 1 m crest freeboard and corresponding 0.4 m turbine operating head are quite small. However, inefficiency becomes an issue at very low head values. This is further discussed in section 4.3 on the power take-off systems. Additionally, to keep the turbines as simple and rugged as possible, it was decided to minimize the number of moving parts. Hence a design with fixed guide vanes and fixed runner blades were chosen. The result was a low head turbine specially designed for the Wave Dragon with an efficiency between 91 and 92% in the

relevant head and flow ranges [22]. These relevant ranges are not likely to include the minimum head value.

The Seawave Slot-Cone Generator is still a conceptual device and thus is difficult to assess for use in California. The details of the design are as yet unpublished. The Multi-Stage Turbine is an interesting concept and can possibly allow the SSG to operate in low wave energy locations. However, as long as the SSG group intends to use Kaplan turbines the same issues as with the Wave Dragon can be expected. In low wave sites the capacity factor will be problematic.

This page intentionally left blank.

Chapter 4

Novel Design Concept

A novel overtopping device design will be proposed in this chapter. It will be comprised of a seawall-style ramp for overtopping, a reservoir combined with a gearing system to transfer low-head water to a higher head, and a turbine-based power take-off system.

Overtopping wave devices as described in chapter 3 must compromise between overtopping volume and head height. In order to have a high enough head to efficiently generate power the crest freeboard of the wave energy converter must be raised to a sufficient height. As a result much of the small amplitude, low energy waves in low energy sites will not overtop and go unused. The objective of the proposed design is to allow utilization of small waves by transferring the low-head resource to a higher head via the proposed gearing system.

In the following sections the benefit of the proposed system will be established. The conditions for when a net gain in energy is achieved by use of a low seawall plus gearing system will be shown along with the increase in capacity factor. Issues regarding the power take-off system and device operation will be discussed. Lastly additional considerations for improving the device and its applications will be presented.

4.1 Seawall Ramp with Gearing System

4.1.1 Overtopping Seawall

Maximizing the wave overtopping can be accomplished by reducing the crest freeboard to zero. However to do so would mean no water can be stored in the reservoir and therefore no head is available for extracting energy. Some level of crest freeboard is required to establish the head. Initially we will use simply shaped seawalls for our design. Later the seawall can be optimized to maximize overtopping. The seawall overtopping rate formulas from chapter 3 will allow us to determine the corresponding overtopping rate for a given wave environment and location. The seawall will serve as a ramp for water to overtop as well as a structure to contain calm water for the transfer reservoir to utilize.

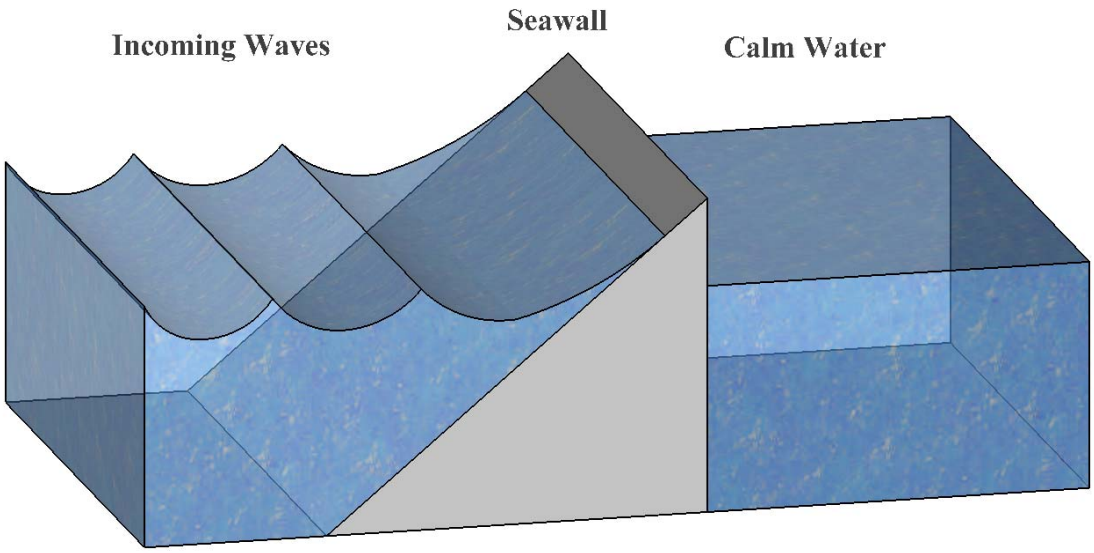

Figure 4.1: Basic seawall configuration.

4.1.2 Gearing System

As described above, the transfer from the low head of the overtopped waves into the high head of the power take-off system is through the gearing system. A schematic of the gearing system is illustrated in Figure (4.2). For clarity the support structure for the system is not shown. The system consists of the overtopping water collec-

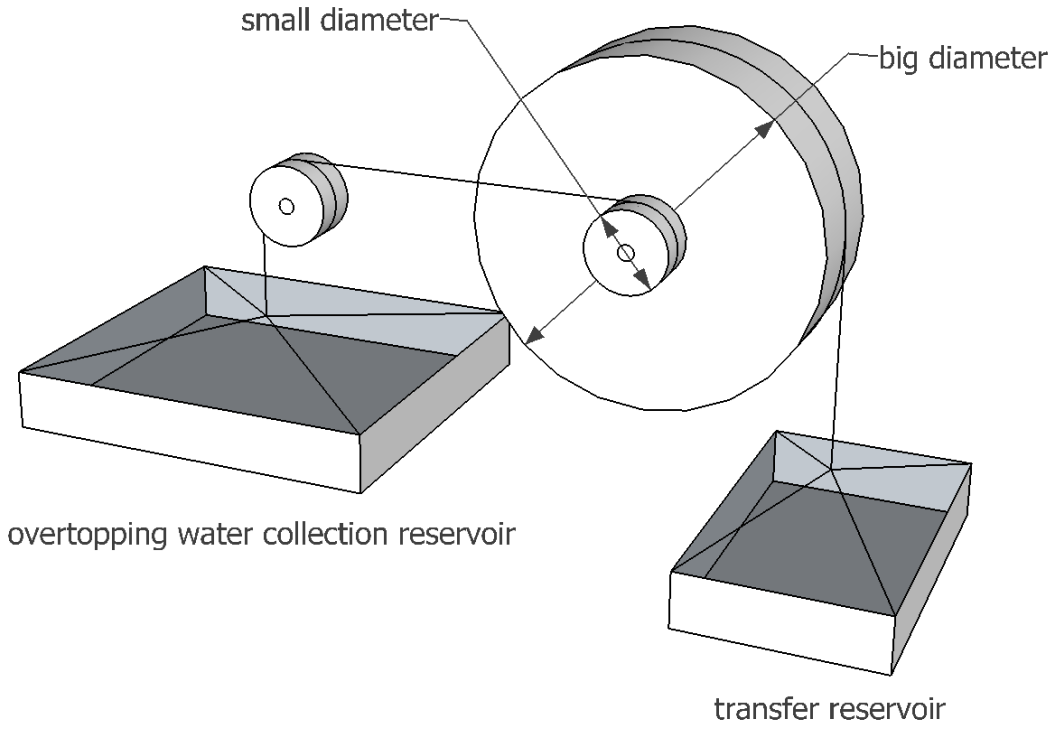

Figure 4.2: Schematic drawing of the gearing system.

tion reservoir, the gears, and the transfer reservoir. The ratio of the gear sizes are determined by the distance the two reservoirs must travel. The overtopping water collection reservoir travels a short distance because the seawall will not have a high crest freeboard. The transfer reservoir must travel a relatively large distance to transfer water to the relatively high head of the power take-off system. The gear ratio is related to the ratio of these distances. In the same way the force due to the weight

of the water in the overtopping water collection reservoir is greater by a factor of the gear ratio than the force due to the weight of the water in the transfer reservoir. Hence the volumes of the two reservoirs are related as follows:

$$\text{Gear Ratio} = \frac{\text{Big diameter}}{\text{small diameter}} = \frac{\text{overtopping reservoir volume}}{\text{transfer reservoir volume}} \tag{4.1}$$

4.1.3 Optimal Overtopping

In this section we will analyze the effectiveness of using a gearing system in conjunction with varying the the crest freeboard. The point of using the gearing system is to increase the volumetric rate of water to the power take-off system resulting in greater energy extraction. To show that the gearing system is effective, we will com-

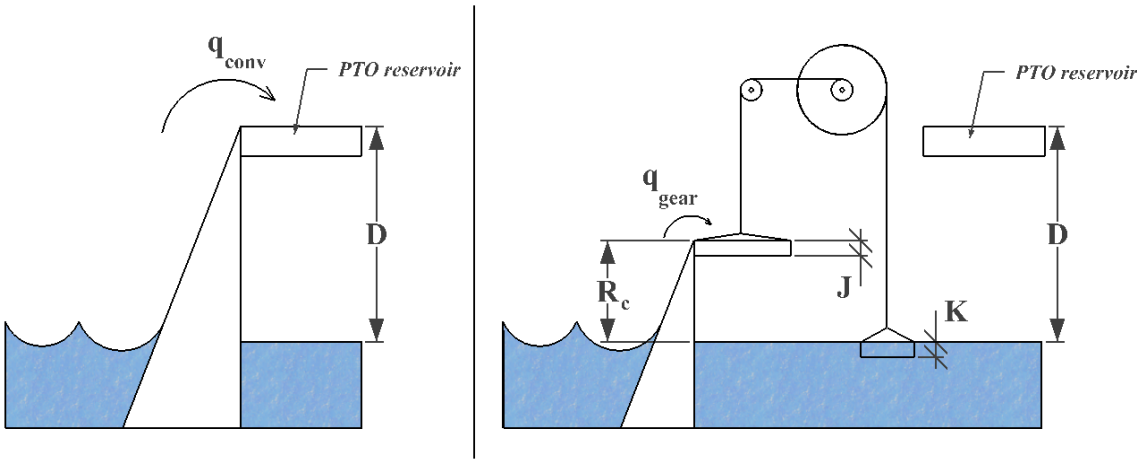

Figure 4.3: Schematic of conventional overtopping (left) and overtopping with gearing system (right).

pare a conventional overtopping device to one with a gearing system. This analysis will use simplified geometries for the reservoirs to illustrate the concept. The notation used is as shown in Figure (4.3). The conventional case we will consider is a simply

shaped inclined seawall with a crest freeboard of 1 unit. This conventional case represents simple overtopping without a gearing system conceptually similar to the Wave Dragon or the Seawave Slot-Cone Generator devices. The gearing system case will also be a simply shaped inclined seawall but with lower crest freeboard. Ultimately we need to show that the volumetric rate of water available to the power take-off system is greater for the gearing system case. To make a fair comparison we must determine the volume of water delivered to the power take-off system at the same height D between the two systems, Q_{conv} and Q_{gear}. In this way the power take-off system is decoupled from the total system. This approach results in a conservative estimate of the effectiveness of using a gearing system. In practice there is likely no performance advantage in maintaining the same PTO reservoir height as in the conventional case. It is likely that the PTO reservoir can be shaped or positioned differently and perform better. Nevertheless for the sake of this comparison analysis we will apply this scenario. For the conventional case the volumetric overtopping rate of water available to the power take-off system is simply the overtopping rate of water, q_{conv}.

$$Q_{conv} = q_{conv} \tag{4.2}$$

For the gearing system case, water must be transferred to the height of 1 unit as opposed to direct overtopping from the waves. This is done using two intermediary reservoirs connected by chains through the gearing system. Therefore although the overtopping rate over the seawall q_{gear} is relatively large compared to q_{conv} the transfer ratio T, and the gear system efficiency η will reduce the volumetric rate for the gearing system case. The transfer ratio T accounts for the gear ratio and the reservoir dimensions for water transfer. The gear system efficiency η accounts for frictional losses, stretching of the chains, water leakage, and other inefficiencies which reduce

the performance of the gearing system.

$$Q_{gear} = q_{gear} \cdot T \cdot \eta \tag{4.3}$$

$$Q_{gear} = q_{gear} \cdot \left(\frac{R_c - J}{D + K} \right) \cdot \eta \tag{4.4}$$

As shown in Figure (4.3) the depth of the two intermediary reservoirs, dimensions J and K should be minimized in order to maximize the volumetric rate of water available to the power take-off system. In the ideal case of perfect efficiency and infinitely long, zero-depth reservoir dimensions for water transfer, this equation simplifies to

$$Q_{gear,ideal} = q_{gear} \cdot \left(\frac{R_c}{D} \right) \tag{4.5}$$

which is simply the overtopping rate times the gear ratio. This represents the maximum overtopping into the PTO reservoir that can be achieved for overtopping devices with a gearing system.

The volume overtopping rates q_{gear} and q_{conv} are determined from the seawall overtopping formula of chapter 3. At a given device location site the water depth at the toe, the seawall slope, the sea bottom slope, and the design significant wave height will all be fixed. Then the overtopping rate can be determined as a function of the crest freeboard R_c. As explained in chapter 3 the form of the overtopping rate q is an exponential curve so depending on the values of crest freeboard the difference between q_{gear} and q_{conv} can be quite large.

Figure (4.4) shows the utility of having a gearing system. The dashed exponentially decaying line represents the overtopping rate as a function of the crest freeboard given by equation (3.5). The open square box indicates the conventional case level of overtopping for a crest freeboard of 1 unit for fixed conditions of significant wave height, seawall incline angle, seabed slope, and relative toe depth. The dash-dot lin-

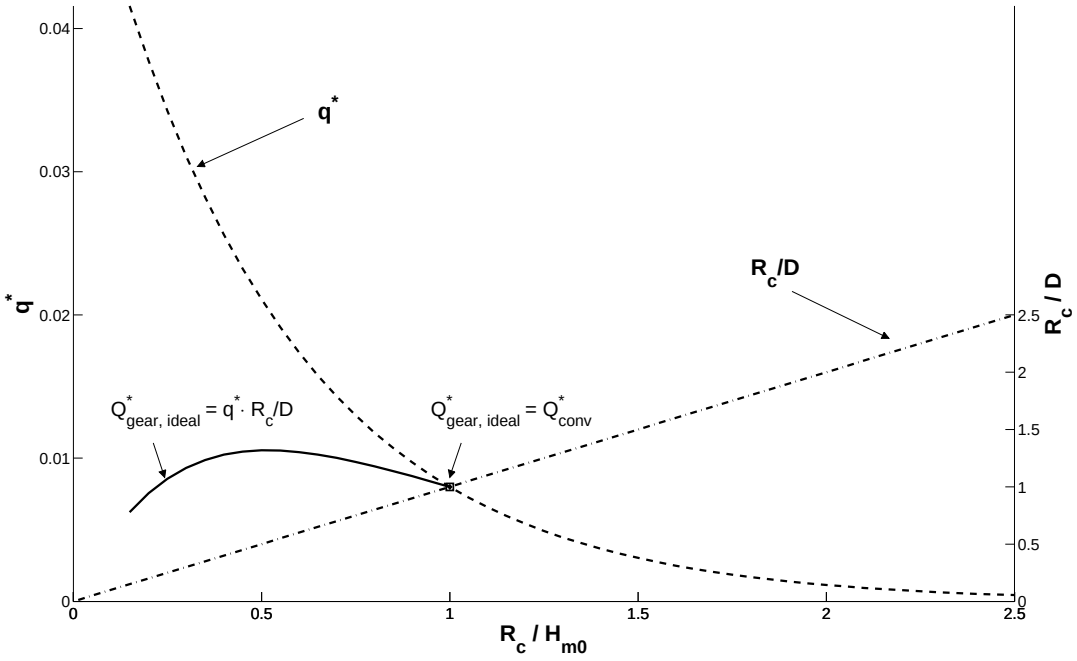

Figure 4.4: Optimizing overtopping rate using an ideal gearing system.

ear line represents the multiplication factor of the gear ratio. Based on these same conditions and for a power take-off system height of $D = 1\ m$ height (same as the conventional case), the solid line which is the dashed and the dash-dot line multiplied, shows the ideal case of Q_{gear} as a function of the crest freeboard. Clearly there is a maximum at around 0.5 m which is more than 30% higher than Q_{conv}. There is also a wide range of crest freeboard values for which an improvement in overtopping is possible over conventional systems. Thus the ability of gearing systems to increase overtopping rates has been shown for ideal cases. Increased overtopping will still occur for more realistic transfer ratio and efficiency values albeit at reduced rates.

The extent of improved overtopping rates can be explored by varying the important parameters of power take-off reservoir height, crest freeboard, and significant wave height. The power take-off reservoir height can range from $R_c \cdot$ gear ratio on the high end to R_c on the low end. For any value less than R_c there is no need for

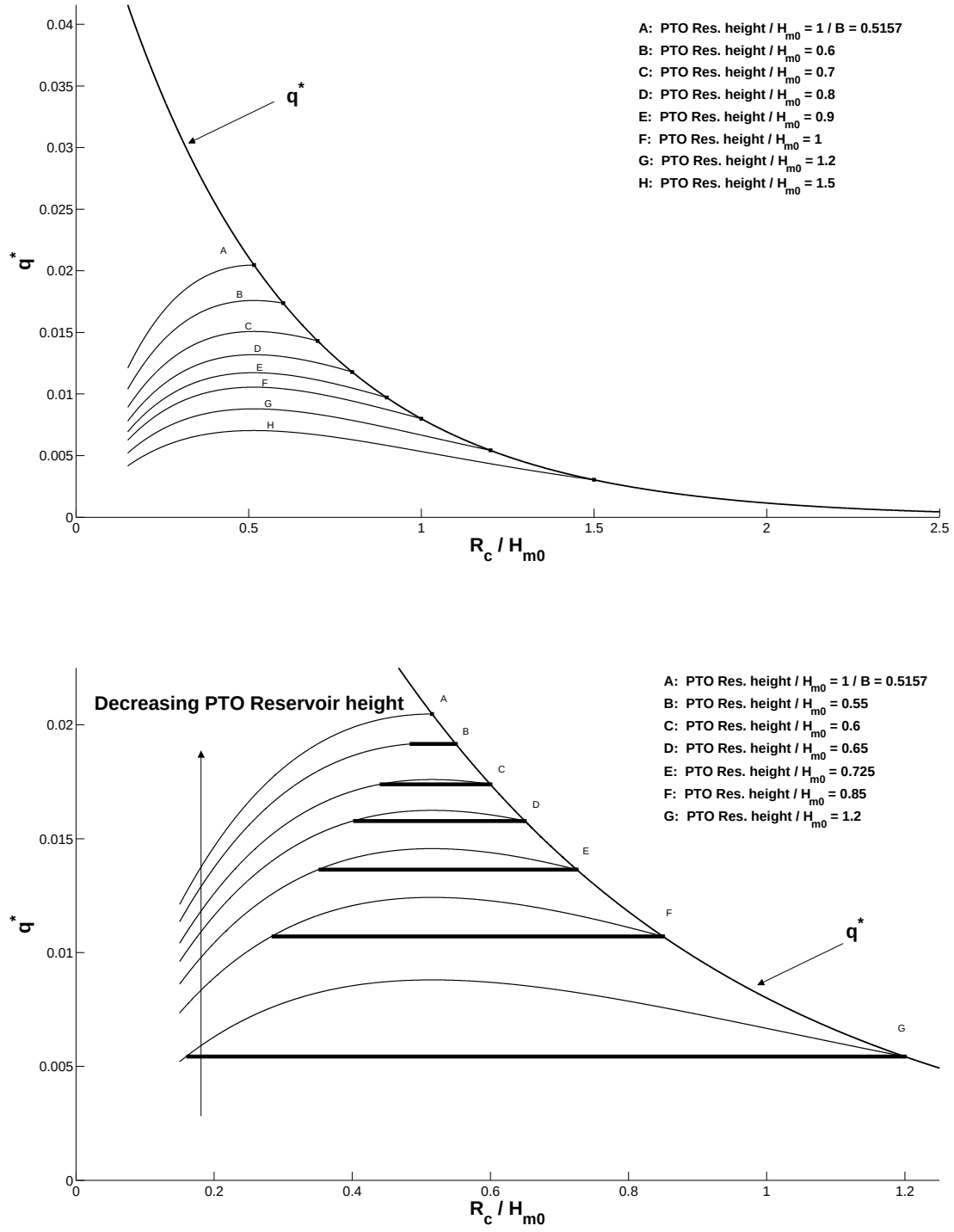

Figure 4.5: Optimizing curves for various power take-off reservoir heights for $H_{m0} = 1\,m$ (top). Effective crest freeboard range decreases as power take-off reservoir heights decrease shown here for $H_{m0} = 1\,m$ (bottom).

a gearing system. By lowering the power take-off reservoir height D from the upper limit, the non-dimensional overtopping rate q^* increases as shown in Figure (4.5). However the range of crest freeboard values for which the gearing system performs better than a conventional system narrows as well. This is also illustrated in the lower half of Figure (4.5) by the thick horizontal lines. The narrowing of this range continues until the PTO reservoir height of the gearing system has reduced to the optimal crest freeboard, $D = R_{c,opt}$. (The optimal crest freeboard will be defined and analyzed below). The maximum possible overtopping with a gearing system occurs at this value of D. In such a case there is no need for a gearing system and this represents the limit of reducing the gearing system back to the conventional system. Note that in this figure the plots do not extend to $R_c = 0$ which would represent the useless case of zero crest freeboard.

Under conditions where the PTO reservoir height D is fixed, for all values of $D \geq R_c$, there is a specific value for crest freeboard where the optimum overtopping rate occurs. It is also the value where the maximum possible overtopping as described above can occur. This value of crest freeboard may be determined analytically by operating on equation (4.4) for the volumetric rate of water flow into the PTO reservoir. In non-dimensional form this can be written as:

$$Q^*_{gear} = \exp\left(-\left(A + B\frac{R_c}{H_{m0}}\right)\right) \cdot \frac{R_c - J}{D + K} \cdot \eta \tag{4.6}$$

We are interested in the inflexion point of this equation, thus we must find the value

for R_c where $\frac{\partial Q^*_{gear}}{\partial R_c} = 0$.

$$\begin{aligned}
\frac{\partial Q^*_{gear}}{\partial R_c} &= \eta \exp(-A) \frac{\partial}{\partial R_c} \left(\exp\left(-B \cdot \frac{R_c}{H_{m0}} \right) \cdot \frac{R_c}{D+K} \right) \\
&= \eta \exp(-A) \left[-\frac{B}{H_{m0}} \cdot \exp\left(-B \cdot \frac{R_c}{H_{m0}} \right) \cdot \frac{R_c}{D+K} + \exp\left(-B \cdot \frac{R_c}{H_{m0}} \right) \cdot \frac{1}{D+K} \right] \\
&= \eta \exp(-A) \exp\left(-B \cdot \frac{R_c}{H_{m0}} \right) \cdot \frac{1}{D+K} \cdot \left[\frac{-B}{H_{m0}} \cdot R_c + 1 \right]
\end{aligned}$$

The above analysis shows that for maximum Q^*_{gear} for a given PTO reservoir height, the optimum value of R_c is given by:

$$R_{c,opt} = \frac{H_{m0}}{B} \tag{4.7}$$

This establishes a simple relationship between the optimum crest freeboard and the significant wave height. As shown in chapter 3 and Appendix C the factor of $1/B$ is a function of α, θ, and h_t/H_{m0}. For the range of the seabed slope variable θ and relative toe depth variable h_t/H_{m0} pertinent to our applications, $1/B$ is effectively constant. However this factor and therefore the optimum crest freeboard is not constant for seawall incline angle α. For our application range of α between 90 to 30 degrees, B_0 and equivalently B varies approximately linearly between the values 2.30 and 1.83, respectively. This tells us that for a given significant wave height, $R_{c,opt}$ is relatively small for a 90° vertical wall and increases approximately linearly as the seawall angle decreases to 30°.

Figure (4.6) shows a surface plot of idealized overtopping rates of optimized crest freeboard overtopping devices for varying seawall incline angle and varying power take-off reservoir heights. As expected the trends shows increasing Q as seawall angle decreases and also as PTO reservoir height decreases. More overtopping occurs for sloped walls than vertical walls. Also more overtopping occurs when the transfer ratio

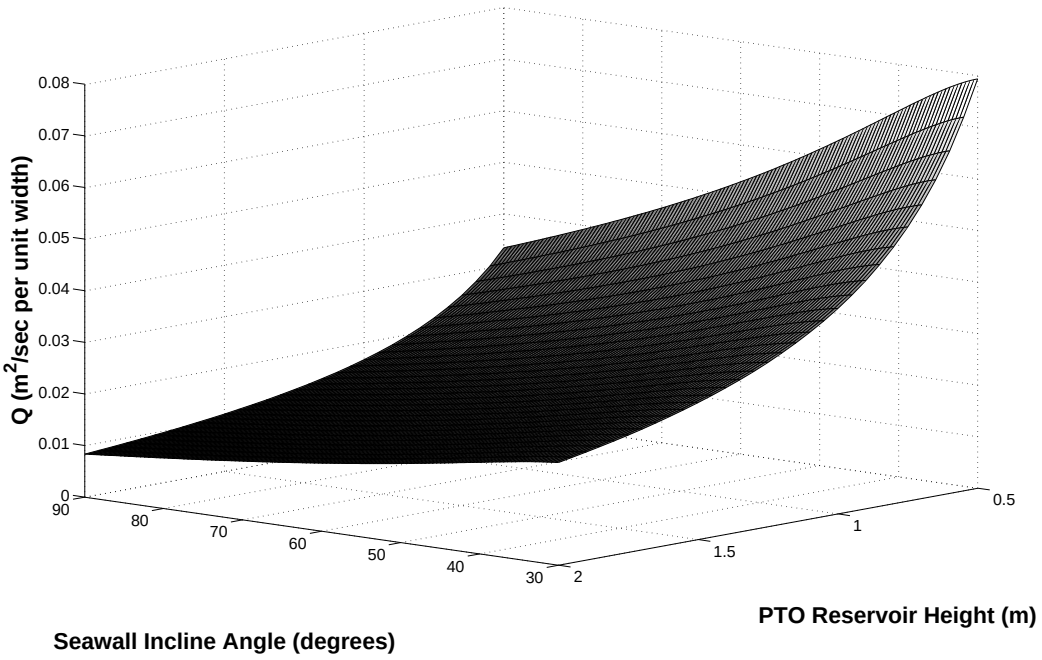

Figure 4.6: Optimum overtopping rate using an ideal gearing system for $H_{m0} = 1\,m$.

is larger due to smaller PTO reservoir height, D.

Table (4.1) shows selected values of the optimum volumetric overtopping flow rate from Figure (4.6). The numbers show that at this significant wave height a seawall of 30° incline angle gives over twice the overtopping rate of a vertical wall. Table (4.2) shows the percent improvement in overtopping due to the gearing system for these selected values over the corresponding values for a conventional system. The percent improvement is higher for the steeper seawall incline angles and larger values of power take-off reservoir heights. This is because under conditions of smaller overtopping such as these the gearing system becomes more effective.

The last important parameter to explore is the significant wave height. Using the optimum crest freeboard we can get an estimate of the limits on wave conditions where a gearing system may be useful. Equation (4.7) indicates that optimum crest freeboard increases linearly with the significant wave height. This is demonstrated in

Table 4.1: Optimized volumetric overtopping flow rate (m^2/sec per unit width) as a function of seawall incline angle and PTO reservoir height for an idealized gearing system for $H_{m0} = 1\,m$.

	PTO Reservoir Height (m)						
Angle (degrees)	0.5	0.75	1.00	1.25	1.50	1.75	2.00
30	0.0794	0.0531	0.0399	0.0319	0.0266	0.0228	0.0199
45	0.0661	0.0441	0.0331	0.0264	0.0220	0.0189	0.0165
60	0.0528	0.0352	0.0264	0.0211	0.0176	0.0151	0.0132
75	0.0423	0.0282	0.0211	0.0169	0.0141	0.0121	0.0106
90	0.0334	0.0223	0.0167	0.0134	0.0111	0.0095	0.0084

Figure (4.7). As before the decaying exponential curves are the seawall volumetric overtopping flow rate for the significant wave heights indicated. The short increasing curves represent overtopping with a gearing system. The squares indicate the optimum crest freeboard. There is a limit where the optimum crest freeboard height reaches the design height of the power take-off system. At this point and for higher values of significant wave height there is no benefit to using a gearing system rather than a conventional overtopping system.

Figure (4.8) shows this optimum crest freeboard as a function of significant wave height and seawall incline angle. The dependence on significant wave height is linear, while the dependence on seawall incline angle is approximately linear due to the behavior of B in the operating range of 30° to 90° as discussed earlier. Table (4.3) provides some selected numerical values for $R_{c,opt}$. As expected the optimum crest freeboard is greater at smaller values of seawall incline angle because the factor of $1/B$ is bigger at smaller angles than at larger angles.

Table 4.2: Percent improvement of the Table (4.1) overtopping rates over a conventional system for the same PTO reservoir height (equivalent to crest freeboard).

	PTO Reservoir Height (m)						
Angle (degrees)	0.5	0.75	1.00	1.25	1.50	1.75	2.00
30	0.00	5.68	25.14	58.06	107.96	181.44	288.81
45	0.00	8.30	31.89	71.33	131.84	222.67	358.45
60	0.04	11.60	40.06	87.49	161.44	274.97	449.01
75	0.37	15.30	49.01	105.41	194.96	335.64	556.83
90	1.03	19.69	59.53	126.81	235.89	411.65	695.61

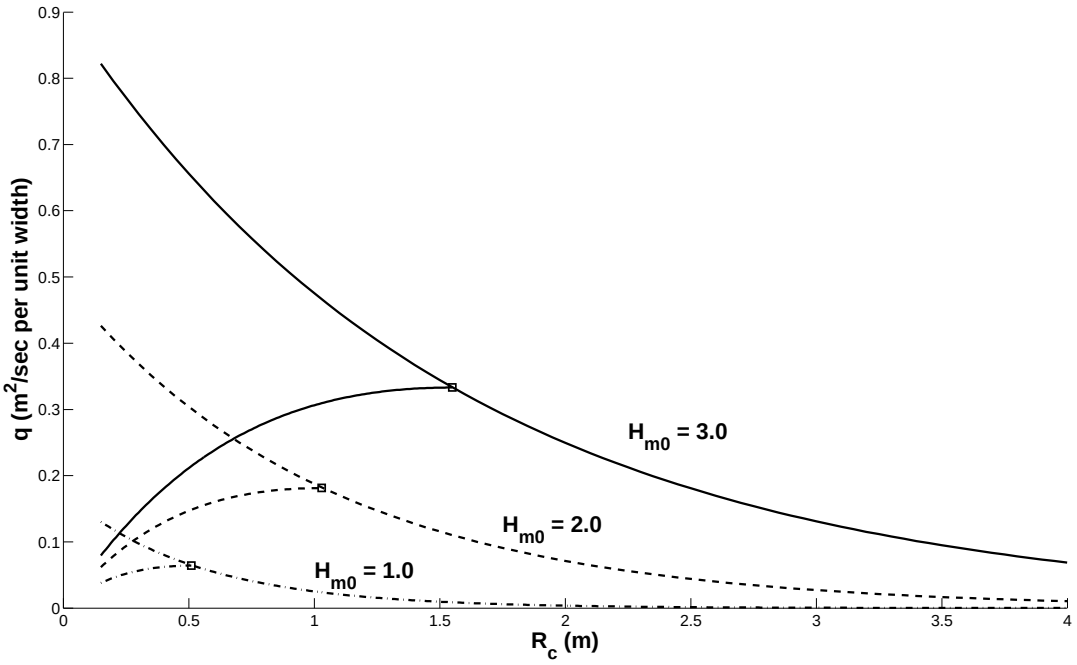

Figure 4.7: Dimensional plot showing the optimum crest freeboard dependence on significant wave height for a seawall incline angle of 45 degrees.

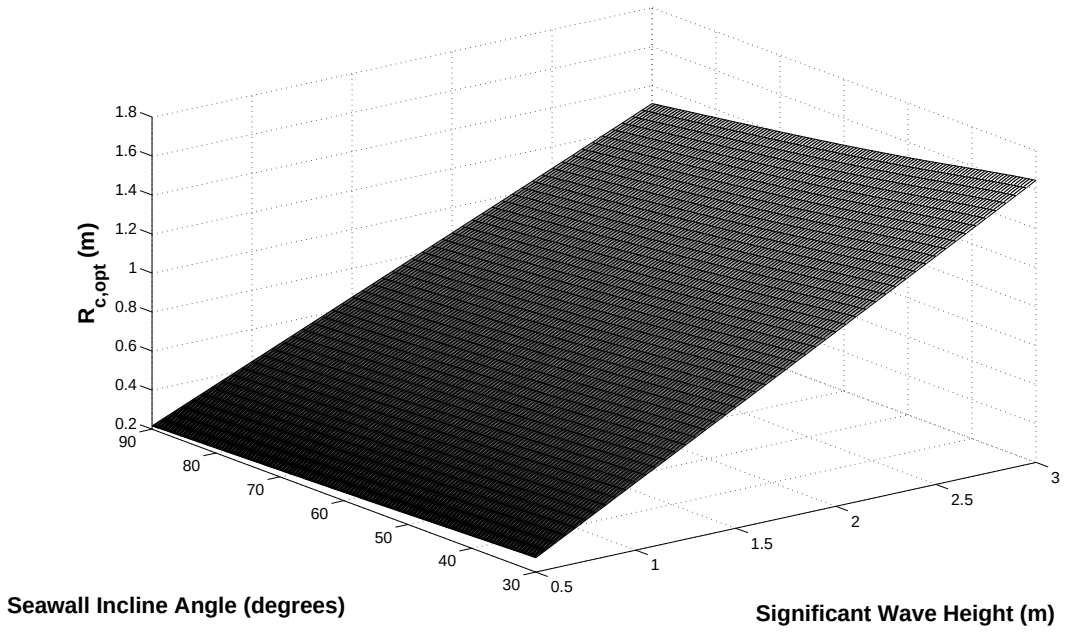

Figure 4.8: Optimum crest freeboard for varying significant wave height and varying seawall incline angle.

Table 4.3: Selected values of the optimum crest freeboard as a function of the significant wave height and the seawall incline angle.

	Significant Wave Height (m)					
Angle (degrees)	0.5	1.00	1.50	2.00	2.50	3.00
30	0.2737	0.5474	0.8211	1.0950	1.3700	1.6475
45	0.2579	0.5157	0.7736	1.0317	1.2907	1.5522
60	0.2428	0.4856	0.7284	0.9714	1.2154	1.4616
75	0.2297	0.4594	0.6892	0.9191	1.1498	1.3828
90	0.2174	0.4348	0.6522	0.8697	1.0881	1.3086

4.1.4 Influence of Transfer Ratio

Now we will look at the parameters that affect the transfer ratio, T. As seen from equation (4.4) and Figure (4.3) T is dependent on the crest freeboard R_c, the depths of the transfer reservoirs J and K, and the height of the power take-off reservoir D. To limit the parameter space we will only consider cases where $J = K$. Now, assuming the crest freeboard is specified (recommended to be at $R_{c,opt}$) we can determine T as a function of J and D. The range for J is $[0 < J < \frac{1}{2}R_c]$ where $J = 0$ represents the ideal case described above. For D, the lower limit is R_c because there is no point to use a gearing system below $D = R_c$ and the upper limit is theoretically infinity however in practice it should be approximately $5R_c$, so $[R_c < D < 5R_c]$.

Figure (4.9) shows the surface plot of T for non-dimensional values of the transfer

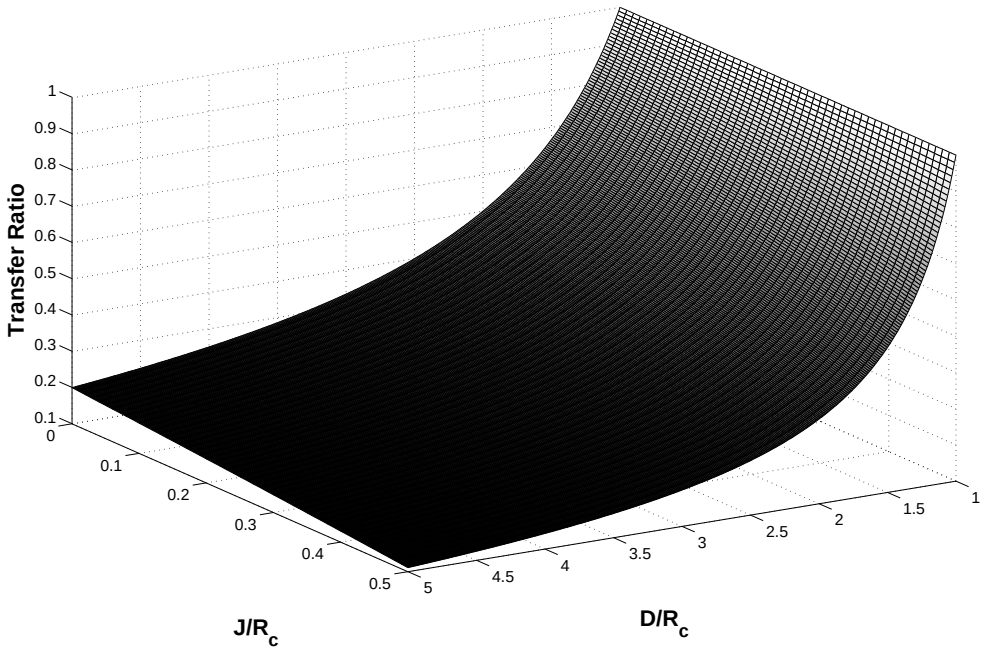

Figure 4.9: Transfer ratio for cases where both transfer reservoirs have the same depth, for cases where $J = K$.

reservoir depths and the power take-off reservoir heights. It shows the transfer ratio

has an inverse-like relationship with D and decreases more quickly for larger J. Also as expected, the transfer ratio also decreases as J increases and does so at larger rates as D increases.

4.1.5 Available Output Power

The available output power is determined by equation (3.1) from chapter 3. Since density ρ and gravity g are constant, the available output power is a function of volumetric overtopping rate Q and head H. We will approximate the head to be equal to the power take-off reservoir height D. The parameters we will look at are the

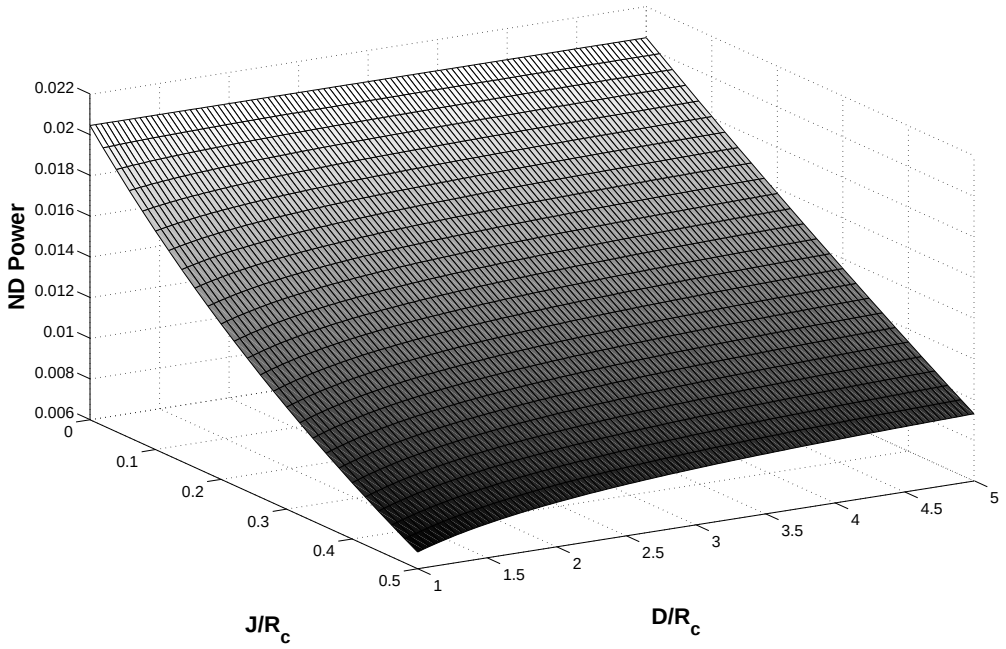

Figure 4.10: Available power output for cases where both transfer reservoirs have the same depth, and where $J = K$.

same as those for the transfer ratio. These are the non-dimensional depths of the transfer reservoirs J and K, and the height of the power take-off reservoir D. Again we will limit the parameter space by requiring $J = K$ and once again assume the

crest freeboard is equal to $R_{c,opt}$. Available output power has the additional factor of D (approximating for H) so now the behavior of the parameters are changed from that of the transfer ratio. Figure (4.10) shows the non-dimensional power as the parameters are varied. The power is non-dimensionalized by $\rho g\sqrt{gH_{m0}^3}R_{c,opt}$. The same range of parameters are used as in the transfer ratio figure. The power behaves similarly as the transfer ratio for varying J, which is smaller power for increasing J. This is because J only affects the power through the transfer ratio. However, power increases as D increases, unlike the transfer ratio. This increase is greater on the low end of the power take-off height range and level offs on the high end. The increase is more pronounced as J increases. The reason power increases for increasing D is because the effect of the additional multiplying factor of D overpowers the inverse-like effects of D in the transfer ratio.

4.2 Increased Capacity Factor

In this section we will look at the increase of the wave resource utilized by using a gearing system. Oftentimes small waves cannot be fully utilized by a conventional system because they have small wave heights and do not have enough energy to overtop the ramp.

The degree to which small waves are under-utilized is shown in Figure (4.11). For three values of power take-off reservoir heights the non-dimensional overtopping is shown as the significant wave height is varied. The dashed line represents the overtopping for conventional systems. The solid line represents the overtopping for gearing systems where the crest freeboard is continuously optimized as the significant wave height varies. Clearly the overtopping is larger for the gearing systems and reduces for increasing significant wave height until the optimized crest freeboard

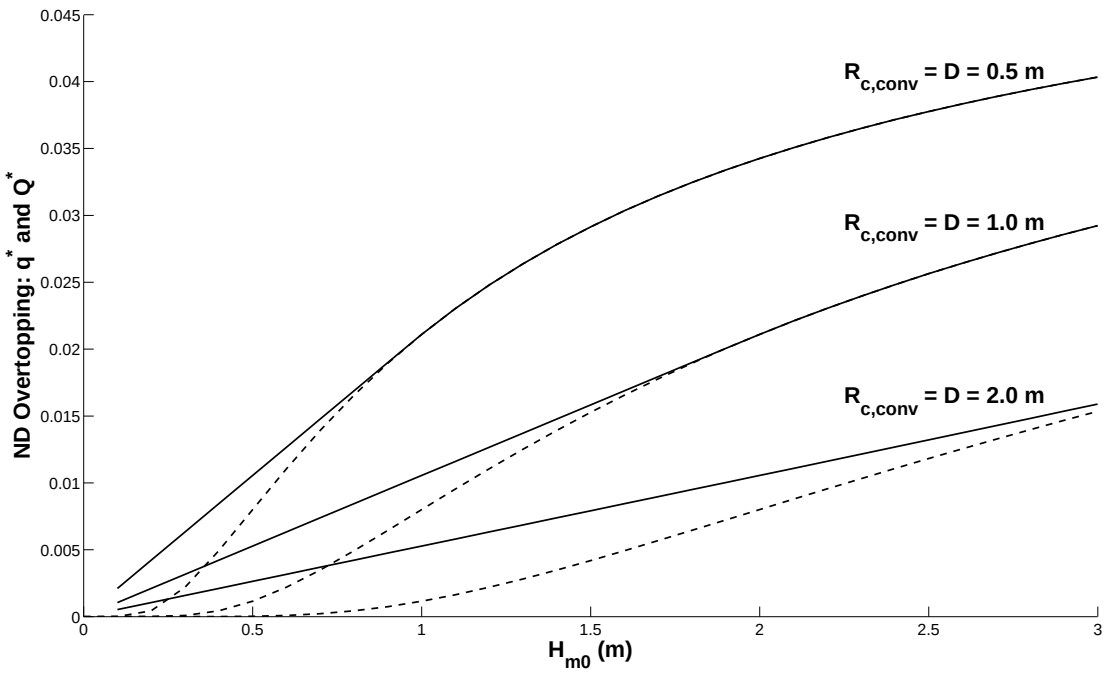

Figure 4.11: Ideal overtopping as a function of significant wave height for varying power take-off reservoir height, D. Solid line is the continuously optimized crest freeboard gearing system. Dashed line is the conventional system.

reaches the value of the power take-off reservoir height. As described earlier, at this point there is no benefit to having a gearing system.

Table (4.4) shows tabulated values of volumetric overtopping rate and Table (4.5) shows tabulated values of the percent increase of the overtopping for a continually optimized crest freeboard gearing system over a conventional system. These tables are useful for analyzing as an upper limit how much additional overtopping can be achieved at a specific location as the significant wave height varies. A simple gearing system with a fixed crest freeboard (not continually optimized) would still show increased overtopping though it would be less than this upper limit. Generally to maximize overtopping it is best to have the lowest PTO reservoir height allowable because as shown in Figure (4.4), though this is not true to maximize output power.

Table 4.4: Volumetric overtopping values (m^3/s) for a 45° incline angle seawall due to an optimized crest freeboard for an ideal gearing system.

	PTO Reservoir Height (m)						
H_{m0} (m)	0.5	0.75	1.00	1.25	1.50	2.00	2.50
0.50	0.0117	0.0078	0.0058	0.0047	0.0039	0.0029	0.0023
0.75	0.0322	0.0215	0.0161	0.0129	0.0107	0.0081	0.0064
1.00	0.0661	0.0441	0.0331	0.0264	0.0220	0.0165	0.0132
1.25	0.1121	0.0770	0.0577	0.0462	0.0385	0.0289	0.0231
1.50	0.1677	0.1214	0.0911	0.0729	0.0607	0.0455	0.0364
1.75	0.2318	0.1757	0.1339	0.1071	0.0893	0.0670	0.0536
2.00	0.3035	0.2382	0.1869	0.1496	0.1247	0.0935	0.0748
2.25	0.3823	0.3082	0.2485	0.2009	0.1674	0.1256	0.1005
2.50	0.4676	0.3852	0.3174	0.2615	0.2180	0.1635	0.1308
2.75	0.5591	0.4689	0.3933	0.3298	0.2770	0.2078	0.1662
3.00	0.6565	0.5589	0.4757	0.4050	0.3447	0.2587	0.2069
3.25	0.7597	0.6549	0.5646	0.4867	0.4196	0.3167	0.2534
3.50	0.8684	0.7568	0.6596	0.5748	0.5010	0.3823	0.3058
3.75	0.9825	0.8644	0.7606	0.6692	0.5888	0.4559	0.3647
4.00	1.1020	0.9777	0.8675	0.7696	0.6828	0.5375	0.4304
4.25	1.2268	1.0965	0.9801	0.8761	0.7831	0.6256	0.5033
4.50	1.3568	1.2208	1.0985	0.9884	0.8894	0.7201	0.5839

4.3 Power Take-off System

Both the Wave Dragon and the Seawave Slot-Cone Generator use or anticipate using Kaplan turbines for their power take-off systems. The Kaplan turbine is categorized as a reaction turbine in which the working fluid completely fills the passageways of the water flow. The angular momentum, pressure, and velocity of the fluid decrease as the turbine rotor extracts energy from the fluid. Reaction turbines are the turbine of choice widely used throughout the world in high-flow, low-head power production.

As shown in Figure (4.12), Kaplan turbines are an inward flow reaction turbine

Table 4.5: Selected values of the percent increase of overtopping for a 45° incline angle seawall due to an optimized crest freeboard for an ideal gearing system.

	PTO Reservoir Height (m)						
H_{m0} (m)	0.5	0.75	1.00	1.25	1.50	2.00	2.50
0.50	31.89	131.84	358.45	867.01	2024.70	10977.86	61508.79
0.75	3.66	31.89	88.79	188.25	358.45	1152.42	3549.55
1.00	0.00	8.30	31.89	71.33	131.84	358.45	867.01
1.25	0.00	1.21	11.87	31.89	61.98	163.85	358.45
1.50	0.00	0.00	3.66	14.57	31.89	88.79	188.24
1.75	0.00	0.00	0.55	6.11	16.64	52.23	111.92
2.00	0.00	0.00	0.00	1.99	8.29	31.87	71.28
2.25	0.00	0.00	0.00	0.28	3.65	19.58	47.15
2.50	0.00	0.00	0.00	0.00	1.19	11.80	31.76
2.75	0.00	0.00	0.00	0.00	0.15	6.79	21.46
3.00	0.00	0.00	0.00	0.00	0.00	3.56	14.34
3.25	0.00	0.00	0.00	0.00	0.00	1.58	9.34
3.50	0.00	0.00	0.00	0.00	0.00	0.47	5.83
3.75	0.00	0.00	0.00	0.00	0.00	0.03	3.38
4.00	0.00	0.00	0.00	0.00	0.00	0.00	1.73
4.25	0.00	0.00	0.00	0.00	0.00	0.00	0.69
4.50	0.00	0.00	0.00	0.00	0.00	0.00	0.15

combining radial and axial features. The fluid flows through the inlet guide vanes and achieves a tangential velocity in a vortex motion before it reaches the propeller shaped runner which spins the rotor [30]. This produces shaft power to run a generator producing electrical power for the electrical grid. Both the inlet guide vanes and the turbine blades are adjustable so their angles can be set to produce the best match for the specific operating conditions. This allows for efficient operation over a range of flow conditions as the flowrate varies or as the available head may vary from season to season. Kaplan turbine efficiencies are typically over 90% but may decrease in very low head applications. Generally, Kaplan turbines are individually designed to

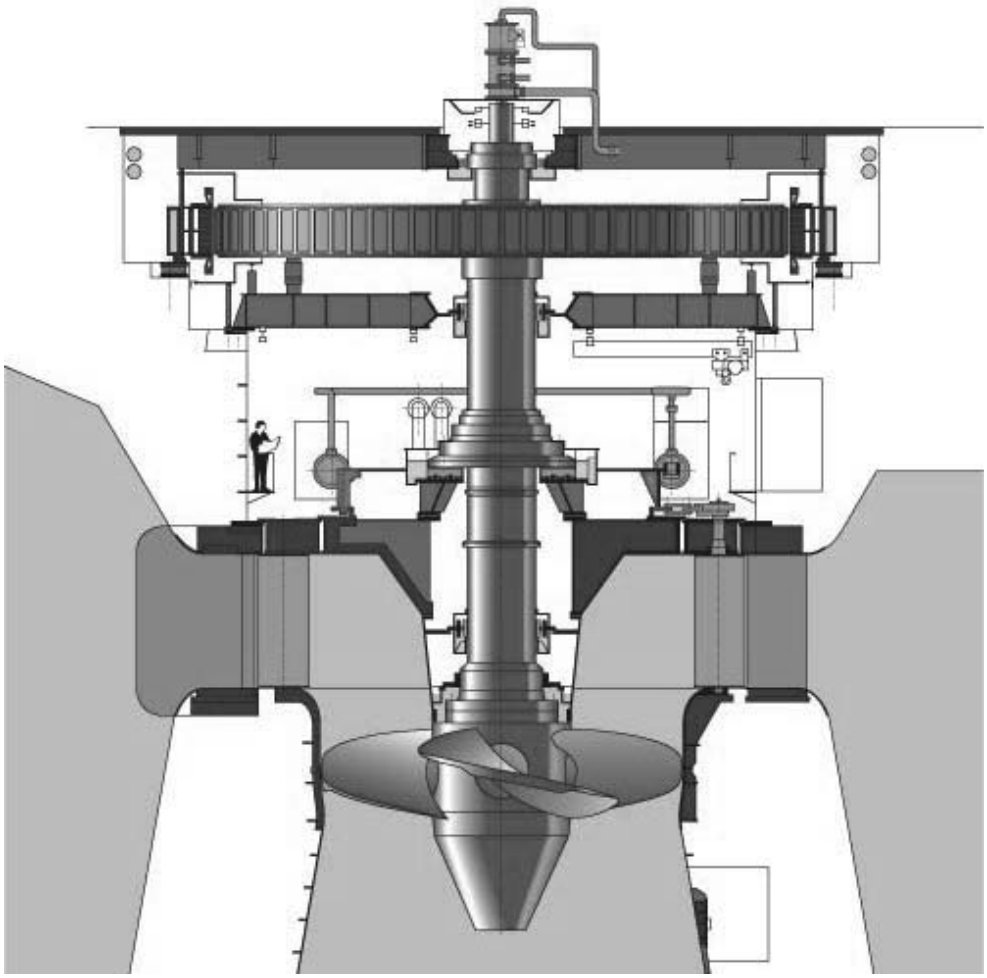

Figure 4.12: Kaplan Turbine schematic.

operate at a specific site and are costly to design, manufacture and install, but operate for decades.

Figure (4.13) is an industrial chart showing the range of conditions for which a Kaplan turbine may operate. This serves as a guide to the level of overtopping flow rates and operating head required by Kaplan turbines. We note that the Wave Dragon turbines have a minimum operating head of 0.4 m however the corresponding minimum flow rate and efficiency are unknown. The lowest operating head on the chart is at 1 m and the minimum volumetric water flowrate at that head is about

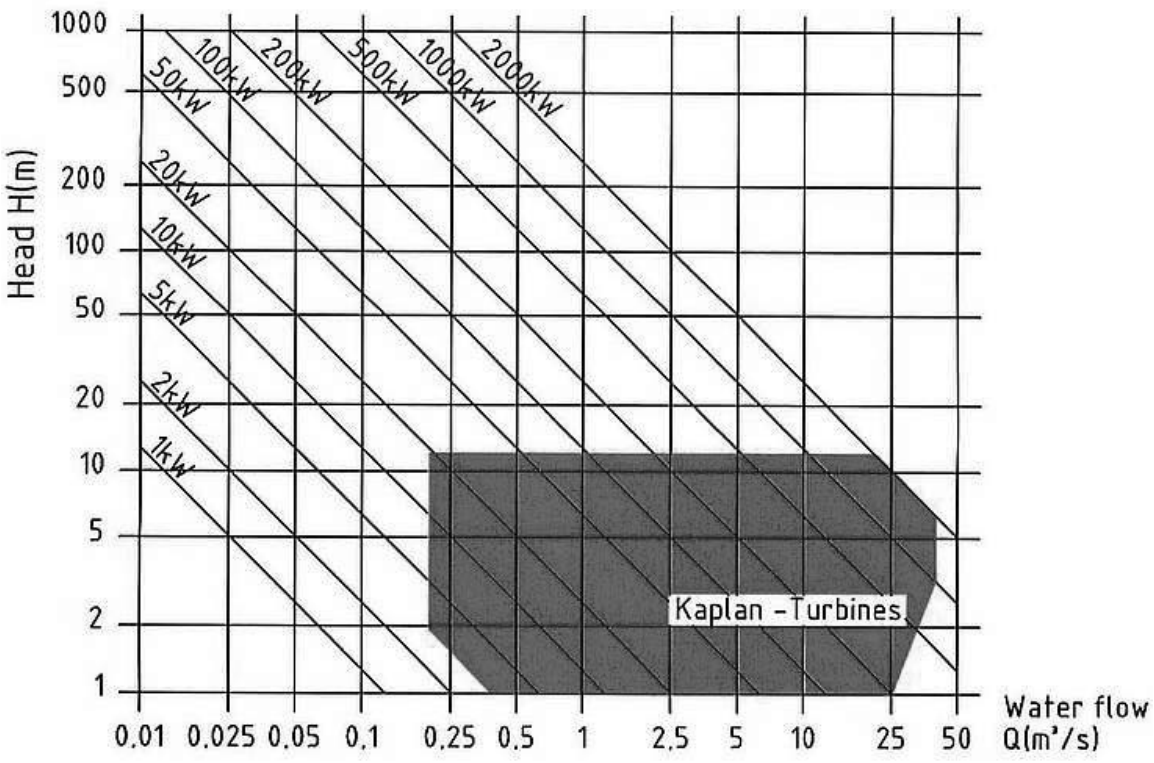

Figure 4.13: Industrial chart for Kaplan Turbine application range.

0.35 m^3/s. At this minimum head height the minimum volumetric overtopping rate is difficult to achieve even for fully optimized crest freeboards of devices with idealized gearing systems. The values from Table (4.4) show that a significant wave height of approximately 2.75 m is necessary for a 45° incline angle seawall. This is quite a large significant wave height and larger than can be expected in many parts of California as shown in Table (2.1).

This brings up the issue of continuous operation versus intermittant operation. A continously operating power generating source is preferable because it is more efficient and easier to integrate the power to the electrical system. However, when the wave conditions are not sufficient to supply the minimum flow rate to the turbine the power take-off system must be stopped and water must be allowed to accumulate in

the reservoir. Intermittant operation will surely need to occur at some point for all devices operating in California. Table (2.2) shows that the minimum significant wave height for most of the buoys drops below 1 m for all the months during the year. The flow rate for such wave conditions will most certainly be less than the minimum flow rate of any Kaplan turbine.

Both the Wave Dragon and the Seawave Slot-Cone Generator have attempted to optimize their devices for intermittant operation. The Wave Dragon is working on a control scheme to time the opening and closing of the turbines in conjunction with the water level of the reservoir to maximize power output. This is necessary because the Wave Dragon is limited in its reservoir size as it is an offshore device. This work is still in development as described in section (3.3.1). The SSG will rely on its Multi-Stage Turbine to limit the number of start/stop sequences by supplying water to the turbine from its various reservoirs as necessary. The MST is as yet untested and still in development.

The power take-off system for devices off the coast of California will need to account for several variables. The consistency and magnitude of the volumetric overtopping rate and the intended application will largely influence the character of power take-off. For low wave environments it may be advantageous to utilize a large reservoir and store the overtopping volume for long time periods and release it during periods of high demand. This option can function as a backup source of power when existing power sources are fully utilized. For high, consistent wave environments the power output can contribute in regular intervals to the base electrical power system. Other applications may require nightime power for lighting sothe overtopping volume can be stored during the day and the power can be output throughout the night. Based on the variables discussed an optimizing strategy for power take-off should be developed specific to the local wave environment at a given location.

4.4 Device Operation

Now the sequence of steps for the device operation will be given. At the start configuration the overtopping water collection reservoir and the transfer reservoir of Figure (4.2) are positioned as in the right hand side of Figure (4.3). The overtopping water collection reservoir is empty and the transfer reservoir is full. As time progresses the incoming waves will overtop the ramp and spill into the collection reservoir. Once enough water has been accumulated the weight of the volume of water in the collection reservoir will overcome the weight of the water in the transfer reservoir multiplied by the gear ratio. The gearing system will function to raise the transfer reservoir up to the height of the power take-off reservoir and the collection reservoir will lower to the calm water surface.

At this point the transfer reservoir will empty its contents into the power take-off reservoir. Following this, the collection reservoir will empty its contents to the calm water surface. Emptying these reservoirs should be done in a time-efficient manner with minimal spillage. At this point the empty reservoirs will return to their initial positions and the open gates to the reservoir will be closed. The weight of the transfer reservoir must be sufficiently greater than the collection reservoir to return to the start positions but this weight differential should be effectively negligible relative to the reservoirs' weight when fully loaded with water. The time spent during the emptying phase of the overall sequence reduces the time which the overtopping water is collected. The reservoirs should be designed to reduce this inefficiency as much as possible.

This processes of transferring the low-head water of small waves into the higher head of the power take-off reservoir will continue at the rate dictated by the wave environment. The rate of power take-off via emptying the power take-off reservoir through the Kaplan turbines is dictated by the chosen strategy for power take-off.

4.5 Additional Considerations

The overtopping device considered in this thesis is a preliminary design and uses a simply shaped ramp for ease in analysis of volumetric overtopping rate. Therefore it is amenable to design improvements for increased overtopping. The option of implementing reflector arms like the Wave Dragon can be explored. It is reasonable to expect similar levels of improvement because both devices are of the wave overtopping type. Likewise the shape of the ramp can likely also be designed with beneficial features, in a manner like the Wave Dragon, for better overtopping.

Another possible approach to increase the power output of this device is to incorporate the multiple tiered reservoir concept of the Seawave Slot-cone Generator. This hybrid style approach would capture energy from the small waves through the gearing system and utilize the tiered reservoirs for the large waves. This could potentially address the issue that the gearing system is ineffective for large waves. Further consideration is needed to determine how to accomodate the both the gearing system and the additional reservoirs.

This page intentionally left blank.

Chapter 5

Application of Concept

The proposed gearing system concepts of chapter 4 will be applied to California's wave environment in this chapter. The datasets from chapter 2 are used for the wave conditions and the resulting energy outputs are provided. The potential improvement on an annual basis by using a gearing system will be shown to vary by location. Starting from southern California to northern California, the gearing system shows great potential improvement to no improvement over a conventional system. The seasonal variation will be highlighted by comparing the average power output of the two systems month-by-month for each location. This demonstrates the more consistent power output for gearing systems.

5.1 Applied to California's Wave Resource

The following procedure outline was applied for each location to determine the results below. We begin with the NOAA buoy data over the past 10 years to get a histogram of the significant wave heights. We fit this histogram with a log-normal distribution and obtain the log-normal probability distribution function. The pro-

posed device concepts require nearshore siting so the wave data must be propagated from the buoy location in deepwater to a nearshore location of depth 10 m. The Goda formulas [16] are applied for this task and we again obtain a log-normal PDF of the nearshore significant wave height. The peak of this PDF will be used as the design wave height for determining the optimal crest freeboard, $R_{c,opt}$. Based on this value the overtopping rate and the power output for the gearing system and the conventional system are computed. A similar procedure is used to compute the monthly output. In this case the starting data is the average monthly significant wave height as provided in Table (2.2). In all gearing system computations the transfer reservoir depths are 0.25 m ($J = K = 0.25\,m$) or equal to $\frac{1}{2}R_{c,opt}$ for cases when $R_{c,opt} < 0.5\,m$. The power take-off reservoir height is at $5R_{c,opt}$ m. The computations for the conventional system assume the power take-off is optimal for 2.0 m PTO heights. These parameters are chosen to compare maximum power outputs for the two systems.

The log-normal distribution is a probability distribution of a random variable X whose logarithm is normally distributed. Empirically this distribution fits our 10-year datasets of significant wave height the best. The formula for the log-normal probability distribution function is:

$$f(x) = \frac{1}{x\sigma\sqrt{2\pi}} \exp\left(-\frac{(\ln x - \mu)^2}{2\sigma^2}\right), \quad x > 0 \tag{5.1}$$

The log-normal parameters μ and σ are:

$$\mu = \ln\left(\mathrm{E}[X]\right) - \tfrac{1}{2}\ln\left(1 + \frac{\mathrm{Var}[X]}{\mathrm{E}[X]^2}\right) \tag{5.2}$$

$$\sigma^2 = \ln\left(1 + \frac{\mathrm{Var}[X]}{\mathrm{E}[X]^2}\right) \tag{5.3}$$

where $\mathrm{E}[X]$ is the expected value and $\mathrm{Var}[X]$ is the varience.

As explained above, the Goda formulas are used to propagate the wave informa-

tion from the buoys located many nautical miles offshore to the nearshore locations where the devices will operate. In practice, more precise significant wave height information at the toe of the structure should be used. If nearshore wave data cannot be taken or is unavailable, it is necessary to conduct a more detailed analysis of wave propagation to nearshore using a powerful, computationally-expensive tool such as SWAN. As described in section (2.5) many coastal processes can occur and influence the nearshore wave environment, so for project design accurate information will be essential. However, for the purposes of this thesis the initial approximations provided by the Goda formulas and linear theory are satisfactory.

The Goda formulas are given in terms of $H_{1/3}$ which we use as an approximate value for H_{m0}.

$$H_{1/3} = \begin{cases} K_s H_0^{'} & : \quad h/L_0 \geq 0.2 \\ \min\left((\beta_0 H_0^{'} + \beta_1 h), \beta_{max} H_0^{'}, K_s H_0^{'}\right) & : \quad h/L_0 < 0.2 \end{cases} \tag{5.4}$$

The parameters β_0, β_1, and β_{max} are given as:

$$\beta_0 = 0.028 \left(\frac{H_0^{'}}{L_0}\right)^{-0.38} \cdot \exp(20 \tan^{1.5}(\theta)) \tag{5.5}$$

$$\beta_1 = 0.52 \exp(4.2 \tan(\theta)) \tag{5.6}$$

$$\beta_{max} = \max\left(0.92, 0.32 \left(\frac{H_0^{'}}{L_0}\right)^{-0.29} \cdot \exp(2.4 \tan(\theta))\right) \tag{5.7}$$

In these equations $H_0^{'}$ is the deepwater significant wave height, L_0 is the corresponding deepwater wavelength, K_s is the shoaling coefficient, and θ is once again the seabed slope.

The information provided by the buoy data will be used for $H_0^{'}$ and L_0. To get the wavelength we use linear theory and following the literature [14] assume a linear relationship between significant wave height and wave period of $T_0 = 1.4H_0^{'} + 4.2$.

Knowing the period and using the deepwater dispersion relationship, equation (2.8), we obtain the wavelength as:

$$L_0 = \frac{gT_0^2}{2\pi} \tag{5.8}$$

Shoaling is a special case of the coastal process of refraction for normal waves across straight, parallel depth contours. We approximate the shoaling coefficient based on work by Folley, et.al [15]. They used SWAN to investigate the transformation of sea-states from deepwater ($> 50\,m$) to nearshore ($10\,m$). Their test run for a seabed slope of $1:500$ shows an approximately 25% reduction of energy. For a traditional wave energy formulation this corresponds to a nearshore significant wave height of 86% that of the offshore significant wave height. This value for the shoaling coefficient K_s is within the range given by Goda and agrees closely with that predicted by linear theory [39] for the range of wave frequency and water depth considered here.

The seabed slope is assumed to vary linearly with angle θ approximated using the buoy depth and distance to shore information. Table (5.1) shows that on this basis the slope is effectively zero.

Table 5.1: Approximate Seabed Slope Angle, θ.

Buoy	Station name	Depth (m)	Dist. to shore (NM)	θ (rad)
46006	SE PAPA	4023	600	0.0036
46022	Eel River	631	17	0.0200
46014	Pt. Arena	274	19	0.0078
46026	San Francisco	52	18	0.0016
46023	Pt. Arguello	384	17	0.0122
46053	Santa Barbara	450	12	0.0202
46025	Santa Monica	882	33	0.0144
46086	San Clemente	1895	25	0.0409

5.1.1 Buoy 46086: Near San Clemente Basin, CA

The San Clemente Basin area at the southern end of the California coast features a low to moderate wave climate suitable for the concepts proposed in chapter 4. Figure (5.1) presents the histogram of the past 10 years of data for significant wave height for Buoy 46086. The log-normal probability distribution function is superimposed over the histogram. Figure (5.2) presents the nearshore log-normal PDF after the wave environment has been propagated to near shore via the Goda formulas. The optimal crest freeboard $R_{c,opt}$ of 0.58 m is computed from the peak in the nearshore log-normal PDF of 1.12 m. Using this PDF and $R_{c,opt}$ the gearing system overtopping is computed for a power take-off reservoir height of $5R_{c,opt}$ m. That along with the conventional overtopping for a crest freeboard of 2.0 m is also shown on the figure. Figure (5.3) shows the improvement in power output by using a gearing system versus a conventional system. For this location there is much improvement throughout the year except the winter months and early spring.

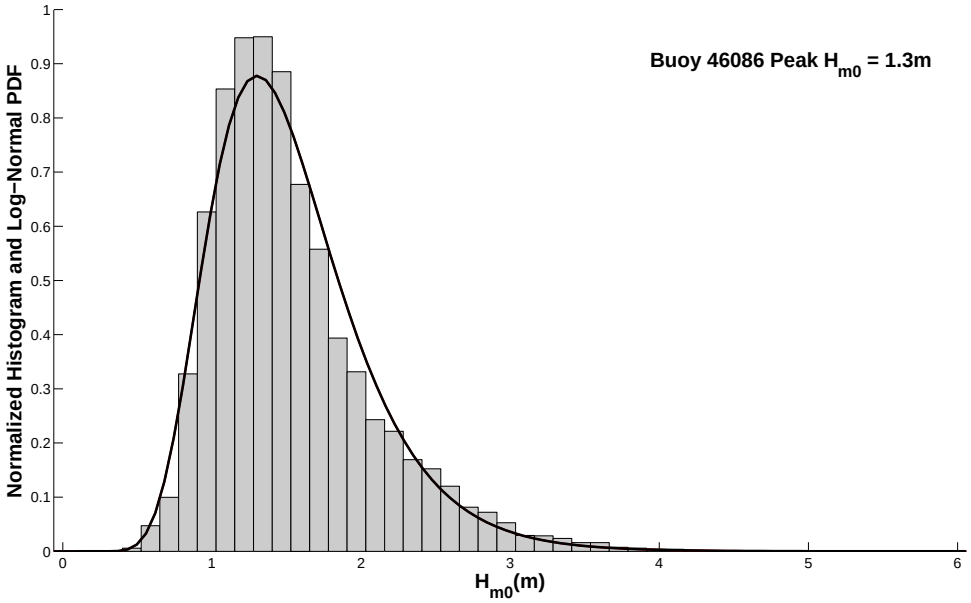

Figure 5.1: Buoy 46086: Histogram of significant wave heights for the past 10 years.

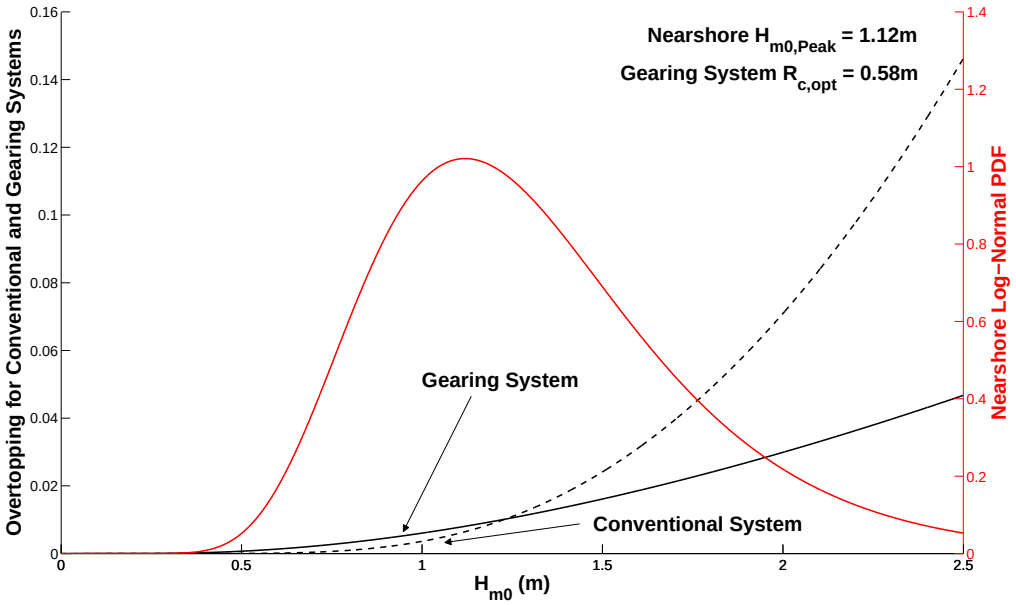

Figure 5.2: Buoy 46086: Nearshore PDF for H_{m0} and overtopping rates.

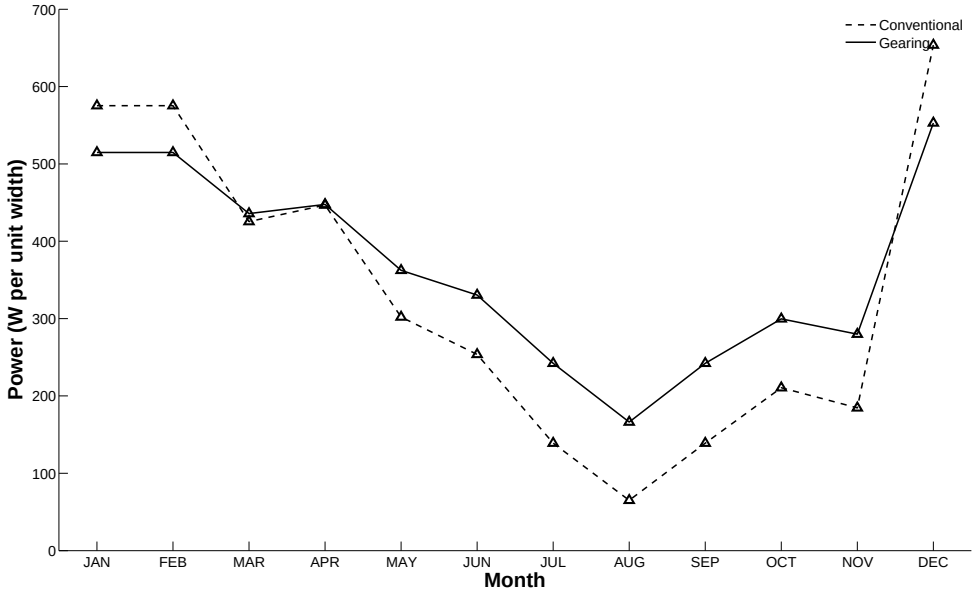

Figure 5.3: Buoy 46086: Average power available for output per month.

5.1.2 Buoy 46025: Near Santa Monica, CA

The Santa Monica location in southern California has the lowest wave climate and is extremely well suited for the concepts proposed in chapter 4. Figure (5.4) presents the histogram of the past 10 years of data for significant wave height for Buoy 46025. The log-normal probability distribution function is superimposed over the histogram. Figure (5.5) presents the nearshore log-normal PDF after the wave environment has been propagated to near shore via the Goda formulas. The optimal crest freeboard $R_{c,opt}$ of 0.43 m is computed from the peak in the nearshore log-normal PDF of 0.84 m. Using this PDF and $R_{c,opt}$ the gearing system overtopping is computed for a power take-off reservoir height of 2.0 m. That along with the conventional overtopping for a crest freeboard of 2.0 m is also shown on the figure. Figure (5.6) shows the improvement in power output by using a gearing system versus a conventional system. For this location there is great improvement throughout the whole year.

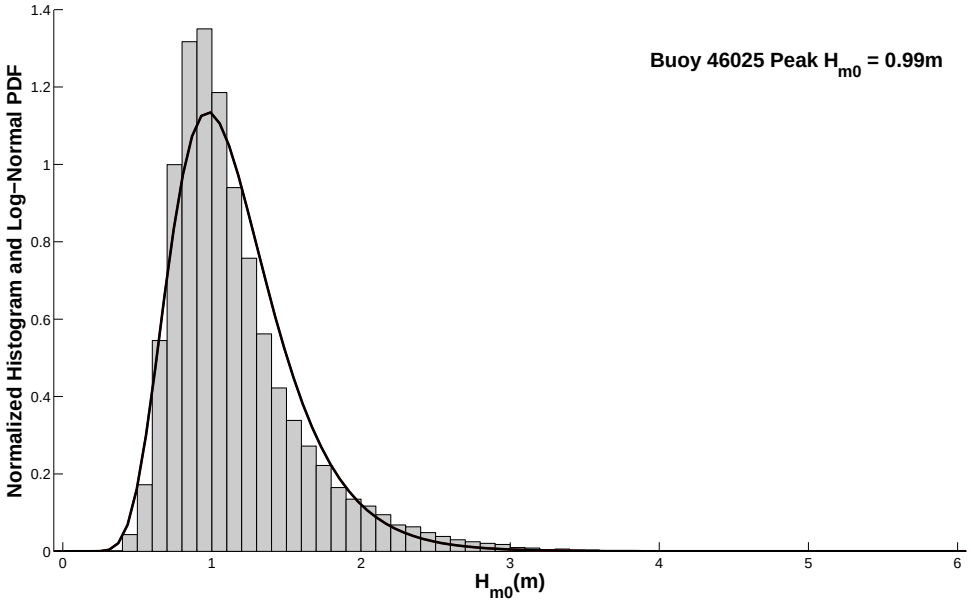

Figure 5.4: Buoy 46025: Histogram of significant wave heights for the past 10 years.

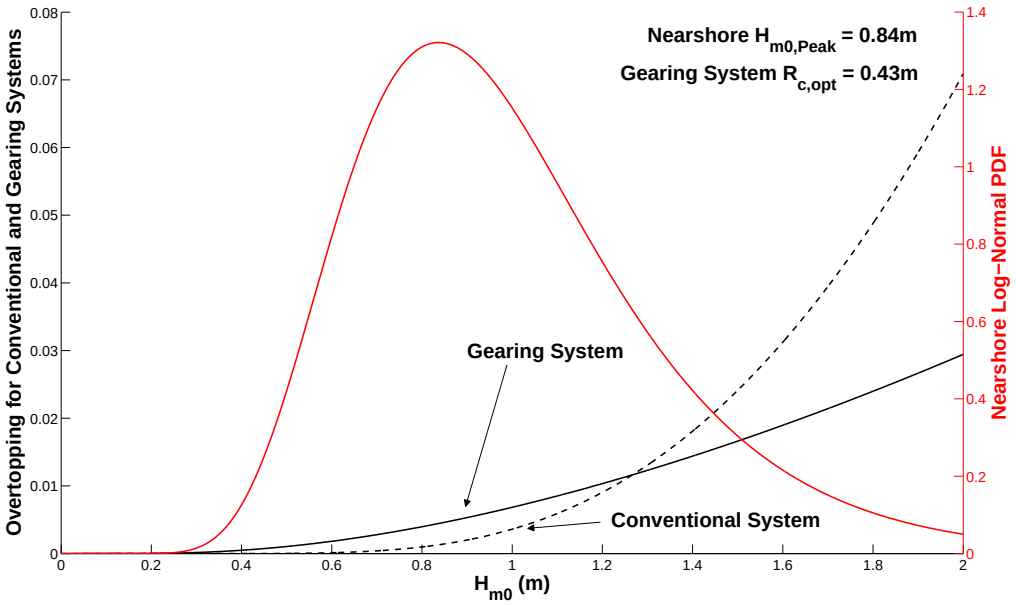

Figure 5.5: Buoy 46025: Nearshore PDF for H_{m0} and overtopping rates.

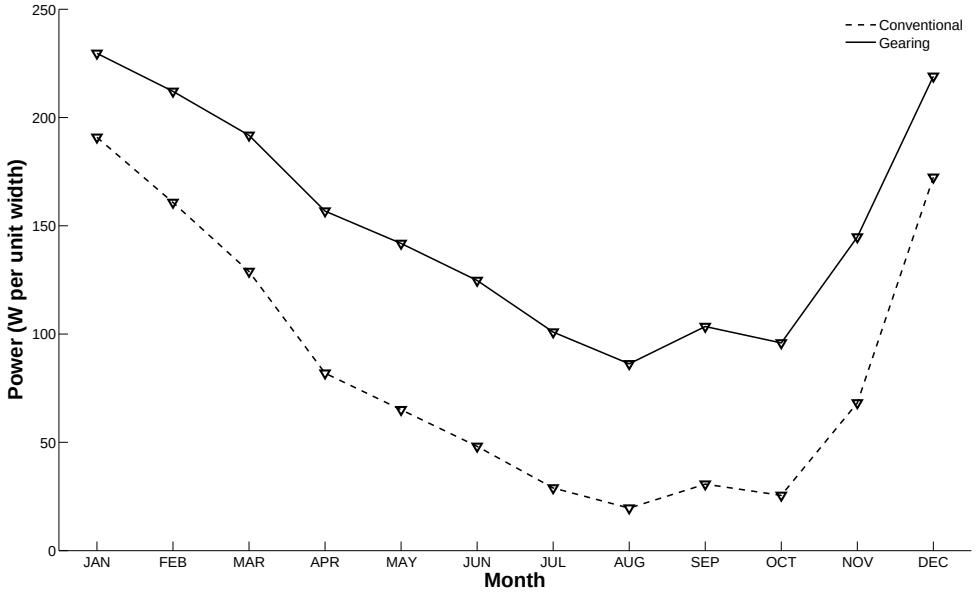

Figure 5.6: Buoy 46025: Average power available for output per month.

5.1.3 Buoy 46053: Near Santa Barbara, CA

The Santa Barbara location in southern California has the second lowest wave climate is well suited for the concepts proposed in chapter 4. Figure (5.7) presents the histogram of the past 10 years of data for significant wave height for Buoy 46053. The log-normal probability distribution function is superimposed over the histogram. Figure (5.8) presents the nearshore log-normal PDF after the wave environment has been propagated to near shore via the Goda formulas. The optimal crest freeboard $R_{c,opt}$ of 0.44 m is computed from the peak in the nearshore log-normal PDF of 0.86 m. Using this PDF and $R_{c,opt}$ the gearing system overtopping is computed for a power take-off reservoir height of 2.0 m. That along with the conventional overtopping for a crest freeboard of 2.0 m is also shown on the figure. Figure (5.9) shows the improvement in power output by using a gearing system versus a conventional system. For this location there is much improvement throughout the year except for December and in January and February the power outputs are very close.

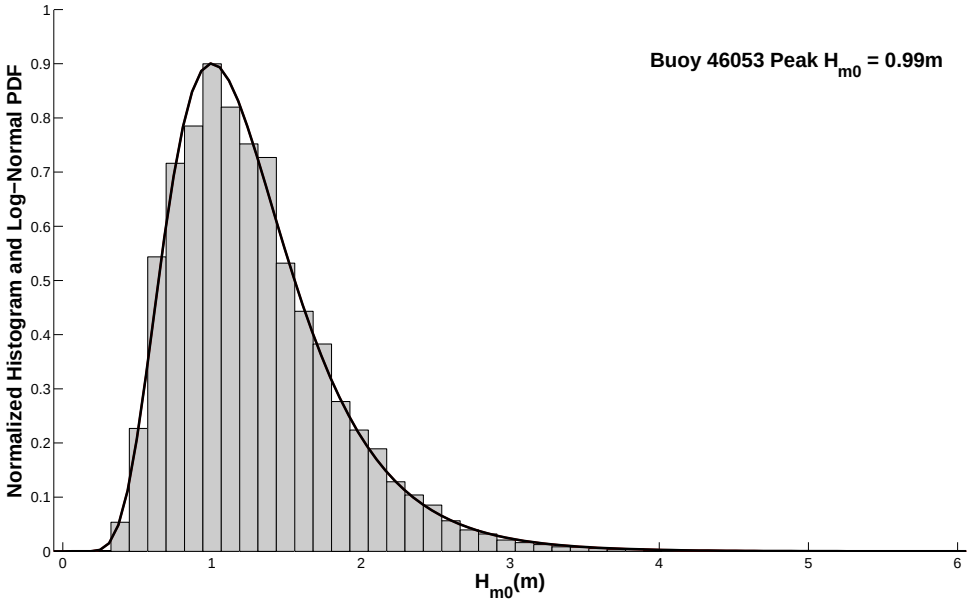

Figure 5.7: Buoy 46053: Histogram of significant wave heights for the past 10 years.

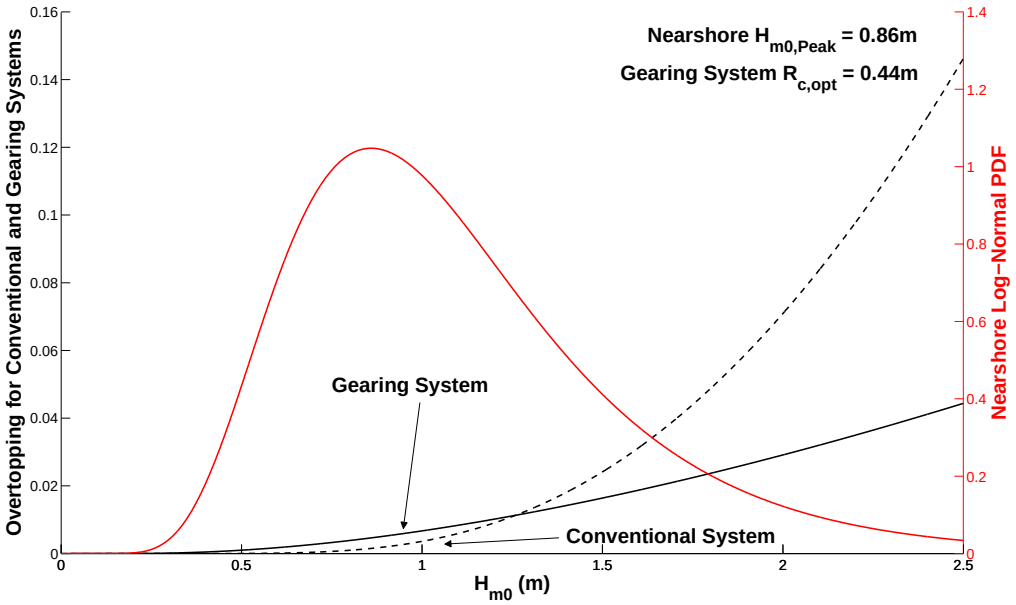

Figure 5.8: Buoy 46053: Nearshore PDF for H_{m0} and overtopping rates.

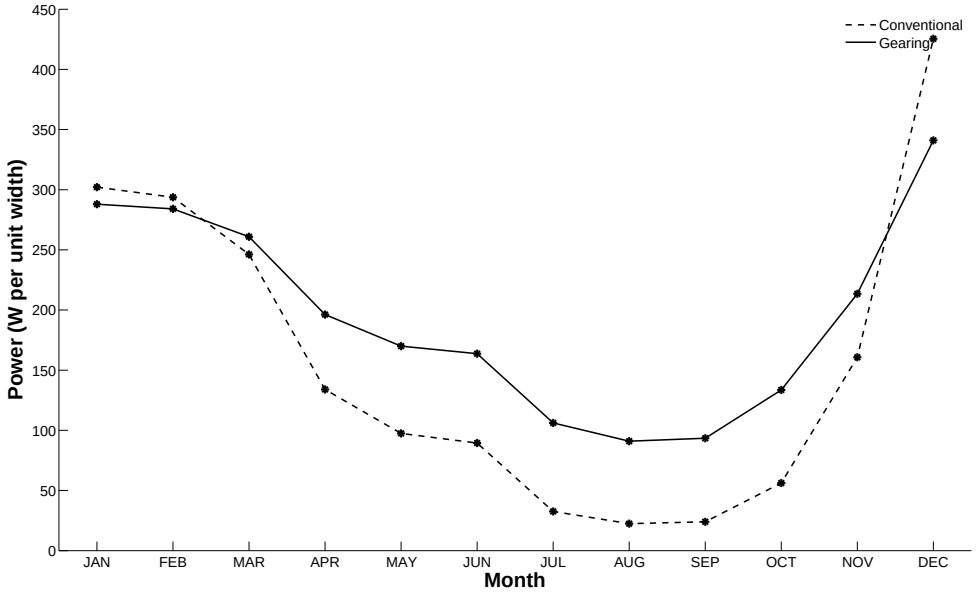

Figure 5.9: Buoy 46053: Average power available for output per month.

5.1.4 Buoy 46023: Near Pt. Arguello, CA

The Pt. Arguello location lies just north of where the coastline changes direction and thus encounters a higher wave climate than the rest of southern California. Therefore it is mildly suited for the concepts proposed in chapter 4. As before, Figure (5.10) presents the histogram for Buoy 46023 with the log-normal PDF superimposed over it. Figure (5.11) presents the nearshore log-normal PDF along with the gearing system and conventional system overtopping rates. The power take-off reservoir height and the conventional system crest freeboard are again 2.0 m. The optimal crest freeboard $R_{c,opt}$ of 0.78 m is computed from the peak in the nearshore log-normal PDF of 1.51 m. Figure (5.12) shows the improvement in power output by using a gearing system versus a conventional system. During the summer months there is improvement, transitioning to no improvement during spring and autumn, and the gearing system underperforms during the winter.

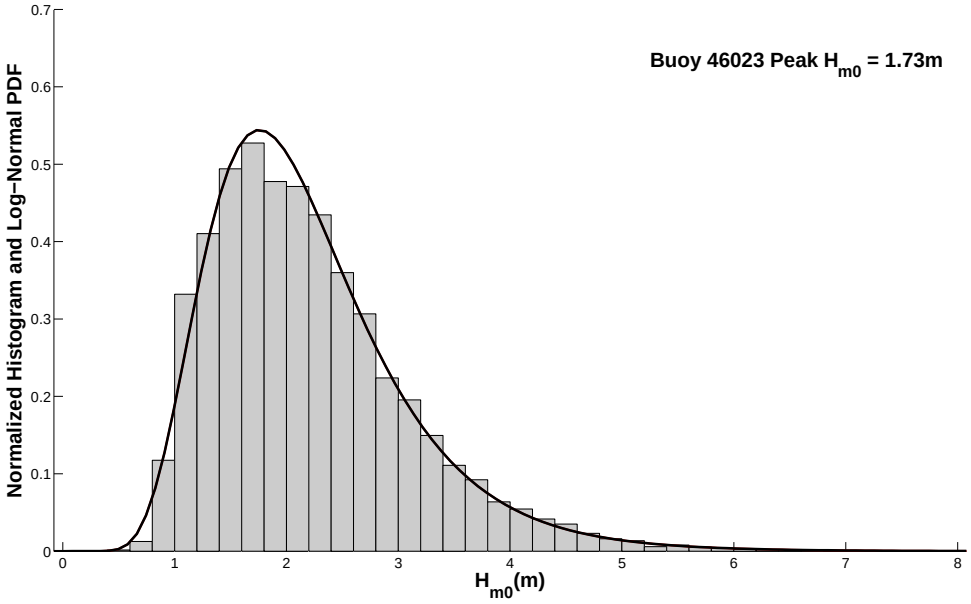

Figure 5.10: Buoy 46023: Histogram of significant wave heights for the past 10 years.

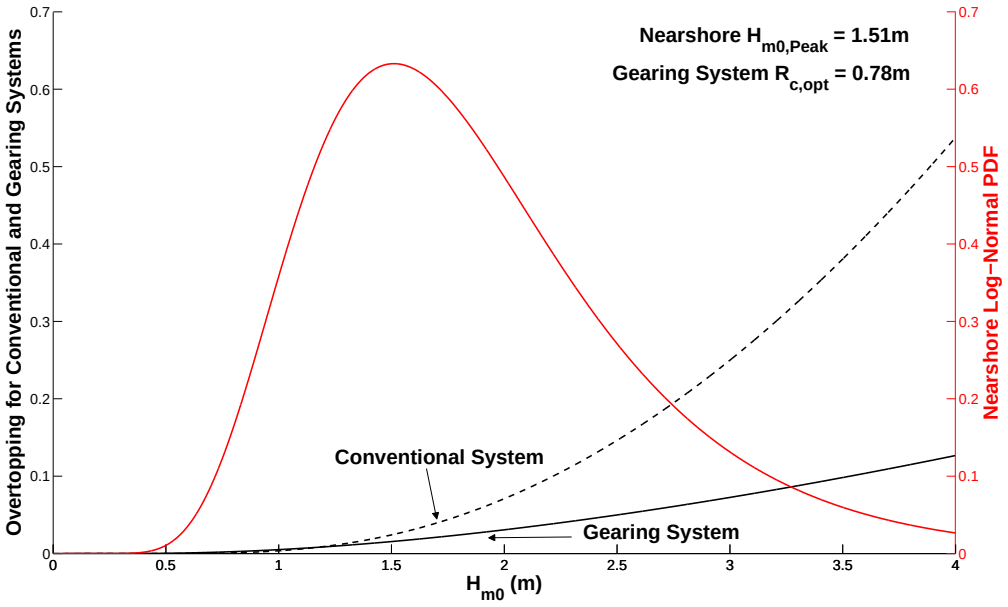

Figure 5.11: Buoy 46023: Nearshore PDF for H_{m0} and overtopping rates.

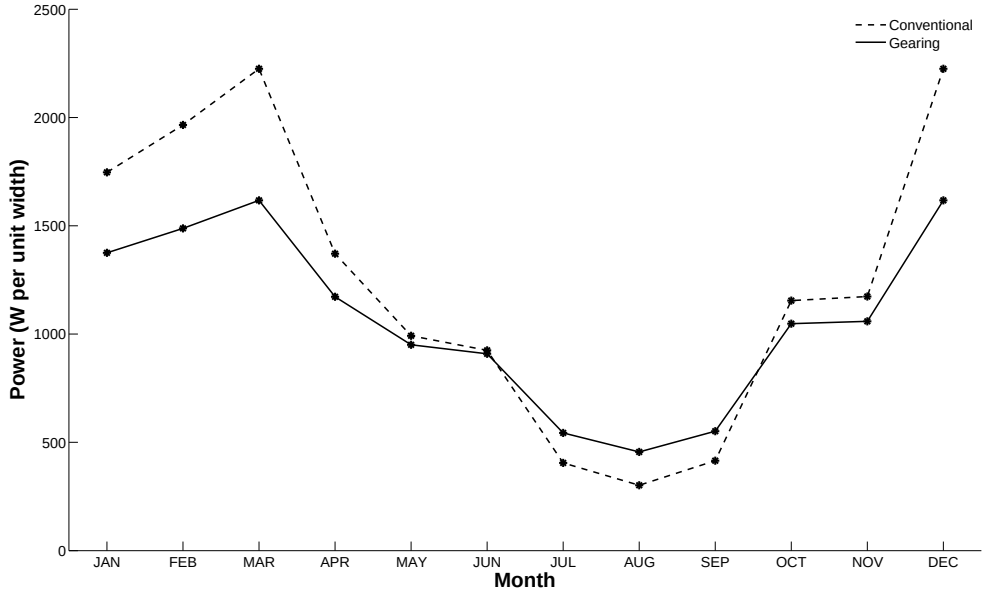

Figure 5.12: Buoy 46023: Average power available for output per month.

5.1.5 Buoy 46026: Near San Francisco, CA

The San Francisco location lies in the northern half of California and is exposed to more wave activity than in southern California. Therefore its suitability for the concepts proposed in chapter 4 is restricted to the summer months. As before, Figure (5.13) presents the histogram for Buoy 46026 with the log-normal PDF superimposed over it. Figure (5.14) presents the nearshore log-normal PDF along with the gearing system and conventional system overtopping rates. The power take-off reservoir height and the conventional system crest freeboard are again 2.0 m. The optimal crest freeboard $R_{c,opt}$ of 0.68 m is computed from the peak in the nearshore log-normal PDF of 1.31 m. Figure (5.15) shows the comparison of power output by using a gearing system versus a conventional system. Only during the summer months there is improvement.

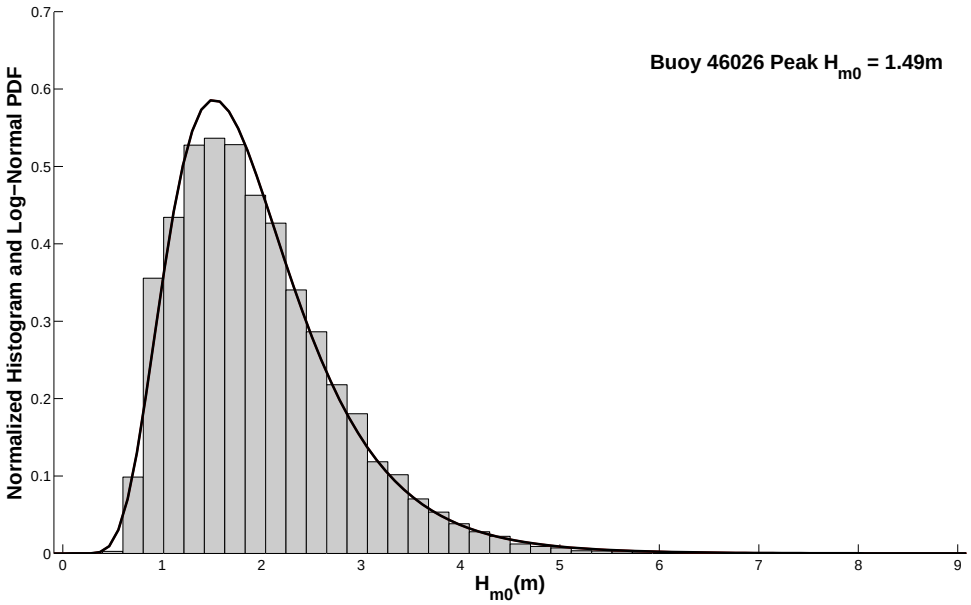

Figure 5.13: Buoy 46026: Histogram of significant wave heights for the past 10 years.

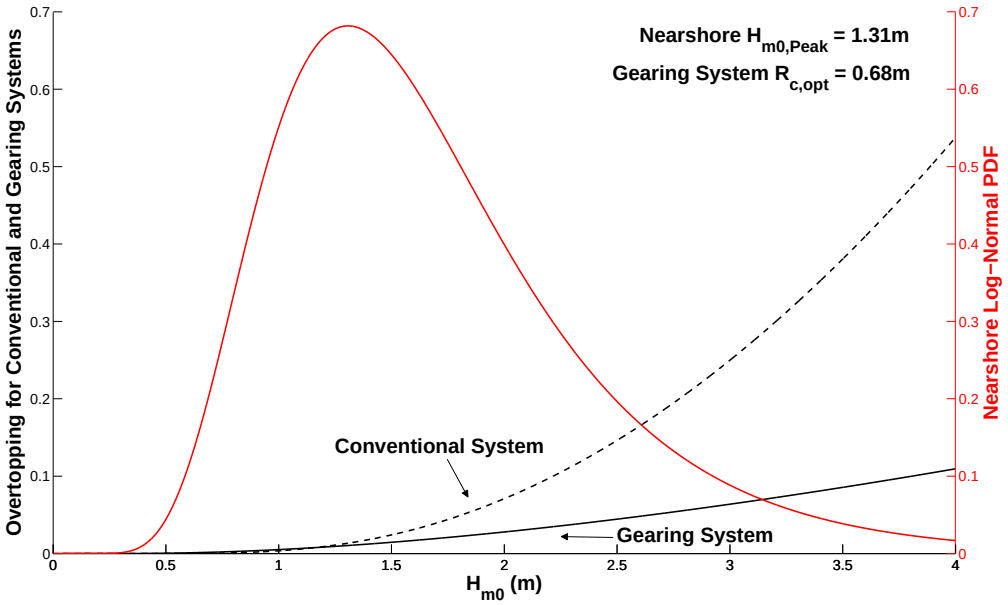

Figure 5.14: Buoy 46026: Nearshore PDF for H_{m0} and overtopping rates.

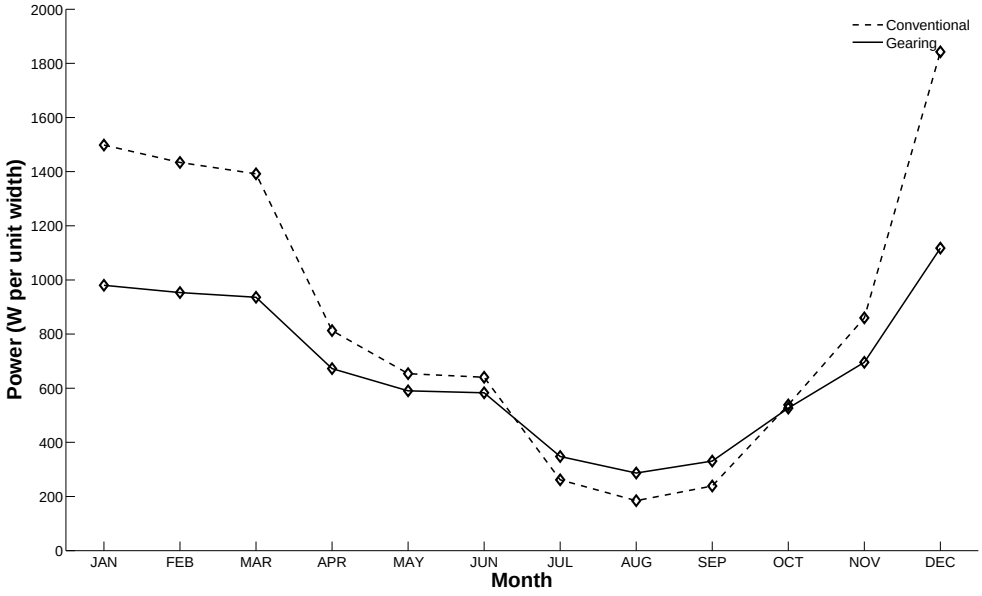

Figure 5.15: Buoy 46026: Average power available for output per month.

5.1.6 Buoy 46014: Near Point Arena, CA

The Pt. Arena location has a relatively strong wave environment year round and with large waves during the winter months. Therefore its suitability for the concepts proposed in chapter 4 is very limited. As before, Figure (5.16) presents the histogram for Buoy 46014 with the log-normal PDF superimposed over it. Figure (5.17) presents the nearshore log-normal PDF along with the gearing system and conventional system overtopping rates. The power take-off reservoir height and the conventional system crest freeboard are again 2.0 m. The optimal crest freeboard $R_{c,opt}$ of 0.76 m is computed from the peak in the nearshore log-normal PDF of 1.47 m. Figure (5.18) shows the comparison of power output by using a gearing system versus a conventional system. August is the only month where the gearing system outperforms the conventional system noticeably, while July and August slightly do so as well.

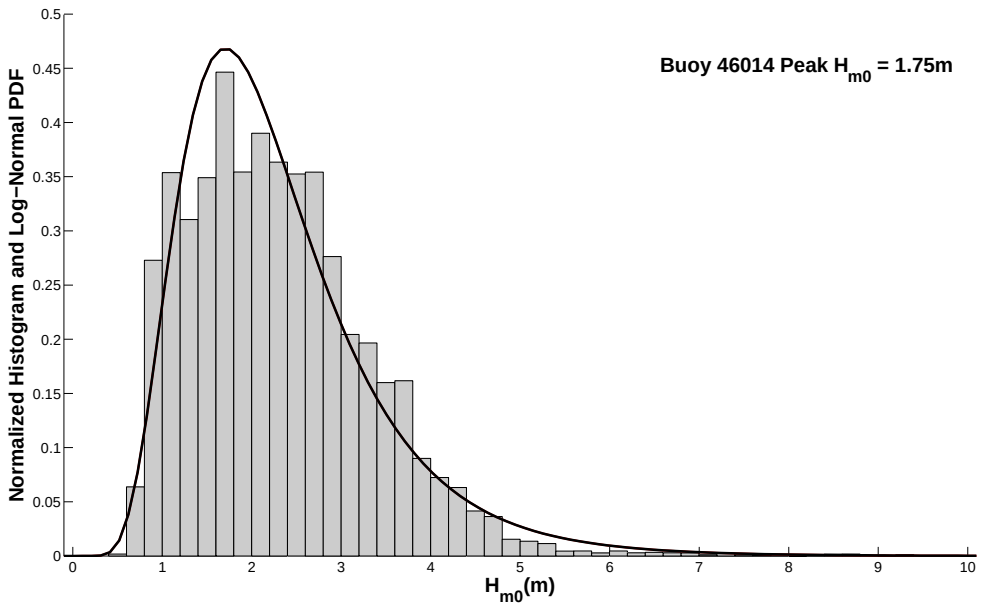

Figure 5.16: Buoy 46014: Histogram of significant wave heights for the past 10 years.

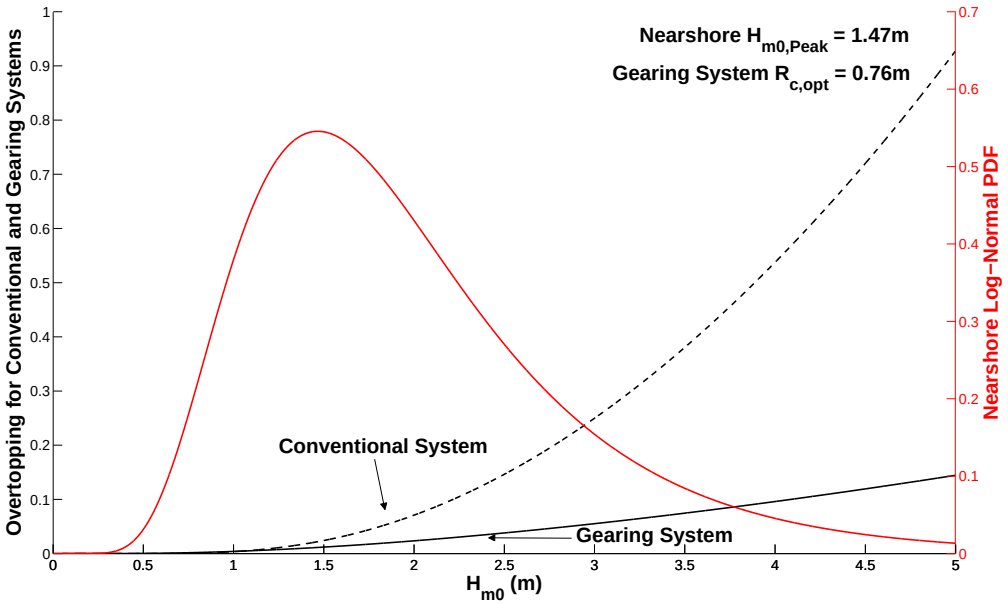

Figure 5.17: Buoy 46014: Nearshore PDF for H_{m0} and overtopping rates.

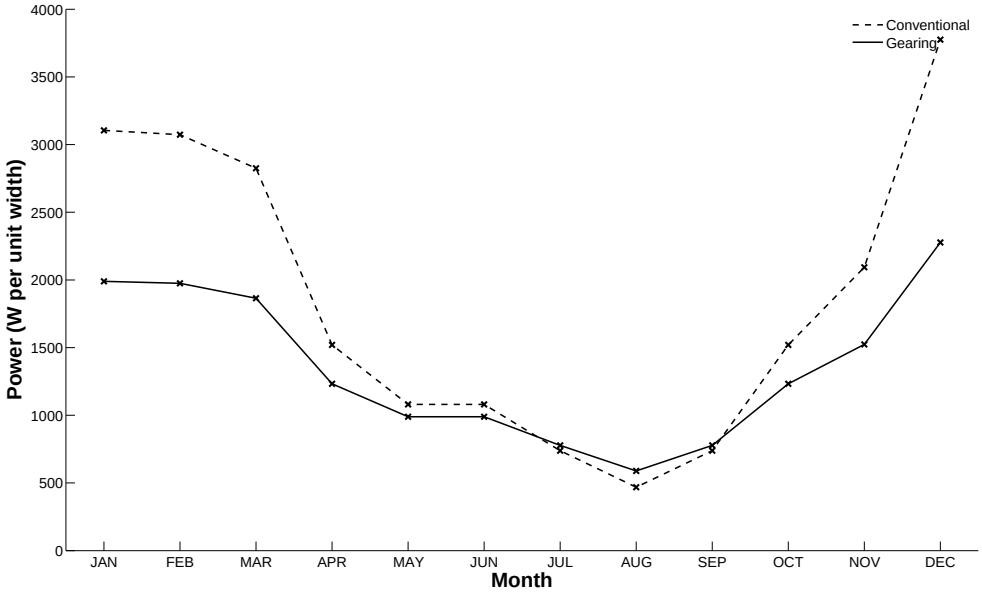

Figure 5.18: Buoy 46014: Average power available for output per month.

5.1.7 Buoy 46022: Near Eel River, CA

The Eel River location on a whole sees a wave environment similar to Pt. Arena but one that is more distinctly divided between a mild and heavy time frame. Therefore its suitability for the concepts proposed in chapter 4 is restricted to the mild times. As before, Figure (5.19) presents the histogram for Buoy 46022 with the log-normal PDF superimposed over it. Figure (5.20) presents the nearshore log-normal PDF along with the gearing system and conventional system overtopping rates. The power take-off reservoir height and the conventional system crest freeboard are again 2.0 m. The optimal crest freeboard $R_{c,opt}$ of 0.79 m is computed from the peak in the nearshore log-normal PDF of 1.53 m. Figure (5.21) shows the improvement in power output by using a gearing system versus a conventional system. Interestingly, the transitions between the heavy and mild wave environments are relatively quick and the gearing system show improvement a little bit beyond just the summer months.

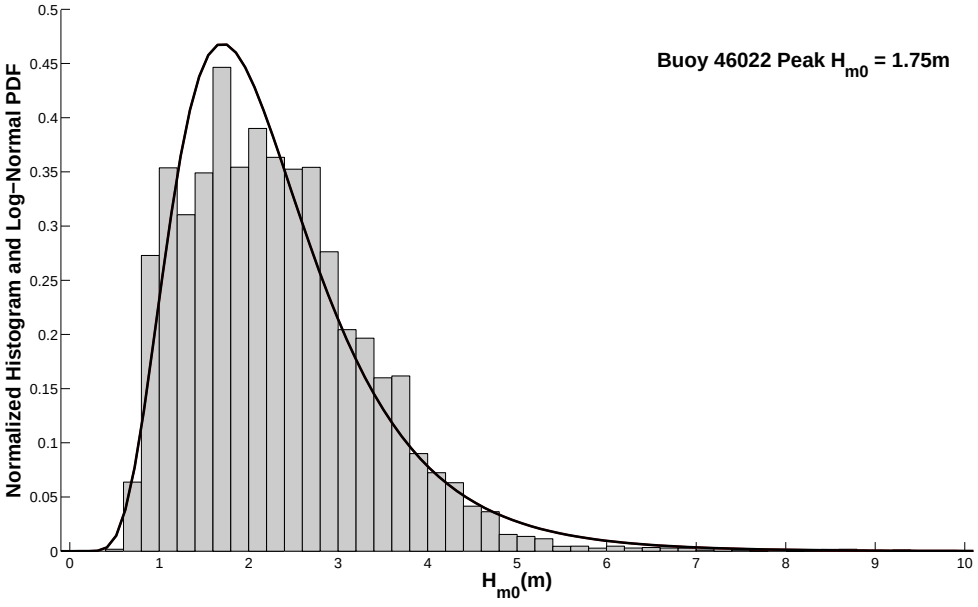

Figure 5.19: Buoy 46022: Histogram of significant wave heights for the past 10 years.

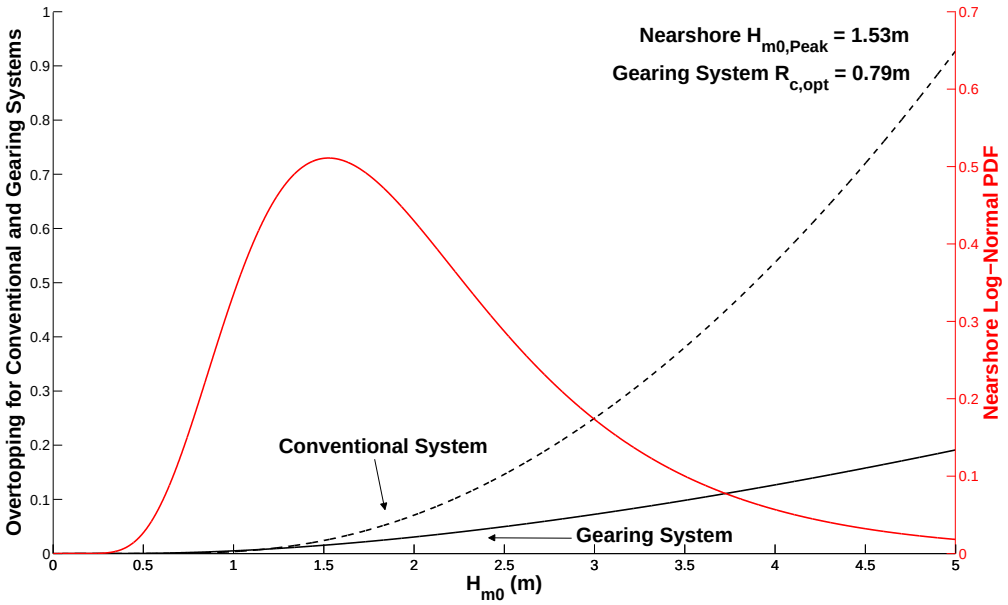

Figure 5.20: Buoy 46022: Nearshore PDF for H_{m0} and overtopping rates.

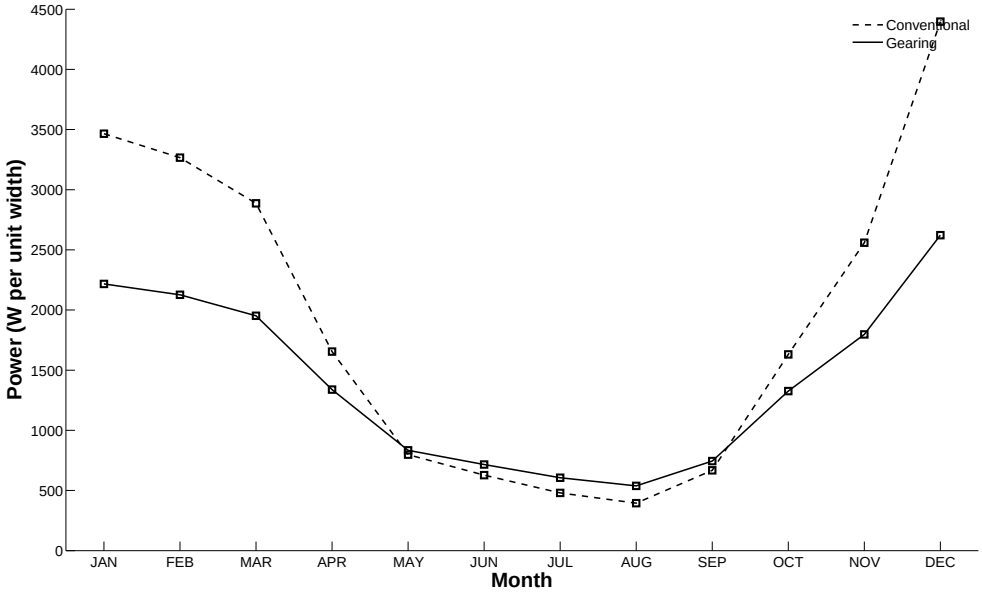

Figure 5.21: Buoy 46022: Average power available for output per month.

5.1.8 Buoy 46006: Near Eureka, CA

The Eureka location at the northern end of California experiences the heaviest wave environment. The monthly wave enviroment is quite similar to Eel River but stronger during the winter. As before, Figure (5.22) presents the histogram for Buoy 46014 with the log-normal PDF superimposed over it. Figure (5.23) presents the nearshore log-normal PDF along with the gearing system and conventional system overtopping rates. The power take-off reservoir height and the conventional system crest freeboard are again 2.0 m. The optimal crest freeboard $R_{c,opt}$ of 0.87 m is computed from the peak in the nearshore log-normal PDF of 1.68 m. Figure (5.24) shows the comparison of power output by using a gearing system versus a conventional system. Like Eel River the gearing system compares well during the middle part of the year.

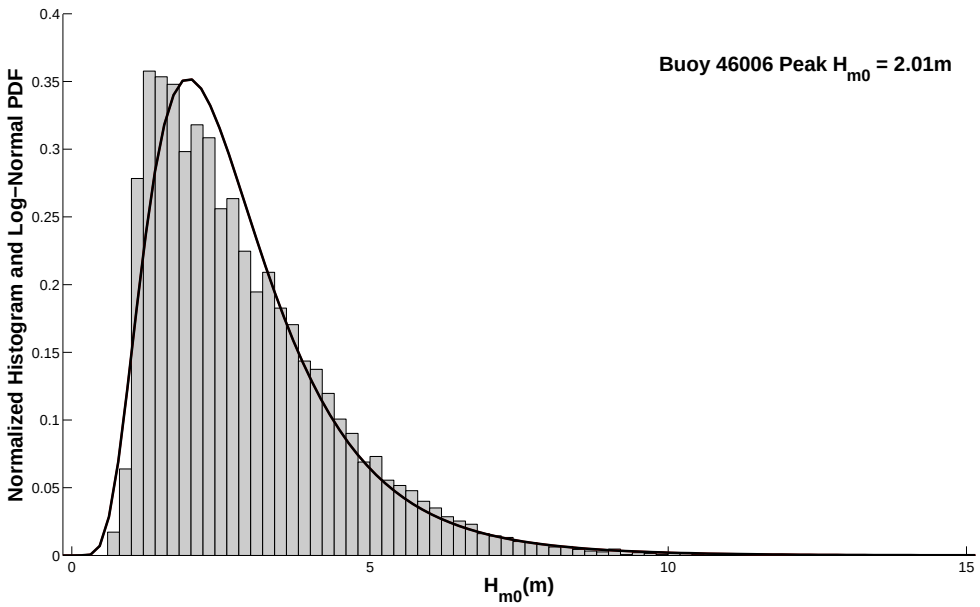

Figure 5.22: Buoy 46006: Histogram of significant wave heights for the past 10 years.

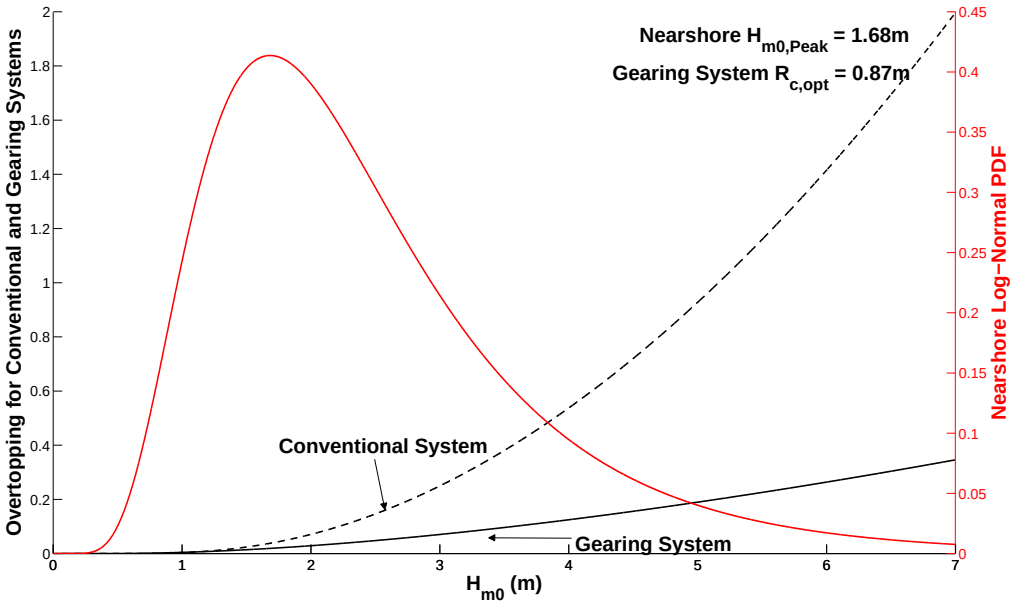

Figure 5.23: Buoy 46006: Nearshore PDF for H_{m0} and overtopping rates.

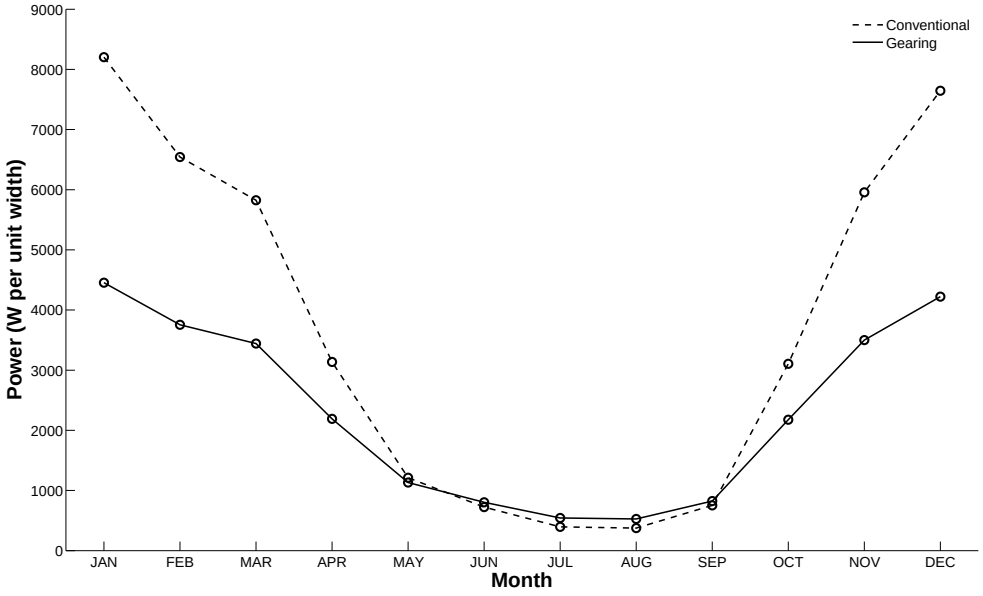

Figure 5.24: Buoy 46006: Average power available for output per month.

5.2 Summary of Results

In the prior section power output of the gearing system and the conventional system were compared on a monthly basis. The gearing system performed better in low wave height conditions but showed no improvement in higher waves. Table (5.2) compares the two systems on a yearly basis. The results show that when the power output is averaged over the whole year the gearing system performs better only at the Santa Monica location. This is because at the other locations in southern California the conventional system power output is large for a relative short time period, predominately during the winter months, which increases the annualized power over that of the gearing system. In northern California the wave environment is generally too large for the gearing system to outperform the conventional system except for the summer months.

Table 5.2: Annualized Power in units of W/m of wave front.

Buoy	Location	Gearing	Conventional
46086	San Clemente	361	403
46025	Santa Monica	156	136
46053	Santa Barbara	203	250
46023	Pt. Arguello	1124	1550
46026	San Francisco	714	1170
46014	Pt. Arena	1297	2051
46022	Eel River	1459	2315
46006	Eureka	2312	4081

However the gearing system can provide higher power output for a greater range of time than the conventional system as shown in Table (5.3). This table provides information based a subset of the significant wave height data for which the gearing system outperforms the conventional system. The critical H_{m0} is the value below

which the power output is greater for the gearing system. The fraction of time column shows what fraction of the year that the waves are below the critical H_{m0} for that particular location. Clearly all locations in southern California have fractions greater than 50%. Those in northern California are all less than 50%. The Gearing Power and Conventional Power columns provided the average power in watts per meter of wave front for these subsets of significant wave height data. Finally the last column shows the improvement of the gearing system over the conventional system for these subsets.

Table 5.3: Statistics and conditions for which the gearing system performs better than the conventional system. Power is in units of W/m of wave front.

Buoy	Location	Critical H_{m0} (m)	Fraction of Time	Gearing Power	Conventional Power	Percent Increase
46086	San Clemente	1.47	69.1	158	103	53.1
46025	Santa Monica	1.31	83.6	99	52	92.1
46053	Santa Barbara	1.32	73.9	90	49	82.9
46023	Pt. Arguello	1.75	49.7	232	175	32.5
46026	San Francisco	1.52	48.1	127	90	41.6
46014	Pt. Arena	1.73	46.7	198	146	35.8
46022	Eel River	1.76	44.0	198	148	33.6
46006	Eureka	1.80	35.7	175	135	29.4

5.3 Expected Extreme Waves

As introduced in chapter 2 the issue of survivability necessitates an analysis of the most probable extreme values of significant wave height for the eight locations. The procedure outline in chapter 2 is applied to the nearshore data and the results are presented in Table (5.4). As expected the most probable extremes values vary by location and increases the farther north the location is. In southern California the most probable extreme significant wave height in 5 years vary from 4.52 to 5.12 m and between 5.52 to 5.70 m for 50 year time periods. These most probable values progress as one travels north to Eureka. The most probable extreme significant values there are 7.12 m and 8.34 m for the 5 and 50 year time periods, respectively.

Table 5.4: Most Probable Extreme Value Significant Wave Height (m) for given number of years.

Location	Number of Years									
	5	10	15	20	25	30	35	40	45	50
San Clemente	5.12	5.29	5.39	5.46	5.51	5.56	5.59	5.62	5.65	5.68
Santa Monica	4.54	4.89	5.09	5.24	5.35	5.44	5.52	5.59	5.65	5.70
Santa Barbara	4.87	5.07	5.18	5.26	5.32	5.37	5.42	5.45	5.49	5.52
Pt. Arguello	6.45	6.56	6.63	6.68	6.72	6.75	6.77	6.79	6.81	6.83
San Francisco	6.41	6.54	6.62	6.68	6.72	6.75	6.78	6.81	6.83	6.85
Pt. Arena	6.76	6.87	6.93	6.98	7.01	7.04	7.07	7.09	7.11	7.12
Eel River	6.57	6.65	6.70	6.74	6.77	6.79	6.81	6.83	6.84	6.86
Eureka	7.29	7.61	7.79	7.92	8.02	8.11	8.18	8.24	8.29	8.34

This page intentionally left blank.

Chapter 6

Conclusions

Conventional designs for overtopping wave energy devices are limited in their applicability to locations which experience large wave activity. This leaves many areas throughout the world as inaccessible for this type of device. The proposed novel design concept is an attempt to utilize this unexploited energy resource. To assess the degree to which this can be done the design concept has been analyzed for various design parameters and applied to eight different wave environments off the California coast.

In order to apply the device design to the eight locations along the California coast the past ten years to significant wave height data were obtained from NOAA data buoys and analyzed. As expected the farther north the location, the larger the wave environment becomes. The monthly trends likewise were in line with expectations. The winter months showed the greatest wave heights due to winter storm activity and the summer months were relatively calm. For all locations even the northernmost of Eureka, during at least one month of the year the gearing system design showed improved power over the conventional design.

The overtopping formulas are based on experimentally derived expressions for overtopping of coastal structures. These expressions for volumetric overtopping rate

have an exponential dependence on significant wave height. The modeling of the gearing system influence the associated volumetric overtopping rate to be initially larger at small significant wave height and grow at a smaller rate than conventional overtopping systems. The design parameters determine at what value of significant wave height the two overtopping rates intersect. This value approximates the maximum significant wave height for which the gearing system outperforms the conventional system.

The southern California locations are better suited for the proposed device. In particular, nearshore to Santa Monica was the most promising location based on percent improvement in power output. In terms of utilization of waves, it was determined that more power could be extracted from 83.6% of all waves at this site. On an annualized basis, nearshore Santa Monica was the only location which demonstrated better performance than a conventional system. This is because at other locations the high power output during the winter months accounted for much of the power. However in the southern California sites on a monthly basis the gearing system performs better for most months out of the year than a conventional system. Generally the gearing system power output demonstrated a more even power output throughout the year than the conventional system. Extreme value analysis also supports operating in southern California locations. The most probable extreme value from 5 to 50 years are much smaller than can be expected at northern California sites. This allows for greater survivability and less stringent design criteria. This work shows that the proposed design concept has potential to access the small wave environments of many more global sites than currently possible.

6.1 Future Work

As described in chapter 3 and 4, the shape of the overtopping ramp is a simple ramp. Research into improved volumetric overtopping rate can be conducted by testing more advanced shapes as demonstrated by the Wave Dragon ramp design.

The propagation of the offshore NOAA buoy data to the nearshore locations was performed using the Goda formulas. While sufficient for the purposes of this thesis, a numerically-intensive, sophisticated analysis of this propagation using the SWAN code can potentially yield more accurate nearshore significant wave heights. Additionally because of the complex bathymetry depicted in Figure (2.16), locations where the coastal processes have amplified wave heights may be discovered. At such locations high power output wave energy devices may be possible.

Finally, hybrid devices should be explored to combine the benefits of the gearing system design for small waves with the higher power output of conventional designs for larger waves.

This page intentionally left blank.

Bibliography

[1] Armstrong, F. and Blundell, K., *Energy ... Beyond Oil*, Oxford University Press, 2007.

[2] Bascom, W., *Waves and Beaches*, Anchor Books, 1980.

[3] Brooke, J., *Wave Energy Conversion*, Elsevier Science, 2003.

[4] Budal, K., and Falnes, J., "A resonant point-absorber of ocean wave power", Nature, 256, pp.478-79, 1975.

[5] Butt, T. and Russell, *Surf Science*, University of Hawaii Press, 2004.

[6] CLASH ('Crest Level Assessment of coastal Structure'), www.clash-eu.org

[7] Count, B., *Power from Sea Waves*, Academic Press, 1980.

[8] Cruz, J., *Ocean Wave Energy Current Status and Future Perspectives*, Springer, 2008.

[9] EurOtop Wave Overtopping of Sea Defences and Related Structures: Assessment Manual, Aug. 2007, www.overtopping-manual.com

[10] Evans, D.V., "A theory of wave-power absorption by oscillating bodies", Journal of Fluid Mechanics, 77 (1976), pp.1-25.

[11] Evans, D.V., "Power from Water Waves", Annual Review of Fluid Mechanics, 13 (1981), pp. 157-187

[12] Falnes, J., *Ocean Waves and Oscillating Systems*, Cambridge University Press, 2002.

[13] Falnes, J., "A review of wave-energy extraction", Marine Structures, 20 (2007), pp.185-201.

[14] Frigaard, P., Kofoed, J.P., and Rasmussen, M.R., "Wave Overtopping Measurements on the Wave Dragon Nissum Bredning Prototype", Proc. of 14th ISOPE Conf., 2004, pp. 210-216.

[15] Folley, M., Whittaker, T.J.T, "Analysis of the nearshore wave energy resource", Renewable Energy, 34 (2009), pp. 1709-1715.

[16] Goda, Y., "Derivation of unified wave overtopping formulas for seawalls with smooth, impermeable surfaces based on selected CLASH datasets", Coastal Engineering, 56 (2009), pp. 385399.

[17] Goda, Y., *Random Seas and Design of Maritime Structures*, World Scientific, 2000.

[18] Holthuijsen, L.H., *Waves in Oceanic and Coastal Waters*, Cambridge University Press, 2007.

[19] Khan, J., and Bhuyan, G., Ocean Energy: Global Technology Development Status, Report prepared by Powertech Labs for the IEA-OES., 2009, [Online], Available: www.iea-oceans.org

[20] Iglesias, G., et.al., "Wave energy potential in Galicia (NW Spain)", Renewable Energy, 34 (2009), pp.23232333.

[21] Kofoed, J.P., et.al., "Influence of buoyancy control performance on power production by the Wave Dragon Nissum Bredning Prototype", Proc. of 17th ISOPE Conf., 2007, pp. 497-504.

[22] Kofoed, J.P., et.al., "Prototype testing of the wave energy converter wave dragon", Renewable Energy, 31 (2006), pp. 181-189.

[23] Kramer, M., and Frigaard P., "Efficient Wave Energy Amplification with Wave Reflector", Proc. of 12th ISOP Conf., 2002, pp. 707-712.

[24] Kundu, P.K and Cohen, I.M., *Fluid Mechanics*, Elsevier Academic Press, San Diego, CA, 2004.

[25] Mansour, A., *ME240A: Advanced Marine Structures I*, UC Berkeley, Spring 2009.

[26] Margheritini, L., Vicinanza, D., Frigaard, P. (2009), "SSG wave energy converter: Design, reliability and hydraulic performance of an innovative overtopping device", Renewable Energy, 34 (2009), pp. 1371-1380.

[27] McCormick, M., *Ocean Wave Energy Conversion*, John Wiley and Sons, 1981.

[28] Mehlum, E., "Tapchan", Hydrodynamics of Ocean Wave-Energy Utilization, IUTAM Symposium Lisbon, Portugal 1985, pp. 51-55.

[29] Mei, C.C., *The Applied Dynamics of Ocean Surface Waves*, World Scientific, 2005.

[30] Munson, B.R., Young, D.F., Okiishi, T.H., *Fundamentals of Fluid Mechanics*, John Wiley & Sons, 3rd Ed., 1994.

[31] Neilsen, F.G. et.al, "Specialist Committe V.4 Ocean, Wind and Wave Energy Utilization", 17th International Ship and Offshore Structures Congress, volume 2, 2009.

[32] Newman, J.N., *Marine Hydrodynamics*, MIT Press, 1977.

[33] http://www.ndbc.noaa.gov/

[34] Özger M., Altunkaynak A., Şen Z., "Stochastic wave energy calculation formulation", Renewable Energy, 29 (2009), pp. 1747-1756.

[35] Previsic, M., and Bedard, R., EPRI report: EPRI WP 011 CA, Dec. 31, 2007. (Online version: www.epri.com/oceanenergy/).

[36] Previsic, M., EPRI report: E2I EPRI WP-004-US-Rev 1, June 16, 2004. (Online version: www.epri.com/oceanenergy/).

[37] Ross, D., *Power from the Waves*, Oxford University Press, 1995.

[38] Shaw, R., *Wave Energy a design challenge*, Ellis Horwood Publishers, 1982.

[39] Sobey, R.J., *CE204: Coastal and Estuarine Analysis Course Notes*, UC Berkeley, Fall 2003.

[40] http://www.swan.tudelft.nl

[41] Tedd, J., Kofoed, J.P, "Measurements of overtopping flow time series on the Wave Dragon, wave energy converter", Renewable Energy, 34 (2009), pp. 711-717.

[42] Tucker, M.J., and Pitt E.G., *Waves in Ocean Engineering*, Elsevier, 2001.

[43] van der Meer, J.W., "Technical Report Wave Run-up and Wave Overtopping at Dikes", Technical Advisory Committee on Flood Defence The Netherlands, Delft, May 2002.

[44] Vicinanza, D., Frigaard, P., "Wave pressure acting on a seawave slot-cone generator", Coastal Engineering, 55 (2008), pp. 553-568.

[45] Wehausen, J.V. and Laitone, E.V. (1960). "Surface Waves", *Handbuch der Physik*, Vol. 9, Springer-Verlag, Berlin, pp. 483–490 (Online version: http://www.coe.berkeley.edu/SurfaceWaves).

[46] Westwood, A., "Refocus Marine Renewable Energy Report", Elsevier, 2005

[47] Young, I.R., *Wind Generated Ocean Waves*, Elsevier, 1999.

This page intentionally left blank.

Appendix A

Linear Theory of Waves

This section presents some standard fundamentals and results of the linear theory of water waves. Further details can be found in standard references by Wehausen [45], Newman [32], and Kundu [24].

A.1 Theoretical Description

This mathematical formulation employs a righthand coordinate system $(\hat{x}, \hat{y}, \hat{z})$ fixed on the undisturbed free surface with z being positive in the upward vertical direction. The fluid domain is infinite in the x and y directions and of constant depth d, in the z direction. The propagation direction of the incident waves make an angle β with the positive x-axis. The fluid is considered to be inviscid and incompressible with surface tension negligible. We take the flow to be irrotational; hence there exists a scalar velocity potential, $\Phi(x, y, z, t)$ such that

$$\mathbf{v} = (u, v, w) = \nabla\Phi = (\Phi_x, \Phi_y, \Phi_z).$$

Thus, the equation for conservation of mass becomes Laplace's equation:

$$\nabla^2\Phi = 0. \tag{A.1}$$

If we insert $\nabla\Phi$ in for $\mathbf{v}$ into the incompressible Euler equation

$$\frac{\partial \mathbf{v}}{\partial t} + (\mathbf{v}\cdot\nabla)\mathbf{v} = -\frac{\nabla P}{\rho} - \mathbf{g}$$

(where P is pressure, ρ is density, and $\mathbf{g}$ is gravity) and switch the order of the differentiation in the local acceleration term, for the x component we get:

$$\frac{\partial}{\partial x}\left\{\frac{\partial\Phi}{\partial t} + \frac{1}{2}\left(\left(\frac{\partial\Phi}{\partial x}\right)^2 + \left(\frac{\partial\Phi}{\partial y}\right)^2 + \left(\frac{\partial\Phi}{\partial z}\right)^2\right) + g\hat{z}\right\} = 0$$

Likewise for the y and z components we get:

$$\frac{\partial}{\partial y}\left\{\frac{\partial\Phi}{\partial t} + \frac{1}{2}\left(\left(\frac{\partial\Phi}{\partial x}\right)^2 + \left(\frac{\partial\Phi}{\partial y}\right)^2 + \left(\frac{\partial\Phi}{\partial z}\right)^2\right) + g\hat{z}\right\} = 0$$

$$\frac{\partial}{\partial z}\left\{\frac{\partial\Phi}{\partial t} + \frac{1}{2}\left(\left(\frac{\partial\Phi}{\partial x}\right)^2 + \left(\frac{\partial\Phi}{\partial y}\right)^2 + \left(\frac{\partial\Phi}{\partial z}\right)^2\right) + g\hat{z}\right\} = 0$$

So,

$$\nabla\left\{\frac{\partial\Phi}{\partial t} + \frac{1}{2}\left(\left(\frac{\partial\Phi}{\partial x}\right)^2 + \left(\frac{\partial\Phi}{\partial y}\right)^2 + \left(\frac{\partial\Phi}{\partial z}\right)^2\right) + g\hat{z}\right\} = 0$$

We can integrate this equation to get Euler's Integral which when taking the constant of integration as $C(t) = \frac{P_a}{\rho}$ takes the form:

$$\frac{\partial\Phi}{\partial t} + \frac{1}{2}\left(\left(\frac{\partial\Phi}{\partial x}\right)^2 + \left(\frac{\partial\Phi}{\partial y}\right)^2 + \left(\frac{\partial\Phi}{\partial z}\right)^2\right) + \frac{P}{\rho} + gy = \frac{P_A}{\rho} \tag{A.2}$$

where P_A is atmospheric pressure.

A.1.1 Boundary Conditions

Next, we must consider the boundary conditions. The kinematic boundary condition on any geometric surface can be written as

$$\mathbf{v} \cdot \mathbf{n} = \Phi_n = \mathbf{V} \cdot \mathbf{n}$$

where $\mathbf{V}$ is the velocity at a point on the surface and $\mathbf{n}$ is the normal vector at the surface.

Assume the geometric surface is $F(\mathbf{x}, t) = 0$. Then $\mathbf{n} = \frac{\nabla F}{|\nabla F|}$. We take the material derivative of F to get $\mathbf{V}$.

$$\frac{DF}{Dt} = \frac{\partial F}{\partial t} + (\mathbf{V} \cdot \nabla)F = 0$$

$$\mathbf{V} \cdot \nabla F = -\frac{\partial F}{\partial t}$$

So,

$$\mathbf{V} \cdot \mathbf{n} = -\frac{F_t}{|\nabla F|}$$

Applying the kinematic boundary condition we arrive at the kinematic boundary condition:

$$\Phi_x F_x + \Phi_y F_y + \Phi_z F_z + F_t = 0$$

Now on apply this to the free surface which is described by $z = Z(x, y, t)$ or $F = z - Z(x, y, t) = 0$. The free surface kinematic boundary condition becomes:

$$Z_x(x, y, t)\Phi_x(x, y, Z(x, y, t), t) + Z_y\Phi_y - \Phi_z + Z_t = 0 \tag{A.3}$$

The dynamic boundary condition states that the pressure everywhere on the free surface equals the atmospheric pressure. Applying Euler's Integral to the free surface

we get:

$$\Phi_t(x, y, Z(x, y, t), t) + \frac{1}{2}|\nabla\Phi|^2 + gZ = 0 \tag{A.4}$$

A.1.2 Linearization

We will make the assumption of small amplitude waves such that the ratio of the wave amplitude to wavelength is very small, $\frac{A}{\lambda} \ll 1$. We will use the following scaling of variables:

$$\begin{aligned} Z &= O(A) && \text{(A.5)} \\ x, y, z &= O(\lambda) && \text{(A.6)} \\ Time = T &= O\left(\sqrt{\frac{\lambda}{g}}\right) && \text{(A.7)} \\ u, v, w &= O\left(\frac{A}{T}\right) && \text{(A.8)} \\ \Phi &= O\left(A\sqrt{\lambda g}\right) && \text{(A.9)} \end{aligned}$$

On the free surface we are linearizing about the calm water line, thus we may replace $z = Z$ by $z = 0$ in the argument to Φ. The linearized problem thus becomes: The field equation remains Laplace's equation:

$$\nabla^2\Phi = 0 \tag{A.10}$$

Euler's Integral becomes:

$$\Phi_t + gz + \frac{P}{\rho} = 0 \tag{A.11}$$

The kinematic free surface boundary condition becomes:

$$\Phi_z(x, y, 0, t) = Z_t \tag{A.12}$$

The dynamic free surface boundary condition becomes:

$$\Phi_t(x, y, 0, t) + gZ(x, y, t) = 0 \tag{A.13}$$

Combining the two, we get the free surface boundary condition:

$$\Phi_{tt} + gZ_z = 0 \tag{A.14}$$

The bottom boundary condition remains:

$$\Phi_z = 0, \quad \text{at } z = -d \tag{A.15}$$

A.1.3 Solution of the Boundary Value Problem

By using the method of separation of variables (using k as the separation constant) the boundary value problem is solved with the following results for the free surface, velocity potential, and dispersion relationship.

$$Z = A \cdot \mathrm{Re}\left(e^{ik(x\cos\beta + y\sin\beta) - i\omega t}\right) \tag{A.16}$$

$$\Phi = \frac{-igA}{\omega}\frac{\cosh k(z+d)}{\cosh kd}e^{ik(x\cos\beta + y\sin\beta) - i\omega t} \tag{A.17}$$

$$\omega^2 = gk\tanh(kd) \tag{A.18}$$

The dispersion relationship relates k, the wavenumber and ω, the angular frequency such that they cannot be arbitrarily chosen.

A wave travels at its phase speed $c = \omega/k$. Applying the dispersion relationship

(A.1.3) and the definition of the wavenumber, $k = 2\pi/L$ to this we get:

$$c^2 = \frac{gL}{2\pi} \tanh\left(\frac{2\pi d}{L}\right) \tag{A.19}$$

This demonstrates that wave speed is a function of wavelength. Longer waves travel faster.

Finally in the case of deep water, $d \to \infty$, some simplifications can be made. Specifically, $\cosh k(z+d)\cosh kd \to 1$, and $\tanh kd \to 1$. Thus,

$$\Phi = \frac{-igA}{\omega} e^{ik(x\cos\beta + y\sin\beta) - i\omega t} \tag{A.20}$$

and

$$c^2 = \frac{gL}{2\pi} \tag{A.21}$$

Appendix B

Stochastic Wave Energy Formulation

This section presents the formulation given in [34] for the wave power which accounts for the cross stochastic properties of wave height and period. Starting by applying the expectation operation is on equation (2.12) we get

$$E(P) = \left(\frac{\rho g^2}{64\pi}\right) \cdot E(T_e H_{m0}^2) \tag{B.1}$$

Using the theory of random processes we can use the definition of the covarience, and the cross-correlation coefficient, ρ_{T_e,H_{m0}^2} to manipulate the expectation term of the product between T_e and H_{m0}^2.

$$Cov(T_e, H_{m0}^2) = E(T_e H_{m0}^2) - E(T_e)E(H_{m0}^2) \tag{B.2}$$

$$\rho_{T_e,H_{m0}^2} = \frac{Cov(T_e, H_{m0}^2)}{\sigma_{T_e}\sigma_{H_{m0}^2}} \tag{B.3}$$

Here σ_{T_e} and $\sigma_{H^2_{m0}}$ are the standard deviations for T_e and H^2_{m0} respectively. By applying these two equations to equation (B.1) we can arrive at

$$E(P) = \left(\frac{\rho g^2}{64\pi}\right)\left[E(T_e)\cdot E(H^2_{m0}) + \rho_{T_e,H^2_{m0}}\sigma_{T_e}\sigma_{H^2_{m0}}\right] \tag{B.4}$$

This equation reduces to equation (2.12) for the case when the correlation coefficient is zero meaning the energy period and significant wave height are uncorrelated. Rewriting equation (B.4) as

$$E(P) = \left(\frac{\rho g^2}{64\pi}\right) E(T_e)\cdot E(H^2_{m0})\left[1 + \frac{\rho_{T_e,H^2_{m0}}\sigma_{T_e}\sigma_{H^2_{m0}}}{E(T_e)\cdot E(H^2_{m0})}\right] \tag{B.5}$$

it becomes clear that equation (2.12) underestimates power by the factor in brackets for positive correlations which are expected since larger waves have longer periods typically. Defining the term in brackets as the correction factor α, we can use the definition of the coefficient of variation C, to write it succinctly as

$$\alpha = 1 + \rho_{T_e,H^2_{m0}} C_{T_e} C_{H^2_{m0}} \tag{B.6}$$

where C_{T_e} and $C_{H^2_{m0}}$ are the ratio of the standard deviation to the arithmetic average of the energy period and significant wave height respectively. This expression shows that for small values of coefficients of variation the correction factor is unnecessary and the traditional formulation is acceptable. But if the coefficients of variation are large the correction factor may become significant.

Appendix C

Variable Dependence of B

This section will investigate the dependence of the coefficient B on the variables of seawall incline angle α, seabed slope θ, and relative toe depth h_t/H_{m0}. As shown in chapter 3 the equation for B is given by:

$$B = B_0 \tanh\left[(0.822 - 2.22\tan(\theta) \times (h_t/H_{m0} + 0.578 + 2.22\tan(\theta))\right] \tag{C.1}$$

$$B_0 = 2.3 - 0.5\cot(\alpha) + 0.15\cot^2(\alpha) - 0.011\cot^3(\alpha) \tag{C.2}$$

Goda explored the dependence of B on h_t/H_{m0} for two cases of seabed slope angle. His results are reproduced in figure (C.1). For both cases which are representative of expected conditions for seabed slope, the results show that after a relative depth of 3 the value of B plateaus to a constant. It is expected that the relative depth at which the proposed overtopping device is in this range of constant B.

Figure (C.2) below show the effect of the seabed slope angle θ on the non-dimensionalized coefficient B/B_0. B is a hyperbolic tangent function characterized by an approximately constant value from 0 to 15 degrees and dramatic decrease from 15 to 25 degrees and then another approximately constant value from 25 to 90 degrees. It is expected that the proposed overtopping device will operate in seabed slope angles

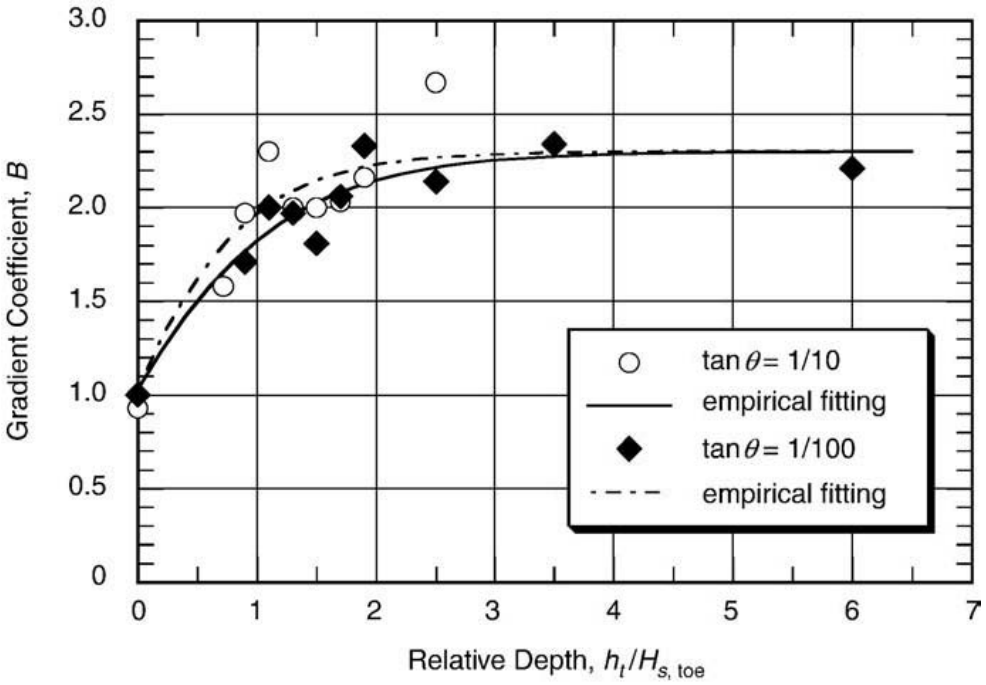

Figure C.1: Dependence of B on relative toe depth h_t/H_{m0}, ref: Goda.

between 0 and 15 degrees and thus B will have an approximately constant dependence on θ.

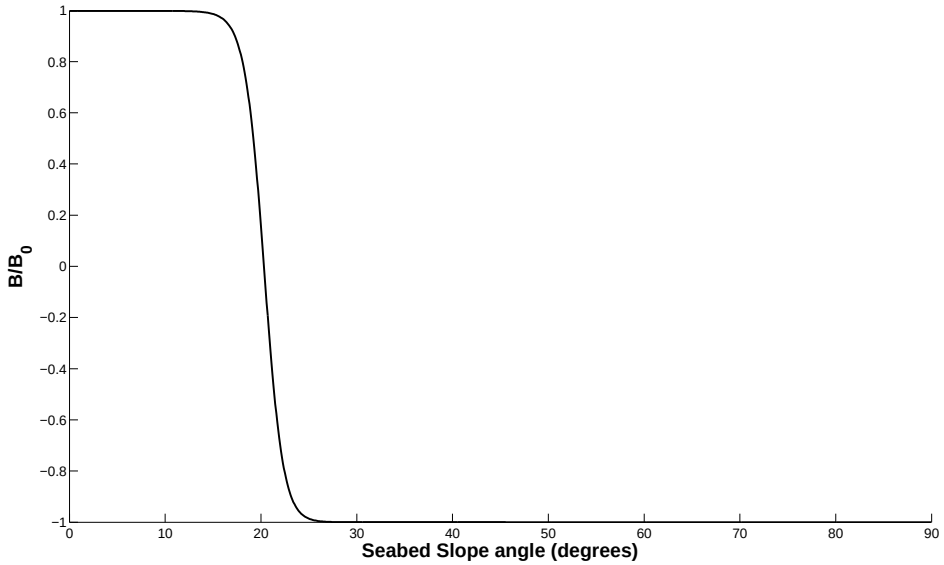

Figure C.2: Dependence of B on seabed slope θ.

The effect of α on B occurs in the B_0 coefficient. As shown in figure (C.3), Goda fit an empirical equation to represent the trend in the data. The use of a cubic equation is based on physical reasoning he cites in various manuals. The region of slopes applicable for our purposes are between slope cotangent values of 0 and 1 as these correspond to seawall incline angles of 90 and 45 degrees. Goda's fit for this region is approximately linear and ranges from 2.30 to 1.94 for 90 and 45 degree incline angles, respectively.

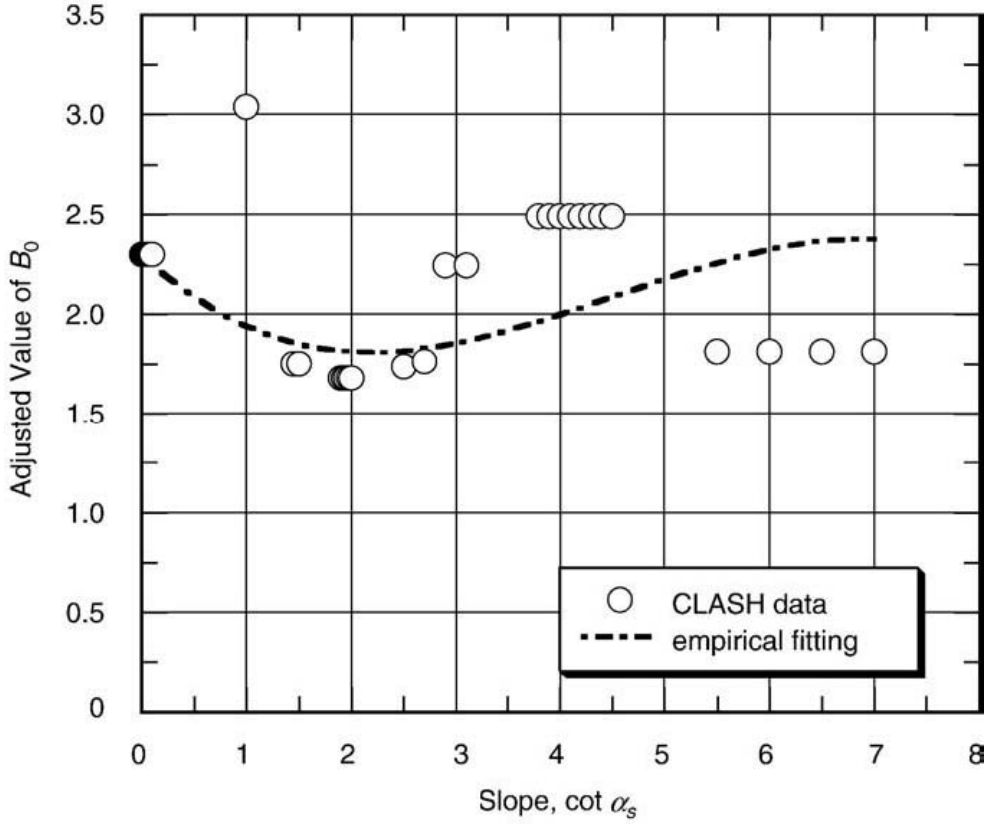

Figure C.3: Dependence of B_0 on seawall incline angle α, ref: Goda.